Order Number 8801723

A study of aerosol separation in granular and fibrous filters

Kao, Ju-Nan, Ph.D.

City University of New York, 1987

U·M·I
300 N. Zeeb Rd.
Ann Arbor, MI 48106

PLEASE NOTE:

In all cases this material has been filmed in the best possible way from the available copy. Problems encountered with this document have been identified here with a check mark __✓__.

1. Glossy photographs or pages _____
2. Colored illustrations, paper or print _____
3. Photographs with dark background ✓
4. Illustrations are poor copy _____
5. Pages with black marks, not original copy _____
6. Print shows through as there is text on both sides of page _____
7. Indistinct, broken or small print on several pages ✓
8. Print exceeds margin requirements _____
9. Tightly bound copy with print lost in spine _____
10. Computer printout pages with indistinct print _____
11. Page(s) _____ lacking when material received, and not available from school or author.
12. Page(s) _____ seem to be missing in numbering only as text follows.
13. Two pages numbered _____. Text follows.
14. Curling and wrinkled pages _____
15. Dissertation contains pages with print at a slant, filmed as received _____
16. Other _____

_____

_____

A STUDY OF AEROSOL SEPARATION IN GRANULAR AND FIBROUS FILTERS

by

JU-NAN KAO

A dissertation submitted to the Graduate Faculty
in Engineering in partial fulfillment of the requirements
for the degree of Doctor of Philosophy,
The City University of New York.

1987

This manuscript has been read and accepted for the Graduate Faculty in Engineering in satisfation of the dissertation requirement for the degree of Doctor of Philosophy.

May 19, 1987

Date

Professor G. I. Tardos

Chair of Examining Committee

May 26, 1987

Date

Professor P. Karmel

Executive Officer

Professor L. Theodore

Professor R. Pfeffer

Professor R. Shinnar

Professor L. Isaacs

Supervisory Committee

The City University of New York

Abstract

A STUDY OF AEROSOL SEPARATION IN GRANULAR AND FIBROUS FILTERS

by

Ju-Nan Kao

Advisors: Professors Robert Pfeffer and Gabriel I. Tardos

A study of a rotating fluidized bed to separate high concentration dusts from flue gases is undertaken. The rotating fluidized bed filter (RFBF) has the advantages of high filtration efficiency, continuous operation and high flow rates of gas per unit area of distributor; thus it appears very attractive for industrial applications.

In the first part of this study, the feasibility of using the RFBF to separate different industrial pollutants containing micron and submicron particles from a contaminated gas stream is demonstrated. A high dust concentration air stream at room temperature as well as exhaust gases from a diesel engine are used to test the RFBF. Efficiency and pressure drop under continuous operation of the filter are measured. Also, experiments to determine minimum granule recirculating rates and ways to clean dirty granules are studied. Furthermore, a preliminary economic comparison of the RFBF with a baghouse and an electrostatic precipitator is given and a conceptual design of a scaled-up pilot size RFBF which can handle 4,000 CFM air and withstand temperatures up to 500 ^{o}F has been given.

In the second part of this work, the influence of electrostatic effects in fibrous and granular beds to separate charged dust particles

in an electric field is studied. The results of experiments with charged particles are used to improved the filtration efficiency of the RFBF for fine dust particles in the size range 0.1 to 1 μm by passing the dusty gas through a corona charger placed at the entrance of the filter. Using precharged particles results in a significant enhacement of the filtration efficiency in the RFBF without an increase in pressure drop through the device and with only a minor complication in the construction of the filter.

This research was carried out under the supervision of Professor G. I. Tardos and Professor R. Pfeffer of the Chemical Engineering Department at the City College of the City University of New York.

ACKNOWLEDGEMENT

I wish to thank Professors Robert Pfeffer and Gabriel I. Tardos for suggesting the subject and for their helpful advice, supervision and encouragement during all stages of this work, Professor Ashok Sangani from the Department of Chemical Engineering, Syracuse University, for offering the use of his flow model and Professor Arthur Squires from Virginia Polytechnic Institute and State University for his expert advice.

Special thanks are also due to Mr. John Bodnaruk, Mr. William Hall and Mr. Ivan Ortiz for constructing the experimental devices, and to Mr. Paul Vinh for his help in running the experiments.

Furthermore, I am indebted to the sponsors of this research, the New York State Energy Research and Development Authority and the New York Power Authority, under contract No. 819-ERER-BEA-86 and to Dr. Burton Krakow and Mr. Roger Heyrman for their support.

Above all, I am most grateful to my dear wife, Jennifer, and parents whose great understanding and patience created the proper conditions for the successful completion of this work

TABLE OF CONTENTS

LIST OF TABLES

LIST OF FIGURES

I. INTRODUCTION

In the United States, coal-fired power plants consume over 500 million tons of coal per year. Since coal contains up to 30% noncombustible mineral matter, enormous quantities of fly ash are produced in the process (R. Carr and W. Smith, 1984c). It is therefore important to find a reliable, efficient, and inexpensive device to remove or recover the fly ash from effluent gases.

The physical and chemical properties of the produced fly ash such as density, particle shape, size distribution, chemical composition, electrical properties, etc., can vary widely depending on the type of coal used and on the plant operating conditions. One of the most important properties is the particle size, a property usually used in dust classification. Thus, particles larger than 10 microns are referred to as "coarse dust" while those smaller than one micron are called "fine dust". Because of the different behavior of these particles with respect to the gas flow, different filtration devices have to be used. In Figure 1 (Dorman, 1974) different dust pollutants are shown on the particle size scale, and the available gas cleaning equipment which can be used for each pollutant is presented. In Table 1 and Figure 2, taken from Stairmand (1965), the dust removal efficiency of different filtration devices is presented as a function of particle size. It can be seen that the coarse dust is separated efficiently by nearly all of the dust arrestors, whereas the fine dust is filtered satisfactorily only by the venturi scrubber, the bag or packed bed filter, and the electrostatic precipitator. These devices are either very expensive (electrostatic precipitator), require a large amount of energy to operate (the venturi scrubber and electrostatic

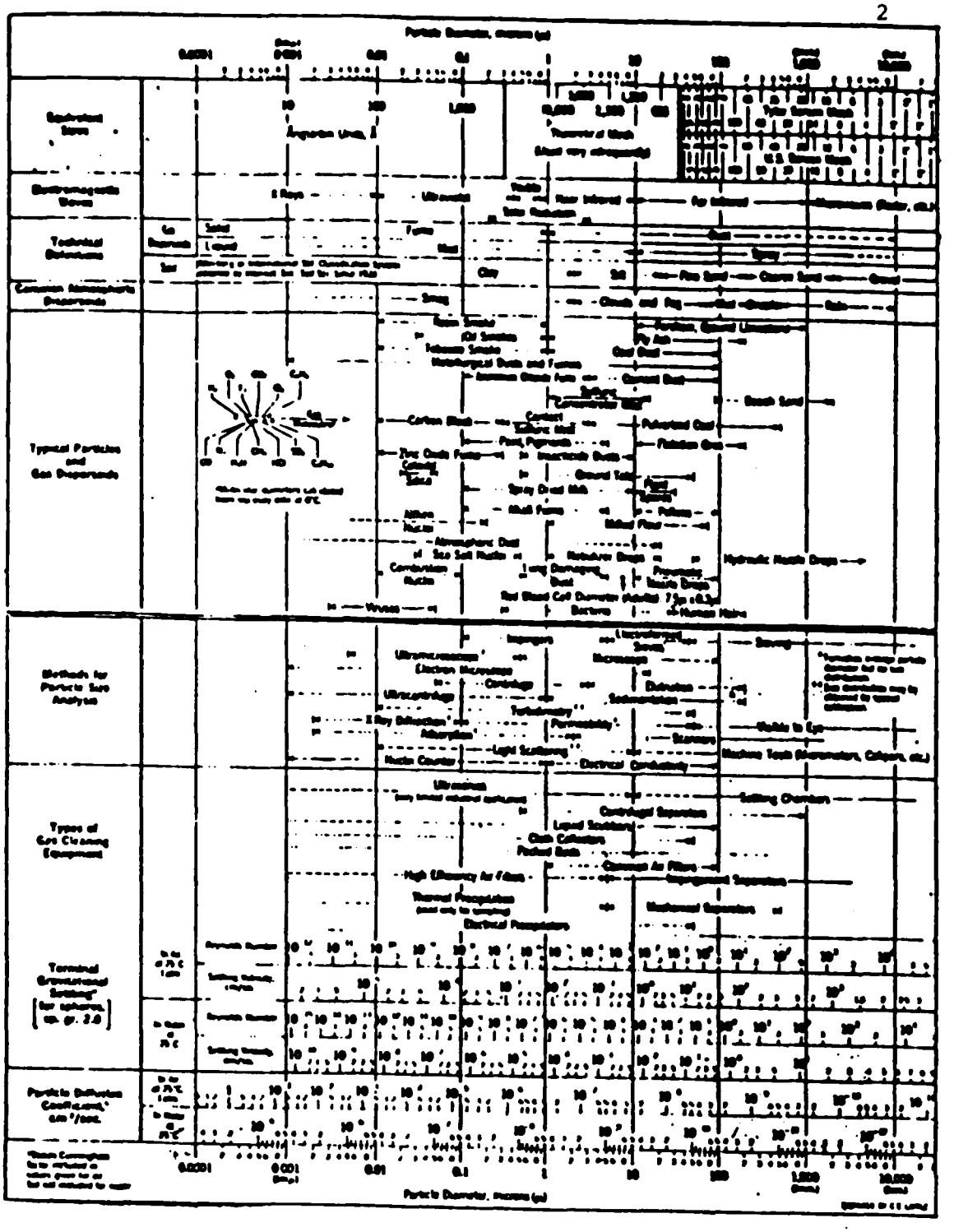

Figure 1. Characteristics of Particles and Particle Dispersoids. (Dorman 1974).

Table 1 Efficiency of Dust-arresting at Various Particle Sizes (Stairmand 1965)

Equipment	Percentage efficiency at		
	50 μ	5 μ	1 μ
Inertial collector	95	16	3
Medium-efficiency cyclone	96	27	8
Cellular cyclone	98	67	22
High-efficiency cyclone	96	73	27
Tubular cyclone	100	88	48
Jet-impingement scrubber	98	88	48
Irrigated cyclone	100	92	62
Self-induced-spray deduster	100	94	68
Spray tower	99	94	55
Fluidised-bed scrubber	> 99	98	58
Irrigated-target scrubber	100	97	80
Electrostatic precipitator	> 99	99	86
Disintegrator	100	98	91
Irrigated electrostatic precipitator	> 99	98	92
Annular-throat scrubber—low energy	100	> 99	96
Venturi-scrubber—medium energy	100	> 99	97
Annular-throat scrubber—medium energy	100	> 99	97
Venturi-scrubber—high energy	100	> 99	98
Shaker-type fabric filter	> 99	> 99	99
Low-velocity bag filter	100	> 99	99
Reverse-jet fabric filter	100	> 99	99

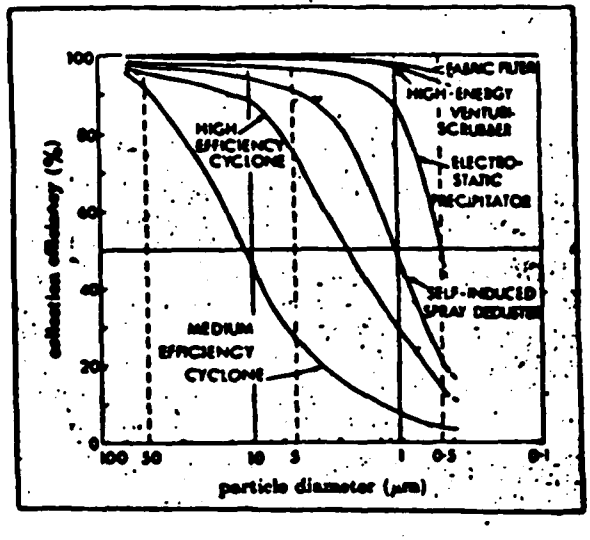

Fig. 2. Efficiencies of typical dust arrestors (Stairmand 1965)

precipitator) or quickly get clogged with dust (bag and packed bed filters). It is therefore obvious that efforts must be made to develop less expensive removal devices which can filter dust particles in the size range 0.01 - 10 μm with the filtration efficiency of a bag or packed bed filter but which do not get clogged with dust (Tardos, 1977).

Although, the continuously operating fluidized bed dust filters (Black and Boubel, 1969; Tardos et al., 1974; Krupp-Koppers, 1974) offer many advantages over other types of packed bed filters including high collection efficiency and low pressure drop, these filters have failed to gain industrial acceptance. This is mainly due to the fact that they are limited to operate at velocities no higher than 1.2 to 1.5 times the minimum fluidization velocity and, therefore, require a very large surface area to handle the high gas throughputs typically found in industrial applications. Operating at higher velocities leads to by-passing of the dusty gas in the form of bubbles, and consequently to poor collection efficiency.

To overcome the limitation of operating the fluidized bed filter at velocities of the order of the minimum fluidization velocity and achieving higher gas throughputs, Pfeffer and Hill (1978) suggested the use of a rotating fluidized bed as a filter device. In a rotating fluidized bed filter (RFBF), the drag force of the gas acting on the bed particles is balanced by the centrifugal force caused by the rotation of the bed and therefore the minimum fluidization velocity increases as the rotating speed is increased so that formation of bubbles can be avoided even at high gas flow rates. This device can therefore be utilized for the removal of fly ash in coal-fired power plants and other industrial filtering applications. The advantages of

using the RFBF are high filtration efficiency, continuous operation without clogging, and a high flow rate of gas per unit area of distributor (Gal et al., 1982; Pfeffer et al., 1986)

During the present work, a rotating fluidized bed dust filter was developed and tested. The rotating fluidized bed filter (RFBF) seems to overcome many of the problems of other granular bed filters. It can operate continuously at high gas flow rates per unit area of distributor, thus making the device relatively small with high capacity. The experimental results demonstrate the feasibility of using the RFBF to separate different industrial pollutants from a contaminated gas stream. Finally, a conceptual design of a scaled-up pilot size RFBF was given; the unit should be suitable to operate in an industrial environment to separate flue gases from a small power plant boiler, an incinerator or from a diesel engine exhaust.

The removal of small charged dust particles from a gas stream using an external electric field is common in granular and fibrous filters. Thus harzardous and/or toxic particles created in industrial processes can be separated from a gas stream by applying strong electric fields across the filter. These type of filters have been shown to be very effective in the removal of small particles in the size range between 0.1 to 2 microns. The physical phenomena in electrostatic granular and fibrous filters are similar to those in electrostatic precipitators. The advantage of the electrostatic granular and fibrous filters is the significant increase in collection surface per unit volume and the reduction in size of the devices required for a given throughput.

In the second part of this work, the influence of electrostatic effects in fibrous and granular beds to separate charged dust particles

in an electric field across the bed is studied. A theoretical model to predict the filtration efficiency of dust particles and pressure drop through the bed is developed and the theoretical results are verified by careful experiments. Furthermore, the results of experiments with charged particles are used to improve the filtration efficiency of the RFBF for fine dust particles in the size range 0.1 to 1 μm by passing the dusty gas through a corona charger placed at the entrance of the filter. Using precharged particles results in a significant enhancement of the efficiency in the RFBF without an increase in pressure drop through the device and with only a minor complication in the construction of the filter.

II. DEVELOPMENT OF THE ROTATING FLUIDIZED BED DUST FILTER

II.1. DESCRIPTION OF APPARATUS AND EXPERIMENTAL PROCEDURES

The rotating fluidized bed filter (RFBF) is essentially a vertical cylinder with porous walls which rotates around its axis of symmetry. Filter material in the form of granules is introduced into the cylinder and is forced to the wall due to the large centrifugal forces produced by the rotation. The drag force of the gas, which flows radially inward through the porous wall, acting on the bed particles is balanced by the centrifugal force. Therefore, the minimum fluidization velocity increases as the rotating speed is increased so that formation of bubbles can be avoided.

A schematic diagram of the rotating fluidized bed is shown in Figure 3 and the experimental RFBF is shown in Figure 4. The apparatus consists of a 0.2 m (7.9 in) diameter, 0.3 m (11.8 in) high distributor contained in a cylindrical plenum. The cylinder's lateral wall is perforated (43% open area) and has 456 holes each 9.5 mm (0.37 in) in diameter. The wall is covered from the inside by a 16 or a 40 mesh screen depending on the size of granules used to keep these from being thrown out of the bed by the centrifugal forces. The distributor (cylinder and screen) can be rotated at rotational speeds which can vary from 140 to 1000 RPM. This corresponds to radial accelerations of 2 to 112 g's. Room air is supplied to the plenum from a compressor which delivers to up to 500 CFM (cubic feet per minute) (14.2 m^3/min) while the flow rate is determined by a rotameter. Liquid aerosol of dioctylphtalate (DOP) is introduced into the inlet air using a Royco 258 smoke generator and particle concentration is measured using a

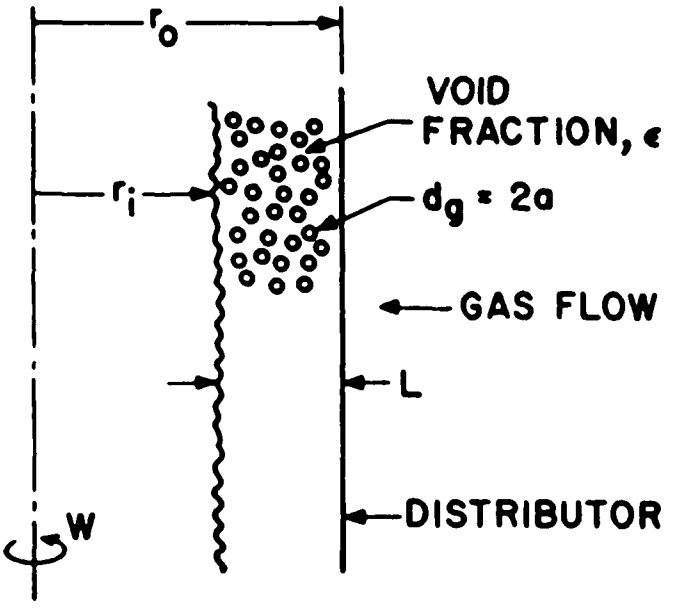

Figure 3. Schematic of a rotating fluidized bed.

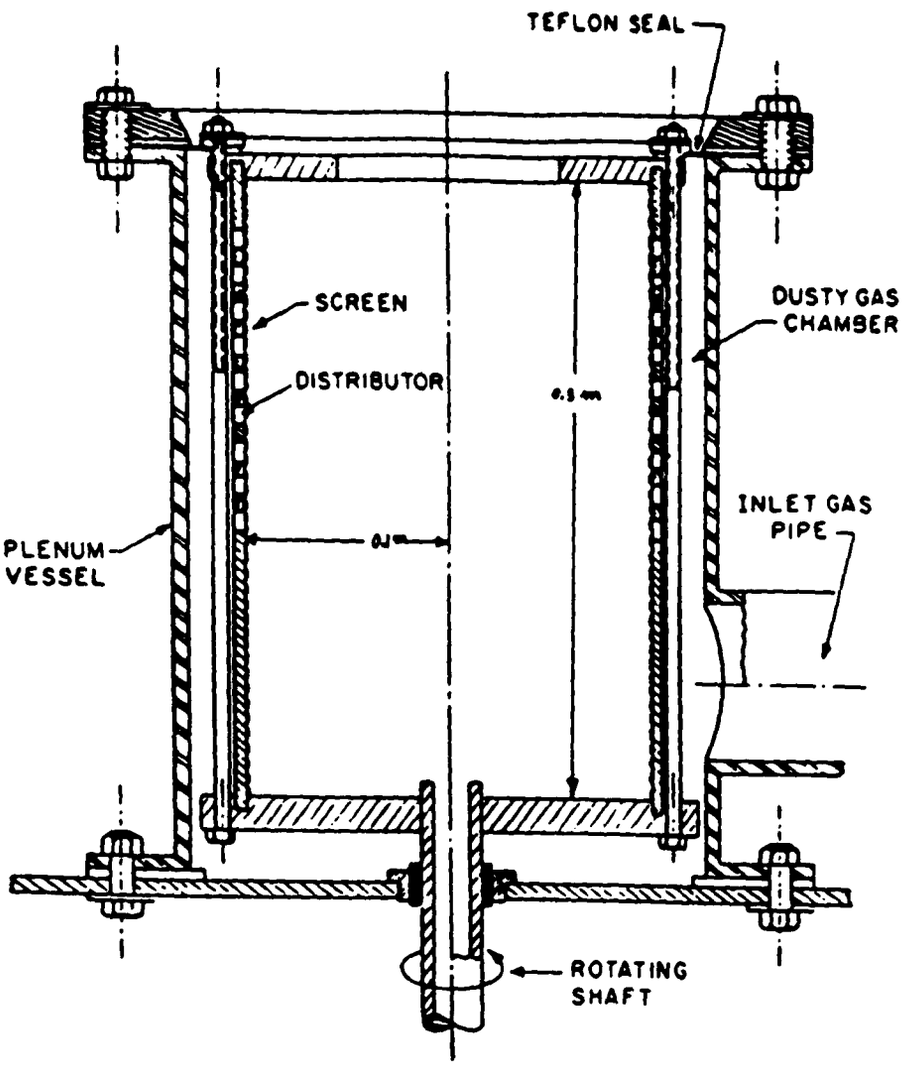

Figure 4. Experimental rotating fluidized bed filter.

Climet particle size and concentration monitoring system. Solid dust is injected pneumatically into the air stream using a generator containing a screw feeder and an ejector or a RODOS dust generator which is capable of generating solid dust to up to 1 g/m^3 (see Appendix D for details). A diesel engine exhaust is also used as a source of polluted air producing airborn carbon and ash particles.

A typical filtration experiment is carried out on the RFBF as follows:

1. A given charge of bed material or granules is loaded into the system.

2. The distributor is accelerated from rest to the desired angular velocity. The free surface of the bed assumes the shape of a paraboloid of revolution.

3. Air is turned on and it flows through the system and through the bed material while the bed starts fluidizing and particles climb up the wall, assuming a cylindrical annular shape.

4. Filtration starts with the introduction of aerosol or dust in to the air stream. The number and size of dust particles at the bed inlet and outlet are measured to obtain the bed filtration efficiency.

5. The continuously operating rotating fluidized bed system is shown in Figure 5. The granules are fed by a feeding system which includes a hopper, a screw feeder, and a source of compressed air and are removed by a discharging system which includes an adjustable baffle and an inertial separator.

6. Experiments with streams containing high concentrations of dust are performed by using both the Rodos and the DOP generators. These can produce about 50 mg/m^3 of dust. The collector granules are

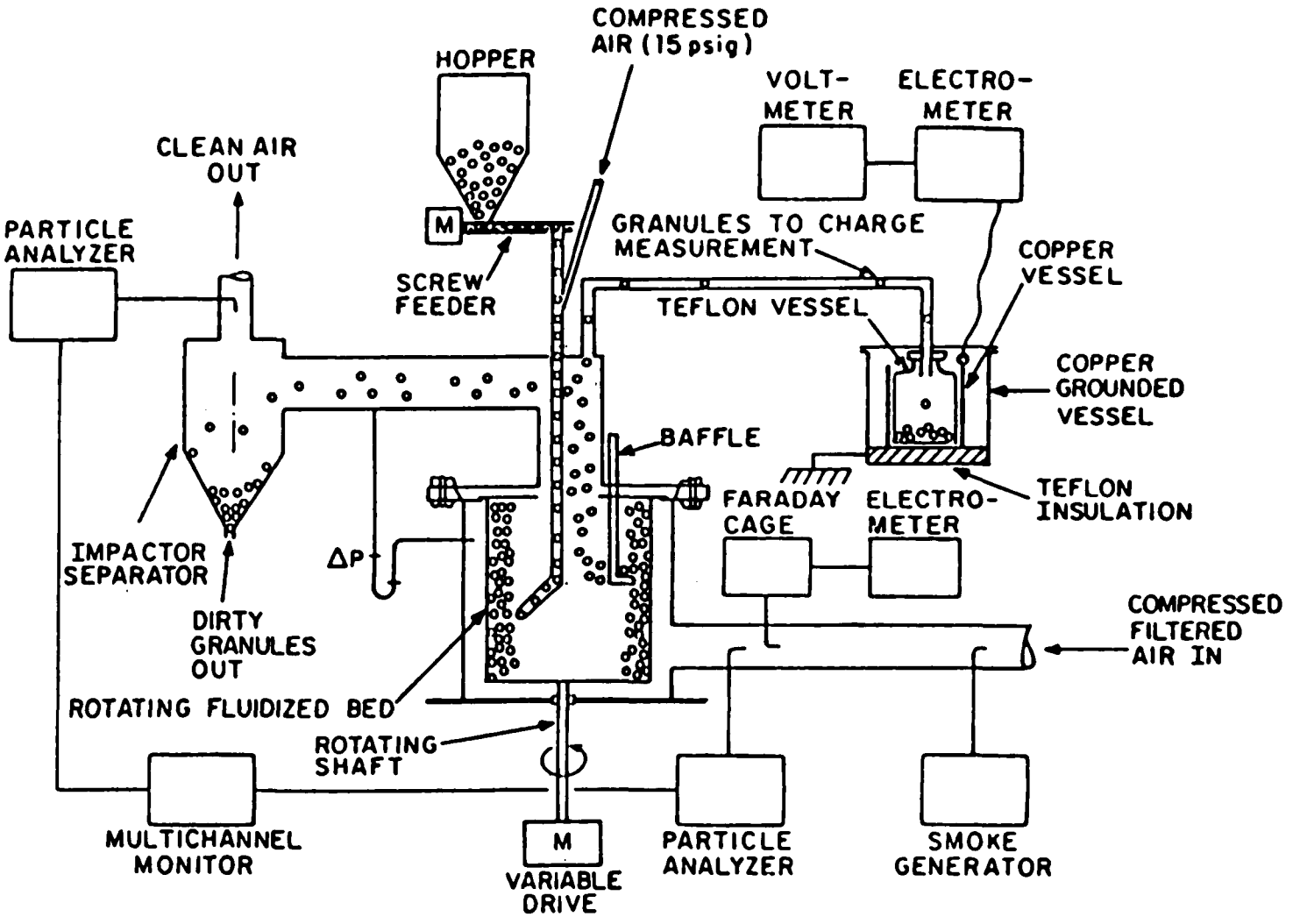

Figure 5. The rotating fluidized bed filter experimental set-up.

introduced continuously in the bed by the feeding system at a predetermined feed rate as a function of the maximum allowable dust loading on the granules inside the bed.

II.2. PRESSURE DROP AND MINIMUM FLUIDIZATION VELOCITY

The pressure drop and minimum fluidization velocity measurements described in this section were performed batch-wise with respect to the granules while the air is flowing continuously.

II.2.1. Theoretical model

When a rotating fluidized bed is operated at a high enough rotational speed, the bed assumes the shape of a cylindrical annulus (Levy et al, 1978). The pressure drop and minimum fluidization velocity in such a bed can be obtained by using the classical relationships for conventional fluidized beds by replacing the acceleration of gravity, g in these relationships by the radial acceleration, a_r produced by the rotation of the distributor. Therefore, the local pressure drop across a conventional fluidized bed is:

$$dp/dr = (1-\epsilon)\ (\rho_g-\rho_f)\ g \qquad (1)$$

where ϵ is the void fraction of the fluidized bed, ρ_g and ρ_f are the densities of the fluidized granules and of air respectively. Replacing g by the radial acceleration, a_r in equation (1) yields:

$$dp/dr = (1-\epsilon)\ (\rho_g-\rho_f)\ a_r = (1-\epsilon)\ (\rho_g-\rho_f)\ U_t^2/r \qquad (2)$$

where U_t is the local tangential velocity. Equation (2) can be integrated by assuming that the tangential velocity varies throughout the bed (U_t=Wr), which upon introduction into equation (2) gives:

$$dp/dr = (1-\epsilon)\ (\rho_g-\rho_f)\ W^2 r \qquad (3)$$

and integrating:

$$\Delta P_f = (1-\epsilon)\ (\rho_g-\rho_f)\ W^2\ (r_o^2-r_i^2)/2 \qquad (4)$$

where r_o is the radius of the bed and r_i is the radius of the inner surface of the granule bed as shown in Figure 3.

When the bed operates at packed bed conditions, the pressure drop is independent of rotation. At steady state, assuming that the gas is incompressible and that the void fraction is constant, the continuity equation for the gas phase is:

$$\frac{d}{dr}\ (rU_r) = 0 \qquad (5)$$

where U_r is the air velocity as a function of radius r. Integration of equation (5) with the assumption that the interstitial air velocity is distributed uniformly over the surface area of the bed yields:

$$rU_r = r_o U_o \qquad (6)$$

or

$$U_r = \frac{U_o r_o}{r} \qquad (7)$$

where U_o is the superficial velocity based on the outside radius, r_o. Since the drag force per unit volume of fluid is the major contribution to the momentum balance (inertial forces can be neglected), and if it is assumed to be represented by Ergun's correlation (1952), the local momentum balance for the gas phase becomes:

$$dp/dr = \phi_1 |U_r| + \phi_2 |U_r|^2 \qquad (8)$$

where:

$$\phi_1 = \frac{150\ (1-\epsilon)^2\ \mu}{\epsilon^3\ (\phi_s d_g)^2} \quad , \quad \phi_2 = \frac{1.75\ (1-\epsilon)\ \rho_f}{\epsilon^3\ \phi_s d_g} \qquad (8a)$$

The gravitational force is negligible because the radial acceleration in the rotating fluidized bed is much higher than that of gravity. In our experiments it ranges from 13 to 63 g's. Substitution of U_r in equation (7) into (8) to convert the air velocity as a function of radius to that based on the outside radius, r_o yields:

$$dp/dr = \phi_1 \left(\frac{U_o r_o}{r} \right) + \phi_2 \left(\frac{U_o r_o}{r} \right)^2 \qquad (9)$$

Integrating over the total bed thickness to account for the change in the cross-sectional area as a function of the radius, r yields (Levy and Chen, 1977):

$$\Delta P_p = \phi_1 U_o r_o \ln (r_o/r_i) + \phi_2 U_o^2 r_o^2 (1/r_i - 1/r_o) \qquad (10)$$

If the sphericity, ϕ_s in equations (8a) is not known, the correlation suggested by Wen and Yu (1966) can be used:

$$\frac{1}{\phi_s \epsilon^3} \approx 14 \qquad \text{and} \qquad \frac{(1-\epsilon)}{\phi_s^2 \epsilon^3} \approx 11$$

and thus:

$$\phi_1 = \frac{1650\ (1-\epsilon)\ \mu}{d_g^2} \quad , \quad \phi_2 = \frac{24.5\ (1-\epsilon)\ \rho_f}{d_g} \ . \qquad (8b)$$

The minimum fluidization velocity in the RFBF can be found by equating the pressure drop across the rotating fluidized bed with that across a packed bed. However, the air velocity is a function of radius, r and it decreases outwards with increasing r resulting in a reduction in fluid drag. In contrast, the centrifugal force increases with increasing r. Consequently, it is concluded that fluidization occurs layer by layer starting with the inner surface outwards as the superficial air velocity increases (Chen, 1986). The average minimum fluidization velocity, U_{mf} is found by equating the total pressure drop

across the packed bed and the fluidized bed (equations (4) and (10), respectively) to obtain:

$$\frac{U_{mf}\rho_f d_g}{\mu} = \left[\left(33.7\frac{C_2}{C_1}\right)^2 + 0.0408 \frac{\rho_f(\rho_g-\rho_f)d_g^3 W^2}{\mu^2} \frac{C_3}{C_1}\right]^{1/2} - 33.7\frac{C_2}{C_1} \qquad (11)$$

where: $C_1 = r_o^2 (1/r_i - 1/r_o)$

$C_2 = r_o \ln(r_o/r_i)$

$C_3 = (r_o^2 - r_i^2)/2.$

In addition to the average minimum fluidization velocity, U_{mf} which is also used by other investigators (Takahashi et al., 1984 and Fan et al., 1985), the surface and critical minimum fluidization velocities, U_{mf_s} and U_{mf_c} are also introduced to further explain the transition from packed to fluidized beds in the rotating fluidized bed filter. As stated earlier, fluidization in the RFBF occurs layer by layer and thus the surface minimum fluidization velocity, U_{mf_s} defined as the velocity at which the bed's inner surface first experiences fluidization is calculated by equating the local pressure drop across the fluidized bed and the packed bed (equations (3) and (9)) evaluated at $r=r_i$. This yields:

$$\frac{U_{mf_s}\rho_f d_g}{\mu}\frac{r_o}{r_i} = [(33.7)^2 + 0.0408\,\frac{\rho_f(\rho_g-\rho_f)d_g^3W^2r_i}{\mu^2}]^{1/2} - 33.7. \quad (12)$$

Similarly, the critical minimum fluidization velocity, U_{mf_c}, defined as the velocity at which the whole bed is fluidized, can be computed using equations (3) and (9) and evaluating at $r=r_o$. The result is:

$$\frac{U_{mf_c}\rho_f d_g}{\mu} = [(33.7)^2 + 0.0408\,\frac{\rho_f(\rho_g-\rho_f)d_g^3W^2r_o}{\mu^2}]^{1/2} - 33.7. \quad (13)$$

From the above definitions and experimental observations, the pressure drop across the RFBF can be divided into three stages corresponding to different air velocities. Figure 6 is a schematic diagram of the configuration of the RFBF at different air velocities. The pressure drop across the bed for the corresponding stages are determined as follows:

Stage I: $U_o \le U_{mf_s}$

Since the superficial air velocity, U_o is less than the surface minimum fluidization velocity, U_{mf_s}, the bed remains packed and the pressure drop is calculated using equation (10):

$$\Delta P_p = \phi_1 U_o r_o \ln(r_o/r_i) + \phi_2 U_o^2 r_o^2 (1/r_i - 1/r_o). \quad (14)$$

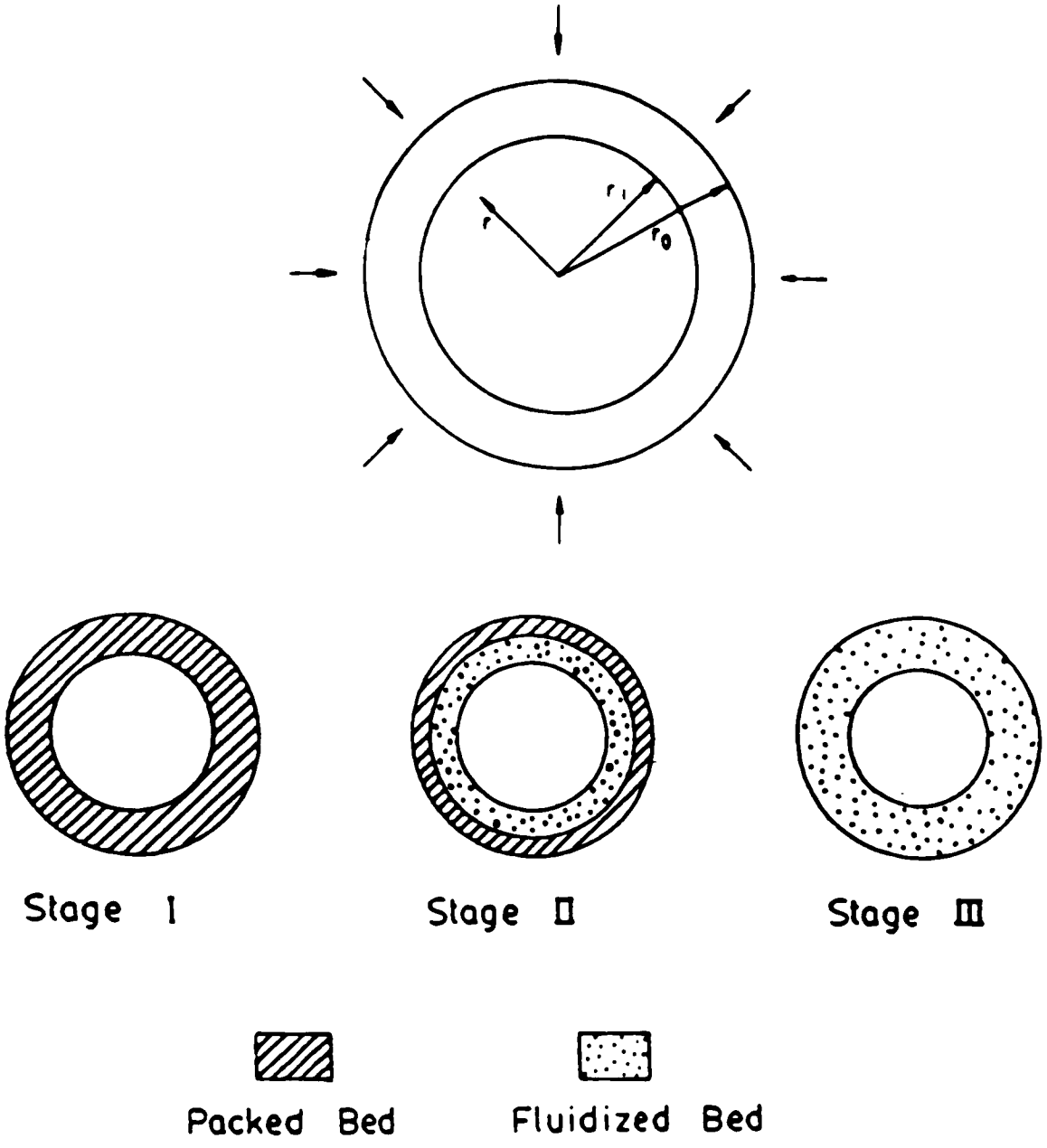

Figure 6: System configurations at different air velocities.

Stage II: $U_{mf_s} < U_o < U_{mf_c}$

For this condition, the bed is partially fluidized and the resulting pressure drop across the bed is a combination of the pressure drop across the fluidized bed and the packed bed:

$$\Delta P = \Delta P_f + \Delta P_p$$

or:

$$\Delta P = (1-\epsilon)(\rho_g-\rho_f)W^2(r_{pf}^2 - r_i^2) + \phi_1 U_o r_o \ln(r_o/r_{pf}) + \phi_2 U_o^2 r_o^2 (1/r_{pf} - 1/r_o). \quad (15)$$

where r_{pf} is the interface of the fluidized and packed beds and can be computed by equating equations (3) and (9) at a given superficial air velocity.

Stage III: $U_o \geq U_{mf_c}$

When the air velocity finally equals to or exceeds that of the critical minimum fluidization velocity, U_{mf_c}, the bed is completely fluidized and the pressure drop is calculated using equation (4):

$$\Delta P_f = (1-\epsilon)(\rho_g-\rho_f)W^2(r_o^2-r_i^2)/2 \; . \quad (16)$$

II.2.2. Results and discussion

Figure 7 shows experimental data for the pressure drop in the RFBF containing 0.3 cm in diameter polyethylene granules (ρ_g=0.932 g/cm^3) as

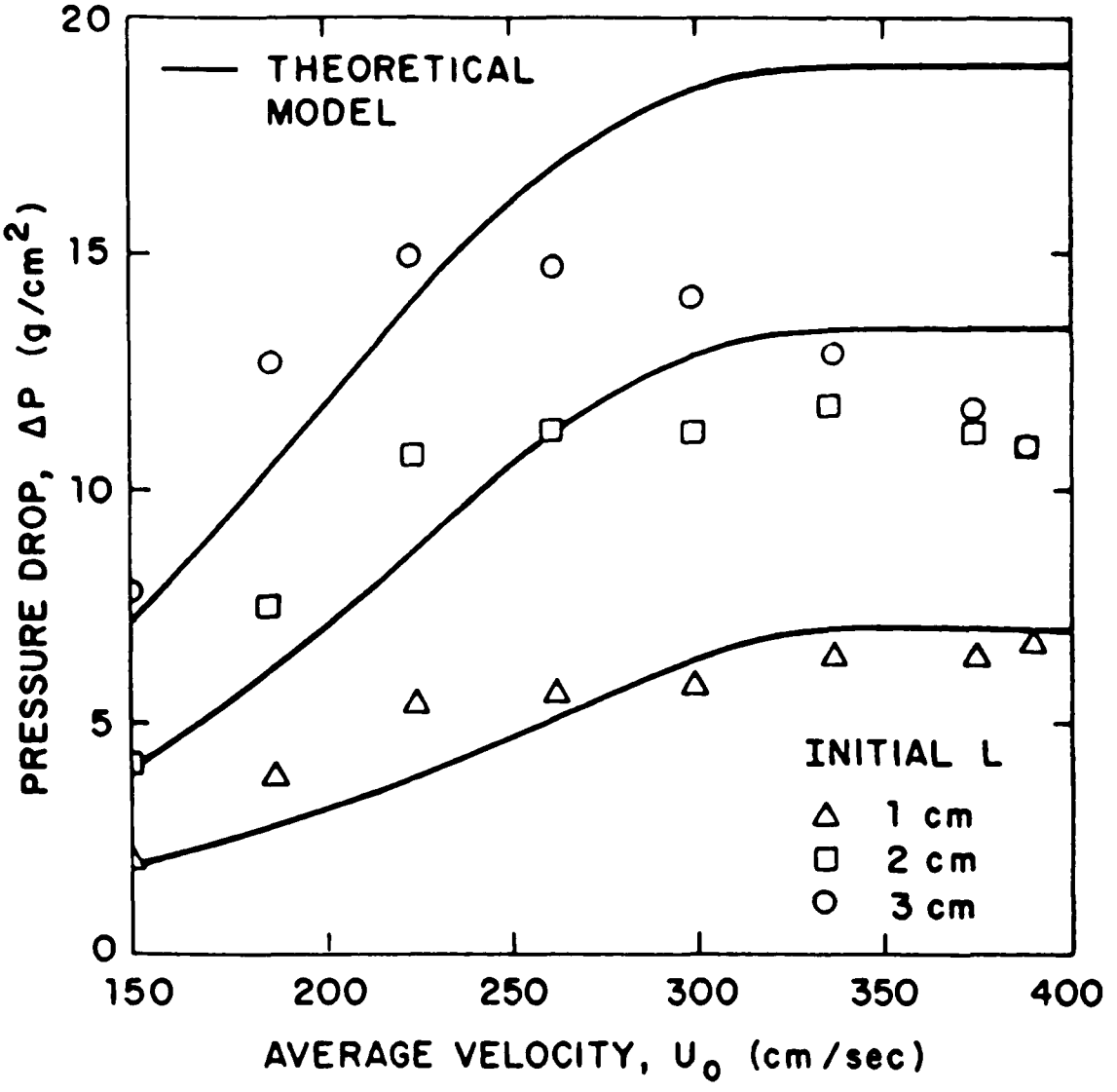

Figure 7. Pressure drop in the rotating fluidized bed for polyethylene granules as a function of air velocity for various initial bed thicknesses.
Rotating speed, W = 345 RPM;
Bed porosity, $\epsilon = 0.4$;
Granule diameter, $d_g = 0.3$ cm;
Granule density, $\rho_g = 0.932$ g/cm^3.

a function of air velocity for various bed thicknesses, as compared to the theoretical model (solid lines) assuming partial fluidization. It is seen that the model predicts the pressure drop for the 1 cm thick bed quite well but overestimates the pressure drop for the thicker beds. The reason for this is that for the 1 cm thick bed, the surface minimum fluidization velocity, U_{mf_s} is 85% that of the critical minimum fluidization velocity, U_{mf_c} (see Table 2) and since these velocities do not differ much, the drag force by the inlet air doesn't exceed the centrifugal force to carry the granules out of the bed. Thus, a completely fluidized bed is achieved as suggested by the flattening of the curve. But, for the thicker beds, the surface minimum fluidization velocity, U_{mf_s} is much lower than that of the critical fluidization velocity; from Table 2, the minimum fluidization velocity, U_{mf_s} is only 71 and 58% of the critical fluidization velocity for the 2 and 3 cm thick beds, respectively. Consequently, at the critical minimum fluidization velocity, U_{mf_c}, the drag force of the inlet air is much higher than the centrifugal force at the surface of the bed . As a result, the drag force of the air continuously carries granules at the surface out of the bed until it is balanced by the centrifugal force of the remaining granules. As shown in Figure 7, the pressure drop curve exhibits a maximum described by Takahashi et al. (1984) and Fan et al. (1985) in the fluidized bed region instead of a plateau as seen for the 1 cm thick bed because in the thicker beds the effective weight of the granules is reduced due to the loss of granules by elutriation. This is highly undesirable because a loss of granules also leads to a drop

Table 2: Minimum fluidization velocities calculated from equations (12) and (13) for various bed thicknesses.

	BED DIAMETER (cm)			
	20		60	
Bed Thickness L (cm)	U_{mf_s} (cm/s)	U_{mf_s}/U_{mf_c}	U_{mf_s} (cm/s)	U_{mf_s}/U_{mf_c}
0	335.2	1.00	592.3	1.00
1	285.5	0.85	562.7	0.95
2	238.5	0.71	533.6	0.90
3	194.5	0.58	505.0	0.85

DATA: For Polyethylene granules

$d_g = 0.3$ cm

$\rho_g = 0.932$ g/cm^3

For Air

$\mu = 1.780 \times 10^{-4}$ g/cm.sec

$\rho_f = 1.204 \times 10^{-3}$ g/cm^3

Rotating Speed, W = 345 RPM

in filtration efficiency. Furthermore, we have conducted experiments operating at the average minimum fluidizing velocity which is between the surface and the critical minimum fluidizing velocity with a bed originally loaded with black polyethylene granules continuously fed with white polyethylene granules and discharging granules from inside the bed continuously at the same rate as the feed. After a given time the bed was examined and found to contain two separate layers of granules, a white layer inside and a predominately black layer near the distributor. This experiment verifies the existence of an interface between the fluidized bed region (white granules) and the packed bed region (black granules) due to partial fluidization. Thus the phenomenon of partial fluidization is strongly dependent on the thickness of the bed and the radius of the bed. As shown in Table 2, the ratio of the surface to critical minimum fluidizing velocity drops down from 0.85 to 0.58 when the bed thickness is increased from 1 cm to 3 cm in a 10 cm bed and back to 0.85 for a 3 cm thick bed when the radius of the bed is increased to 30 cm. Therefore partial fluidization is very significant in the 3 cm thick bed (10 cm radius) but relatively unimportant in the 1 cm thick bed (10 cm radius) and in the 3 cm thick bed of radius 30 cm. This phenomenon is very important in designing a rotating fluidized bed in order to avoid the problem of non-uniformity of the bed which could lead to a drastic reduction in heat and mass transfer rates.

II.3. OPTIMUM OPERATION AND MIXING CHARACTERISTICS IN THE RFBF

II.3.1. Optimum operating conditions of the RFBF

An aerosol particle is captured in a granular bed if it collides with the granule's surface and if it sticks to it. A particulate reaches the granule's surface due to one or more filtration mechanisms which include inertia, interception, diffusion, gravity settling and electrostatic attraction. The effect of diffusion and gravitation in the RFBF is small except for particles smaller than about 1 μm in diameter where diffusion may become dominant or for very large particles where gravitation may become significant. Also, if the aerosol and granules are electrically charged, electrostatic effects may become important (see Section III and Appendix A2 for details).

Experimental and theoretical work was performed on the bench-scale size RFBF using both liquid and solid aerosols: filtration efficiency and pressure drop data were obtained under various conditions of gas velocity, rotational speed, granule size, etc. in order to determine optimal operating conditions. It was found that inertial effects are dominant under the conditions studied; a detailed description of the experiments is given in Appendix A1.

Inertia effects can be characterized by a dimensionless parameter, St (Stokes number) which is defined as

$$St = \frac{2\rho_p r_p^2 U_o C}{9\mu a} \qquad (17)$$

where ρ_p is the density of the aerosol particle, r_p is its radius, U_o is the average air velocity, C is the Cunningham correction factor, μ is the air viscosity, and a is the radius of the filter granule. Figure 8 shows the filtration efficiency of DOP and alumina dust as a

function of the Stokes number, St. Since particles smaller than 1 μm have a very low Stokes number it is clear that the low filtration efficiency observed for these small particles is due to their extreme small inertia. The apparent "tail" at the left of Figure 8 is due to the contribution of other filtration mechanisms, such as diffusion rather than inertia. Thus, the RFBF should be operated at Stokes number larger than 0.04 in order to reach at least 90% filtration efficiency. This value can be obtained by adjusting parameters in the Stokes number such as the average air velocity, aerosol and granule size, etc. A more detailed description of the above results is given in Appendix A1 and Figures A18-20.

In Figure 9, results are given for an experiment where the rotating fluidized bed filter was operated continuously with granules fed to and discharged from the system for over 3 hours using DOP aerosols. The concentration of DOP was kept constant at about 1.3×10^5 particles/liter (3.68×10^6 particles/ft^3) and granules were fed to the bed at a rate of 0.8 liter/hr (2.8×10^{-2} ft^3/hr) so that the average residence time of the granules inside the bed is about one hour. As shown in the figure, the filtration efficiency remains constant at 98-99% for aerosol particles larger than 2 μm (St=0.06). This experiment demonstrates that the RFBF can be operated continuously and at high efficiencies without mechanical problems. DOP was used during these experiments because these aerosols are used for on-site filter testing according to EPA regulations. Similar results under different operating conditions are reported in Appendix A1.

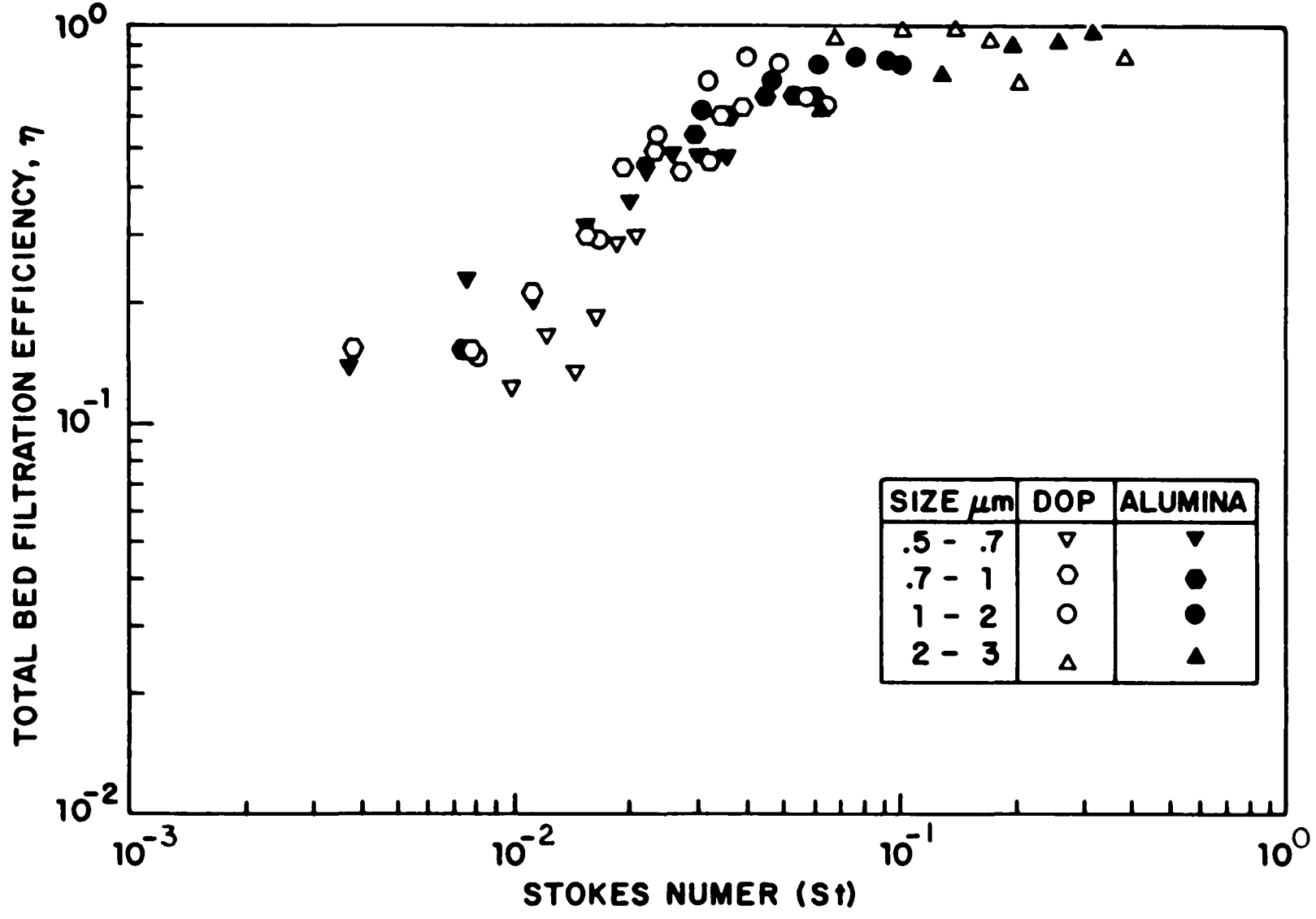

Figure 8. Total bed filtration efficiency as a function of the Stokes number for DOP aerosol and solid dust in the RFBF containing 0.3 cm diameter polyethylene granules. Bed thickness, L=3 cm; Bed porosity, ϵ=0.4; Rotating speed, W= 345 RPM; Relative humidity, RHu=45-47%.

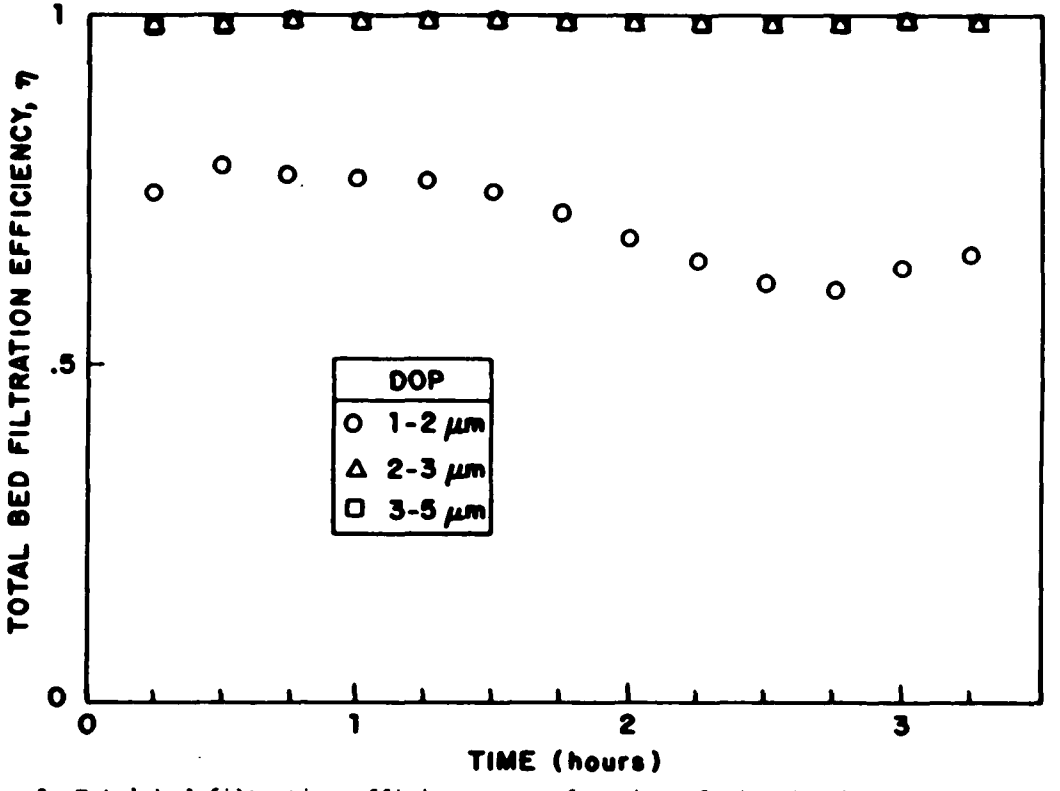

Figure 9. Total bed filtration efficiency as a function of time in the continuously operated RFBF containing 0.3 cm diameter polyethylene granules. Bed thickness, L=1.2 cm; Rotating speed, W=345 RPM; Air velocity, U_o=340 cm/sec; Feed rate of granules, $\dot{V}$=0.8 liter/hr; DOP aerosol concentration, 1.3×10^5 particles/liter.

II.3.2. Mixing and fluidization in the continuously operating RFBF

Work was also undertaken to optimize the fluidization and mixing behavior of the granules in the bed. Thorough mixing is important in continuous operation because granule removal from a poorly mixed bed can result in retention of dirty granules and elutriation of clean ones. In this work, the continuously operating rotating fluidized bed filter was used as shown in Figure 5. It is essentially the same as the batch system with the addition of a feeding and a discharge systems for the granules. The feeding system consists of a hopper, a screw feeder and a source of compressed air. The clean particles are forced pneumatically to the surface of the bed by the high pressure air stream (about 15 psig), at a rate determined by the screw feeder at the bottom of the hopper. The discharge system is composed of a baffle in the bed and an inertial separator. As the radial velocity of the gas through the granules increases above minimum fluidization, granules move towards the center of the rotating cylinder and from there out of the filter into the exit gas stream. Normally this carry-over of granules from the bed is small but can be increased by the baffle which stops the rotation of some granules. The centrifugal force on these granules drops to zero when they hit the baffle and the drag force from the inlet air can easily carry them downstream to the inertial separator where they are separated from the filtered air. The distance between the edge of the baffle and the screen on the inside surface of the rotating cylinder is adjustable and determines the thickness of the bed.

Experiments were carried out to determine the residence time distribution of the granules in the RFBF. For this purpose black polyethylene granules are first loaded into the bed and after the bed

reaches steady state at a given set of operating conditions, white polyethylene granules at a constant flow rate are fed into the RFBF. A mixture of black and white polyethylene granules are simutaneously discharged at the same rate as the feed rate by the baffle that controls the bed thickness. At each ten minute interval, a sample of granules carried out of the bed by air is collected for a period of 1 minute. Black and white polyethylene granules are then separated from each other and their respective volumes recorded.

Residence time distribution

The residence time distribution in the RFBF for a step-function input will be compared with a plug flow and a mixed flow model. The characteristics of a uniform velocity profile with no axial mixing for a plug flow model require that the residence time, τ, be a constant:

$$\tau = \frac{V}{\nu} \qquad (18)$$

where V is the volume of granules (cm^3) in the RFBF and ν is the feed rate (cm^3/min) of granules into the bed. The plug flow model which indicates that at $t < \tau$ the concentration of white granules is zero and at $t \geq \tau$, it is equal to one. For a mixed flow model, the response to a step-function input can be calculated by writing a mass balance around the RFBF. At time t, after the granules are fed into the system, mass conservation gives:

$$C_o \nu \Delta t - C_t \nu \Delta t = V \Delta C_t \qquad (19)$$

where C_o is the concentration of granules in the feed which is 100%, C_t is the effluent concentration of granules at time t, ΔC_t is the change in concentration during Δt and V is the volume of granules in the bed. Dividing equation (19) by Δt and taking the limit as $\Delta t \rightarrow 0$ yields:

$$dC_t/dt = \frac{\nu(C_o - C_t)}{V} = \frac{(C_o - C_t)}{\tau} \quad . \qquad (20)$$

With the initial condition $C_t = 0$ at $t \leq 0$, the solution to equation (20) is:

$$(C_t/C_o) = 1 - e^{(-t/\tau)} \quad . \qquad (21)$$

The broken lines in Figures 10-12 represent the mixed flow model and the solid lines the plug flow model; as discussed earlier, complete fluidization in the RFBF can only be achieved at air velocities above the critical minimum fluidization velocity, U_{mf_c} due to the fact that the RFBF is fluidized layer by layer. The residence time distribution (RTD) curves at U_{mf_c} for bed thicknesses of 0.9, 1.0 and 1.9 cm and for white polyethylene granules feed rate of 5.4, 120 and 55 cm^3/min (0.011, 0.25, 0.12 ft^3/hr), respectively, are shown in Figures 10, 11 and 12. All experimental data points lie close to the mixed flow model (broken line) for both very short average residence times, τ, of 5 minutes and less (Figure 11) as well as for long average residence times of 100 minutes and longer (Figure 10). It was found

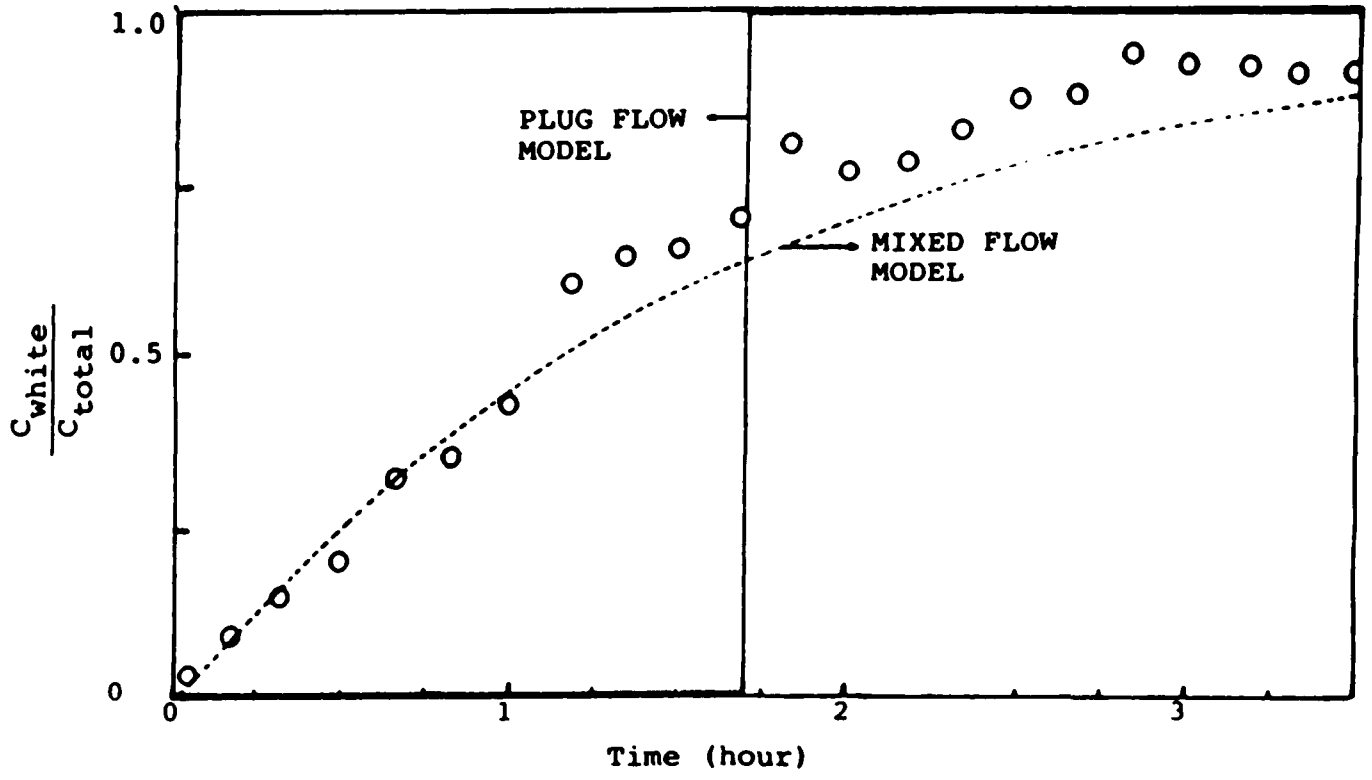

Figure 10. Residence time distribution in the RFBF with bed thickness, L = 0.9 cm, feed rate of granules (white polyethylene granules), $\mathcal{V}$ = 5.4 cm^3/min, average velocity, U_o = 340 cm/sec, rotating speed, W = 345 RPM.

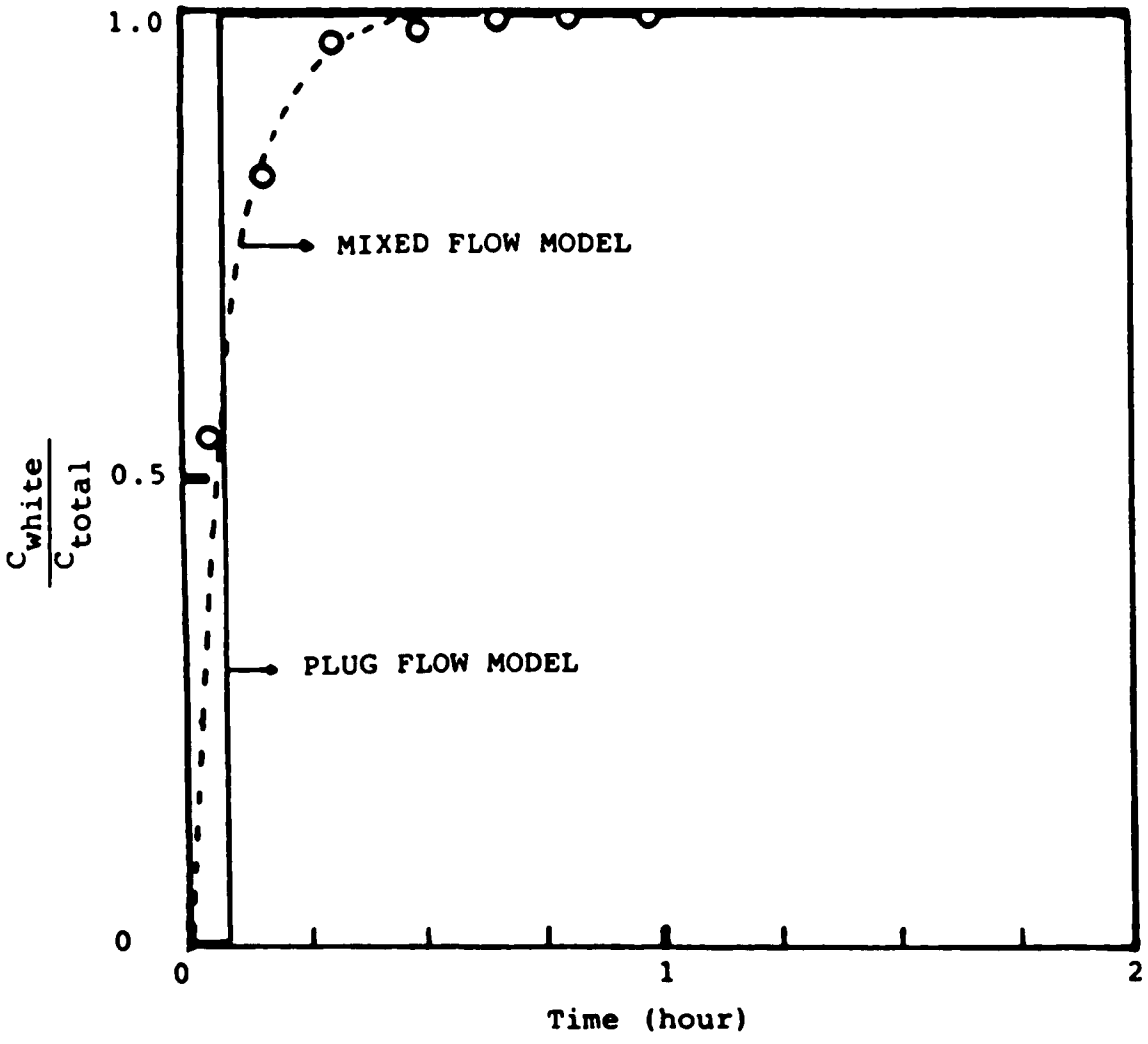

Figure 11. Residence time distribution in the RFBF with bed thickness, L = 1 cm, feed rate of granules (white polyethylene granules), $\dot{V}$ = 120 cm^3/min, average velocity, U_o = 340 cm/sec, rotating speed, W = 345 RPM.

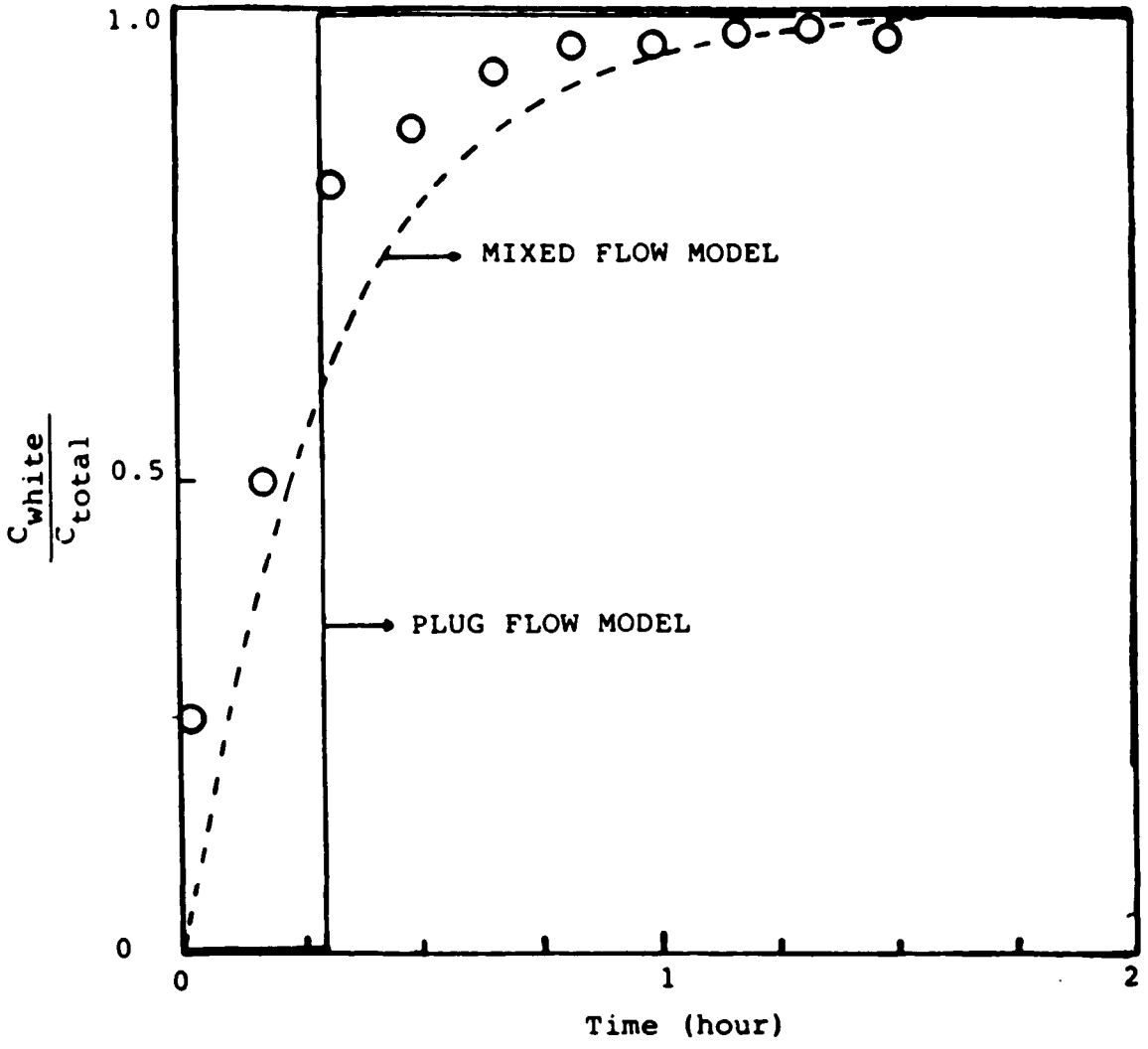

Figure 12 Residence time distribution in the RFBF with bed thickness, L = 1.9 cm, feed rate of granules (white polyethylene granules), $\mathcal{V}$ = 55 cm^3/min, average velocity, U_o = 340 cm/sec, rotating speed, W = 345 RPM.

that the final composition of granules (black and white polyethylene granules) in the bed did not correspond to the composition of the last collected sample in the above experiments. However, in a continuously operating mixed flow model the composition of granules at the exit and inside the bed should be the same. This indicates that there is a dead volume in the bed. In fact, this volume defined as the difference between the volume of the original black polyethylene granules remaining in the bed and the volume at the exit, was 11, 8 and 11% for the 0.9, 1.0 and 1.9 cm thick beds, respectively.

Since all experiments are carried out at U_{mf_c}, one would expect that there should be a complete mixing in the bed and consequently the dead volume should be minimum or non-existent. The presence of the dead volume implies, however, one or both of the following possibilities: a) by-passing of the white granules fed into the bed directly to the exit due to the construction of the present experimental set-up. From Figure 5, it is seen that incoming granules being fed into the bed can easily hit the baffle and be carried out by the drag force of the inlet air. b) the polyethylene granules in the bed experience a low degree of mixing.

Figure 13 shows the residence time distribution for a 1.3 cm (solid hexagons) and a 0.6 cm thick bed (empty circles) operating at a gas velocity equal to the surface minimum fluidization velocity, U_{mf_s} (packed bed region) and 25% over critical minimum fluidization velocity, U_{mf_c}, respectively. At packed bed conditions, the by-passing of white granules is quite pronounced as shown by the steeper rise in the RTD curve (solid hexagons). This by-passing is not only due to the

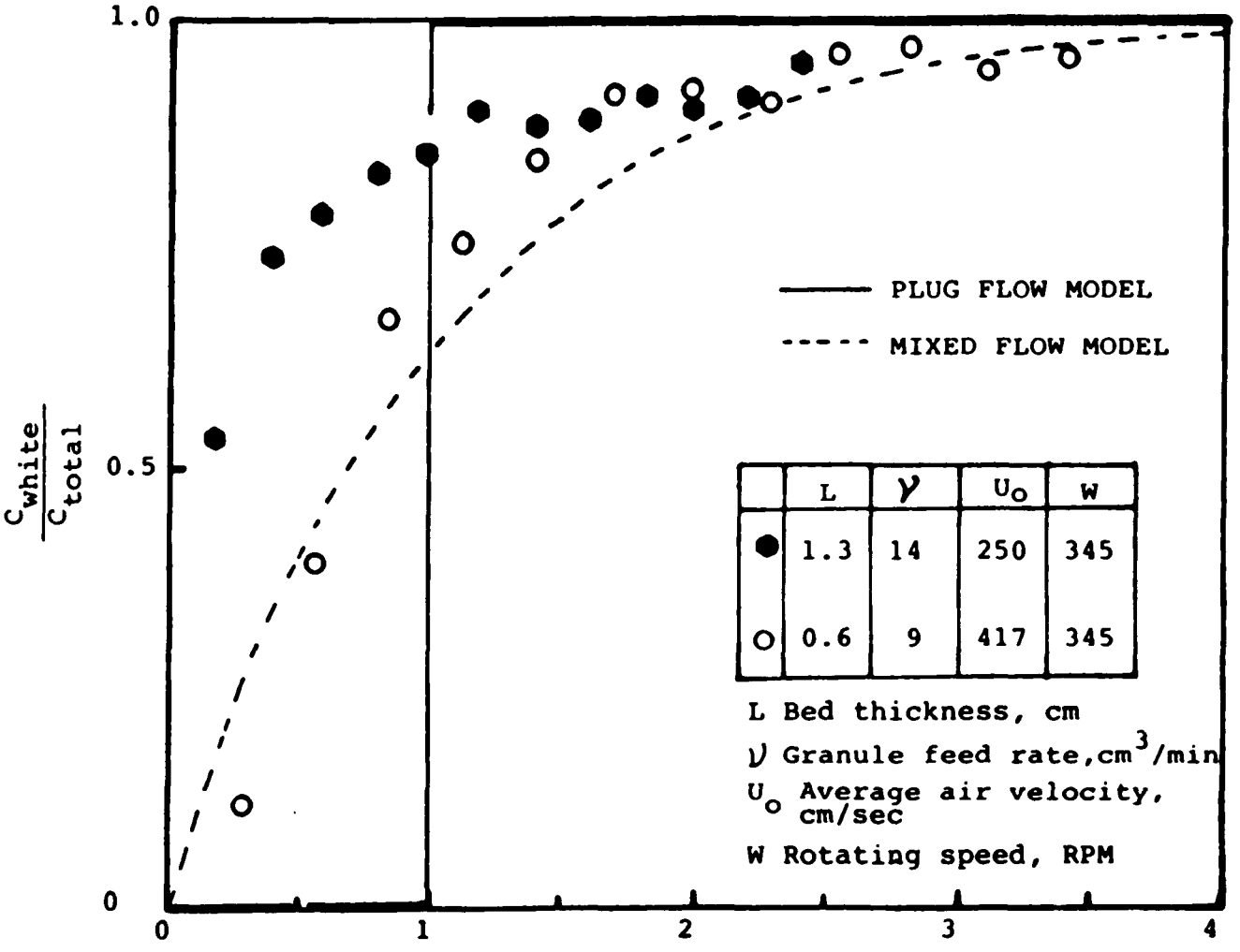

	L	ν	U_o	W
●	1.3	14	250	345
○	0.6	9	417	345

Figure 13. Residence time distribution in the RFBF at different air velocities where τ is the average residence time (V/ν).

experimental set-up but also depends on the bed's operating conditions. Since the bed is operated in the packed bed region, the original black polyethylene granules are packed against the cylinder wall and thus greatly lower the probability for black polyethylene granules at the bed's surface to interchange positions with the incoming white granules. The consequence is that white granules from the feed will tend to hit the baffle more often and are instantly carried out of the bed. This corresponds to a plug flow model at zero or a very short residence time. The dead volume at this operating condition is 20% as compared to 10% when the bed is operated at 25% above the critical minimum fluidization velocity, U_{mf_c} (empty circles); for this condition, the experimental data lie much closer to the mixed flow model. This is expected because at velocities higher than U_{mf_c}, the granules are freely suspended in the bed and uniformly distributed along the bed's surface thus creating a better interchange between black and white granules.

Using a stroboscope, the motion of certain granules near the cylinder wall in the operating bed was observed for up to ten minutes and found that they hardly moved with respect to the neighboring granules. It is known that fluidization is always accompanied by uniform mixing in a conventional fluidized bed (Figure 14a) because a velocity profile exists in such a bed due to the no-slip boundary condition at the wall. Consequently, the granules are well mixed in a conventional bed. Figure 14b shows the present experimental set-up where it can be seen that fluidization occurs with granules being suspended but limited mixing occurs because the air velocity is uniformly distributed around the cylinder's wall. Thus, interchanging

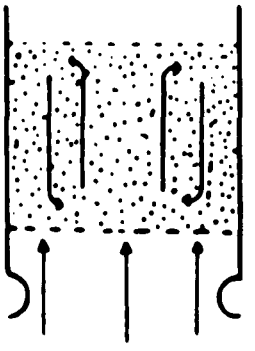

a) Conventional fluidized bed

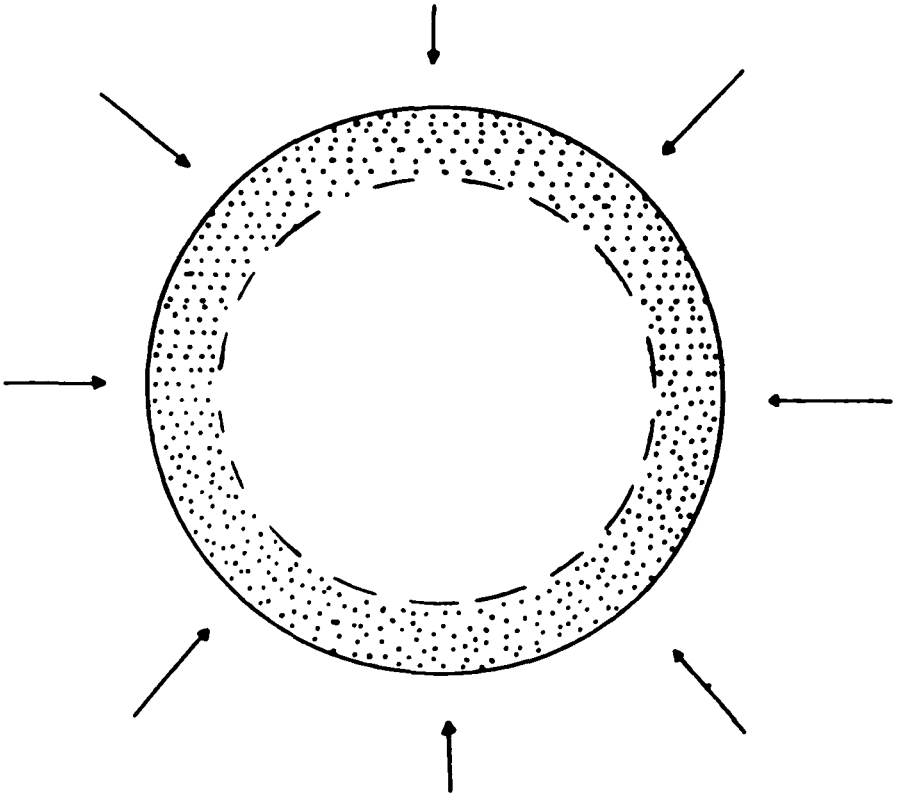

b) Rotating fluidized bed

Figure 14. Flow pattern of a conventional fluidized bed (a) and a rotating fluidized bed (b).

of positions between granules occurs only due to the granules' free motion which results in the existence of a dead volume even at high air velocities. To eliminate the dead volume, a more uniform mixing in the rotating fluidized bed filter, as exhibited in the conventional fluidized bed, can be created by the introduction of fixed baffles into the bed. These baffles will not only create better mixing but also, distribute the air velocity throughout the bed more uniformly depending on their geometric configurations. The design of such baffles is given in Section II.5.

II.4. EXPERIMENTS WITH HIGH CONCENTRATION DUSTS-RESULTS AND DISCUSSION

In this section, experiments are reported where the RFBF was tested with airborne fly ash at high dust concentrations. The purpose of these experiments was to demonstrate the feasibility of operation of the RFBF with fly ash collected from the electrostatic precipitator of a municipal incinerator.

II.4.1. Experiments with high concentration dusts

Using the Rodos feeder (see Appendix E for details), it was possible to generate about 50 mg of fly ash per cubic meter of air flowing through the RFBF which is about 50 to 100 times higher than the aerosol concentration used previously as generated by the home-built unit. However, the concentration of fly ash generated is still below the accepted industrial standard.

At high dust concentrations, the dust loading on the filtering granules becomes an important factor in the operation of the RFBF. In order to separate high concentration dusts in the RFBF at a high filtration efficiency, granules must be kept relatively clean. The

ability to predict granule dust loading allows for the estimation of the saturation time of the granules which, in turn, determines the residence time of the granules in the bed.

The theoretical calculation to determine dust loading assumes that the dust particles are spherical and will cover the granule's surface with only one layer. The dust loading, L_{load}, is defined as the ratio of the weight of dust on the granule's surface to the weight of the granule itself:

$$L_{load} = \frac{W_p}{W_g} \qquad (22)$$

where W_p is the weight of the dust particles and W_g is the weight of the granule. W_p and W_g are given as:

$$W_p = \frac{4}{3}\pi\alpha[(a + d_d)^3 - a^3]\rho_p \quad \text{and} \quad W_g = \frac{4}{3}\pi a^3 \rho_g \qquad (23)$$

where α is the volume fraction of the dust particles in the granule's surface layer and can be taken as 0.6, a is the radius of the granule, d_p is the dust particle diameter taken to be the average diameter for all sizes, and ρ_p and ρ_g are the densities of the dust particles and granules, respectively. Substituting the expressions for W_p and W_g in equation (23) into (22), yields:

$$L_{load} = 0.6 \left[\frac{(a+d_p)^3 - a^3}{a^3} \right] \frac{\rho_p}{\rho_g} . \qquad (24)$$

Calculated values of the maximum dust loading, L_{load} of fly ash on various granules of different sizes per kilogram of granules are given in Table 3.

Experiments to confirm the degree of accuracy for the computed dust loading were performed by operating the RFBF batch-wise until saturation was reached (when the filtration efficiency of fly ash of all sizes dropped to zero). A saturated sample of granules from the bed was then weighed and washed. After drying, the sample is weighed again to determine by difference the weight of dust deposited on the granules. All experimental data are within 33% of the dust loading, L_{load} predicted by equation (24) as seen in Table 3.

Based on the bed thickness, the granule's density, the dust loading, the concentration of dust in the gas stream and the gas flow rate, the saturation time of granules is given as:

$$t_{sat} = \frac{V_g \rho_g L_{load}}{F_{dust} Q_{gas}} \qquad (25)$$

where V_g is the volume of granules in the bed, F_{dust} is the amount of dust in the gas stream (mass/volume) and Q_{gas} is the volumetric flow rate of the gas.

In order to maintain a constant filtration efficiency in a continuously operating RFBF, it is desirable to replace the dirty

Table 3: Maximum dust loading on different granules.

Granules	Theoretical Values*	Experimental Values*
Glass Beads (d_g = 0.10 cm)	1.8	2.2
Porcelain (d_g = 0.20 cm)	2.8	3.7
Polyethylene (d_g = 0.30 cm)	3.8	2.7

* Unit: g of fly ash/Kg of granules

granules in the bed with clean ones before the granules are completely saturated with dust particles. Therefore, the residence time, τ should be no more than 80% of the saturation time

$$\tau = 0.8\ t_{sat} \qquad (26)$$

which requires the granules feed rate, ν to be:

$$\nu = \frac{F_{dust} Q_{gas}}{0.8\alpha\rho_g L_{load}}. \qquad (27)$$

Using typical numbers based on our existing unit and those measured in Table 3, equation (27) predicts that ν is about 7 liters of granules per hour which indicates that the bed's inventory of granules has to be replaced about every 15 min.

It is clear from the above that due to the high dust concentrations, it is desirable to add a prefilter to capture particles larger than 2 μm before they enter into the bed so that the saturation time of the granules is increased and the granule feed rate reduced. For this purpose, a fine 400 mesh screen (37 μm opening) was placed on the outside the cylindrical distributor of the bed. The filtration efficiency of the RFBF for DOP aerosols has been studied using only the screen and a combination of the screen and a 2 cm (0.8 in) thick bed containing 0.1 cm diameter glass beads. As shown in Figure 15, for DOP larger than 2 μm, the efficiency of the RFBF when using the screen only (solid triangles) is almost equal to that when glass beads are present (empty triangles). It remains at or above 90% for the entire range of air velocities studied. However, for smaller aerosols, the combination

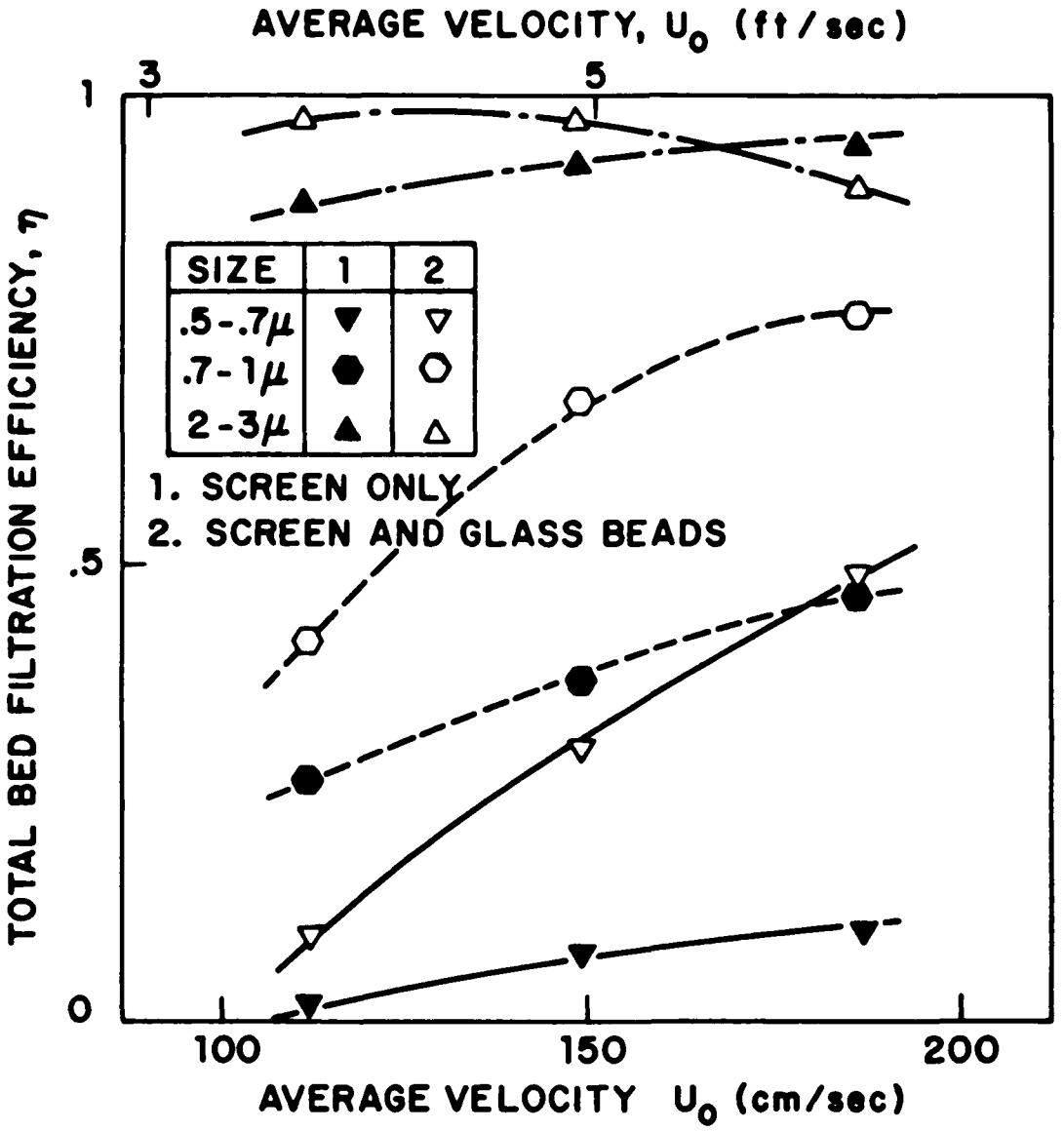

Figure 15. Total bed filtration efficiency as a function of air velocity for DOP aerosols in a RFBF containing 0.1 cm diameter glass beads and a very fine 400 mesh screen (37 microns in opening) around the cylinder. Bed thickness, L=2 cm (glass beads), relative humidity, RHu=18-30%.

of screen and glass beads improves the filtration efficiency significantly. For example, at an air velocity of 150 cm/sec (5 ft/sec), the efficiency of the RFBF for 0.5-0.7 μm and 0.7-1.0 μm particles when using only the screen is 7% (solid inverted triangle) and 38% (solid hexagon), respectively, as compared to 30% (empty inverted triangle) and 67% (empty hexagon) when using the combination of screen and glass beads. Thus, the screen acting as a prefilter removes most of the aerosols larger than 2 μm and the glass beads will provide filtration surfaces for the smaller aerosols. It is advantageous, therefore, to operate the bed with a prefilter and granules inside to improve the efficiency and to extend the saturation time of the granules.

In order to obtain a further understanding of the characteristics of the screen, the filtration efficiency of the RFBF for fly ash using only the screen as a function of time was studied and the results are shown in Figure 16. For the 2-3 μm dust particles, the efficiency remains above 80% and for the 3-5 μm dust particles above 90% during the entire experimental run. However, after the bed is operated for about 20 min., the pressure drop across the bed begins to increase significantly as a result of deposited fly ash on the screen which is gradually building up into a cake. The increase in pressure drop is undesirable in the RFBF but since it has been shown that the use of the prefilter (the screen) is quite effective in enhancing the filtration efficiency for larger particles, the installation of a brush on the outside of the cylinder and along the height of the bed to continuously scrape off the cake is proposed. This will prevent cake formation and the resulting increase in pressure drop.

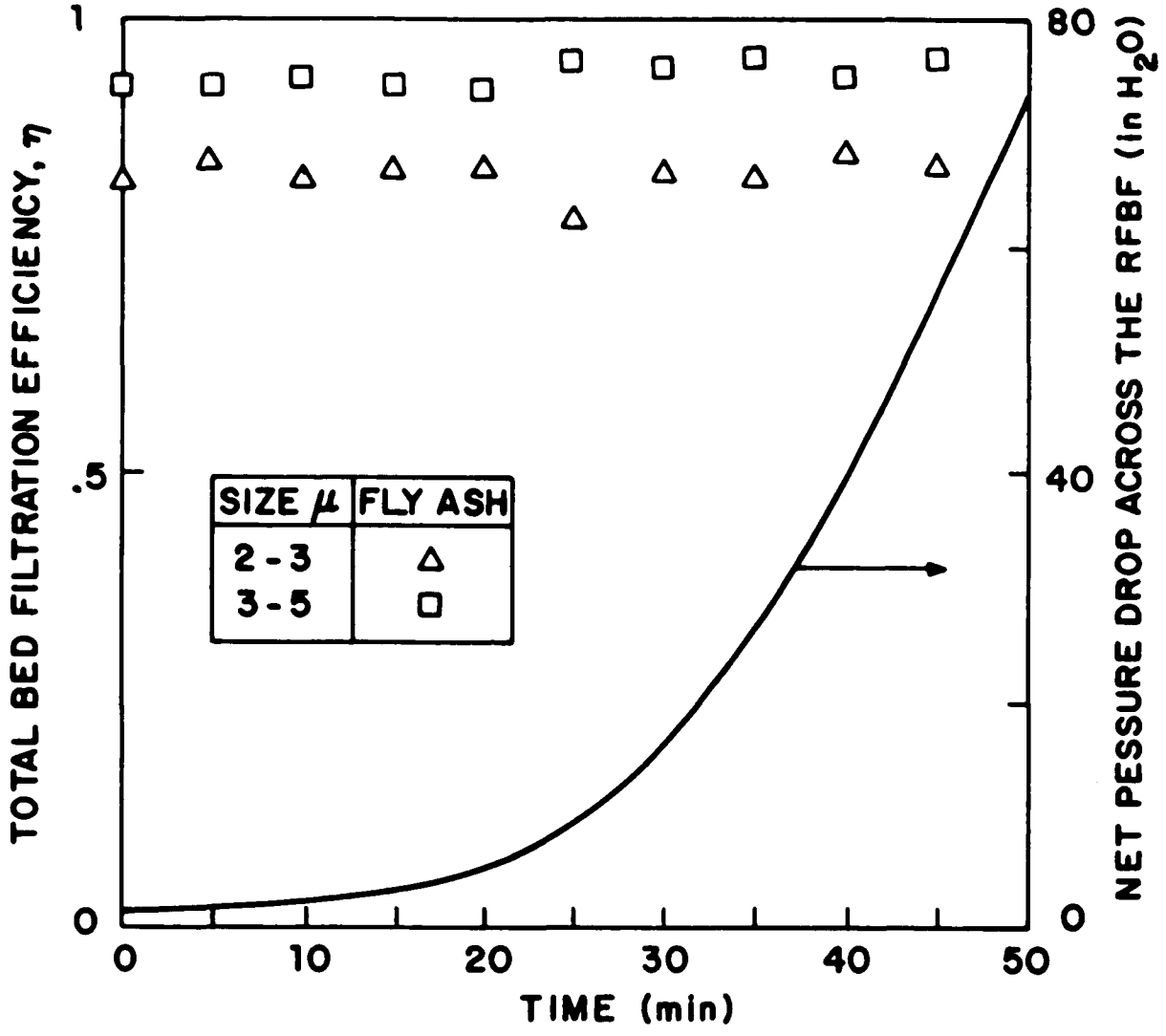

Figure 16. Total bed filtration efficiency as a function of time in the RFBF with screen outside the cylinder (no granules inside) and the pressure drop through the bed at rotating speed, W=140 RPM, average velocity, U_o=150 cm/sec (5 ft/sec), relative humidity, RHu=0%.

II.4.2. Continuous operation of RFBF and granule recirculation

The continuously operating rotating fluidized bed with glass beads for fly ash removal at high concentrations was studied with and without the prefilter. The results given in Figure 17 were obtained with the bed operated continuously for 35 minutes under fluidization conditions with the prefilter (400 mesh screen) and the granules present. The concentration of fly ash was kept constant at about 50 mg/m^3 and glass beads were fed to the bed at a rate of 12 liter/hr (0.4 ft^3/hr) so that the average residence time of the granules inside the bed was about 10 minutes. At the end of the run the pressure drop across the bed was around 30 inches of water and the filtration efficiency for particles larger than 2 μm (St=0.03) was stable at about 90%.

In a separate experiment, the bed was operated with and without the prefilter to investigate the contribution of the prefilter while a high concentration of fly ash was being filtered. As seen in Figure 18 (cycles and triangles), the filtration efficiency increases by about 20 to 40% when the prefilter is present. The prefilter also helps to remove large particles from the inlet stream and prolong the saturation time of the granules inside the bed since the efficiency for particles larger than about 3 μm is practically 100%. Also shown in the figure are some data taken at a higher air temperature. The inlet gas stream temperature was raised to 110 ^{o}F by disconnecting the cooling system of the air supply. As seen, the filtration efficiency stayed constant at about 85% when the temperature increased from 70 ^{o}F to 110 ^{o}F.

During continuous operation of the RFBF, it is necessary to remove dirty granules from the bed, clean them and recycle them into the bed. For this purpose, a three phase fluidized bed was constructed as shown

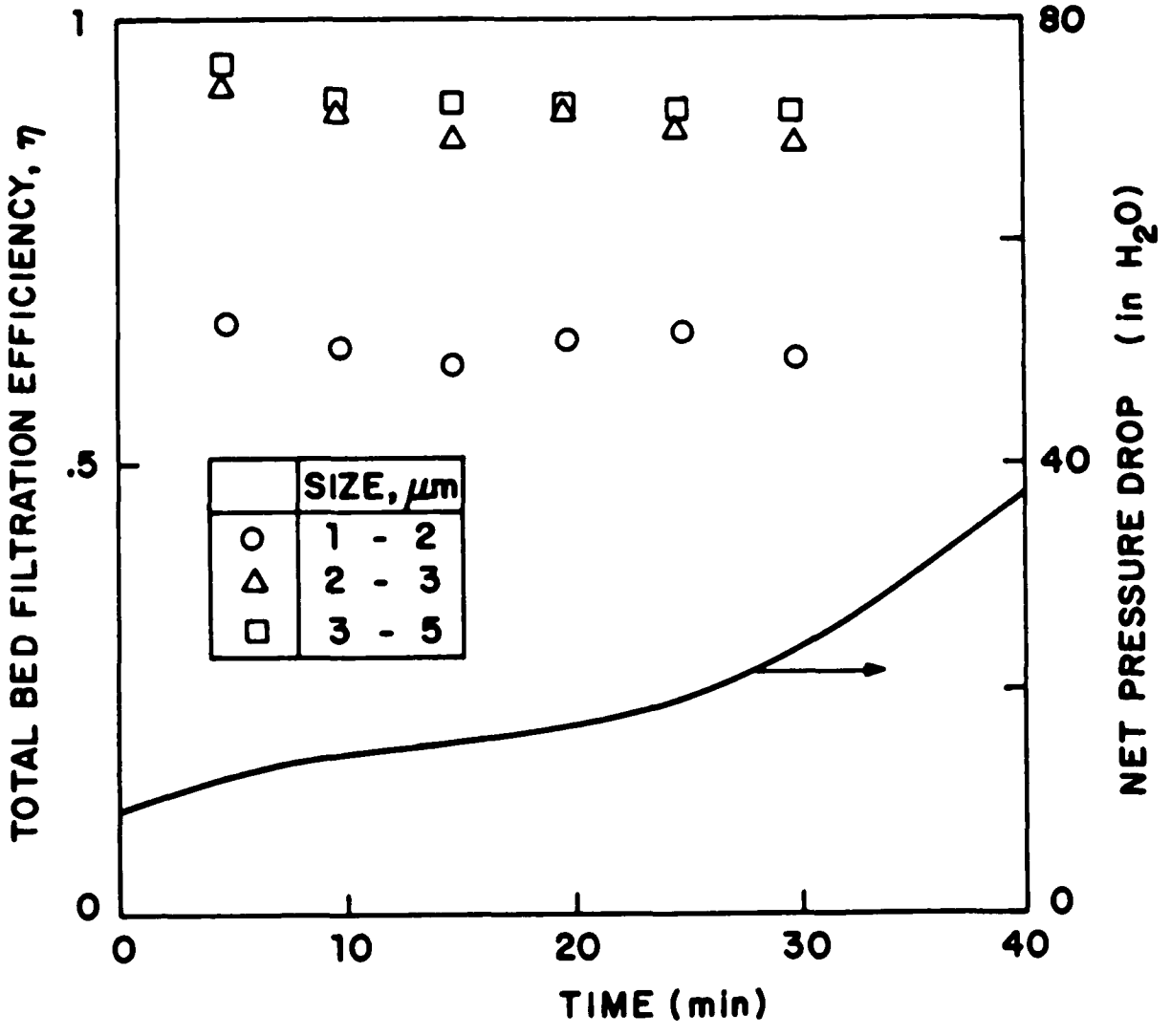

Figure 17. Total bed filtration efficiency of the RFBF as a function of time in the continuously operating RFBF containing 0.15 cm diameter glass beads. Bed thickness, L=3 cm; Rotating speed, W=220 RPM; Air velocity, U_o=180 cm/sec (6 fl/sec); Average residence time, $\bar{\tau}$=10 min; Fly ash concentration, 50 mg/m^3; Relative humidity, RHu=22%.

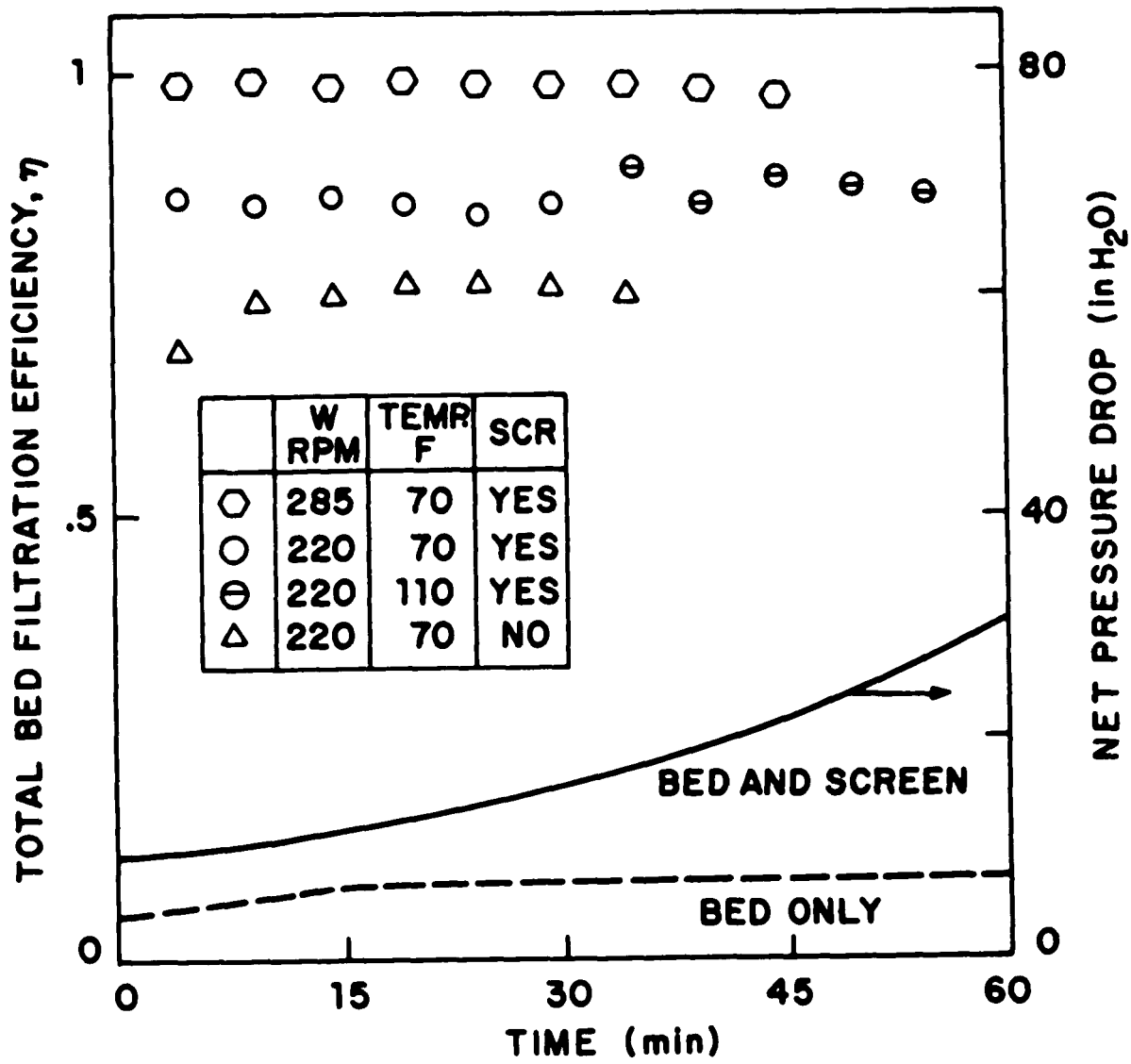

Figure 18. Total bed filtration efficiency of the RFBF as a function of time in the continuously operating RFBF containing 0.15 cm diameter glass beads. Bed thickness, L=3 cm; Air velocity, U_o=150 cm/sec (5 ft/sec); Average residence time, $\bar{\tau}$=10 min; Fly ash concentration, 50 mg/m^3; Dust particle size, d_p=2-3 μm.

in Figure 19. Dry clean air is introduced from the bottom of the bed through a distributor while water is introduced from the top through a spray nozzle. The contaminated water is subsequently drained and the washed granules are dried by the air flow. Figure 20 shows the dust loading on 0.15 cm diameter glass beads as a function of washing time. The experimental work was carried out batchwise following these steps:

1) Dirty granules were loaded into the bed and water was added to cover the whole bed.
2) Air flow rate was adjusted to fluidize the bed.
3) Dirty water was drained from the bed after 10 minutes.
4) Samples were taken for dust loading measurements.

The dust loading on the samples after each batch shows an exponential decay. The dust loading drops from the saturation value of 2.4 g/kg to 0.15 g/kg in about 10 cycles (100 min). After being washed, the granules are dried in air and then transported to the feeding hopper for reuse.

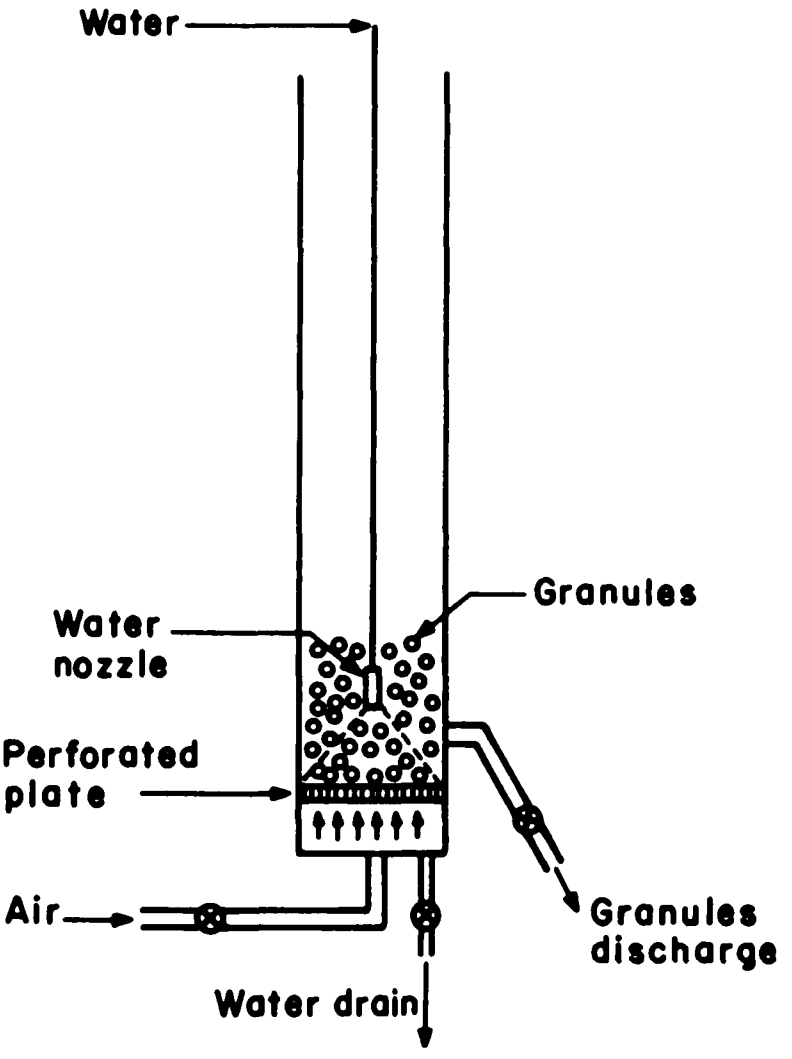

Figure 19. The three phase fluidized bed.

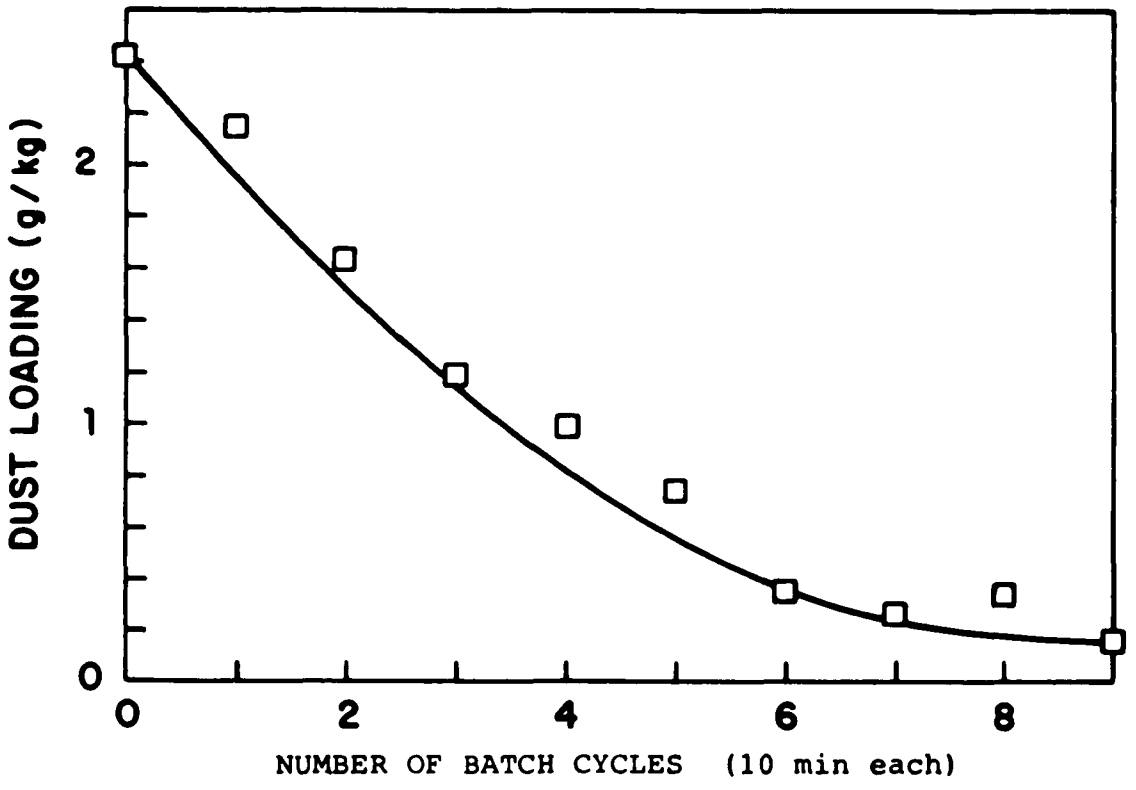

Figure 20. Dust loading of 1.5 mm glass granules in a three phase fluidized bed as a function of batchwise washing operation with water in dry air.

II.5. ECONOMIC EVALUATION AND THE PILOT SIZE RFBF

II.5.1. Economic comparsion of the RFBF with other filters

A comparison of the RFBF, baghouse filters (BF), and electrostatic precipitators (EP) is shown in Table 4. Data are taken from Carr and Smith, 1984a,b; Oglesby and Nichols, 1978; Pontius et al., 1984; Reynolds et al., 1983; White, 1963 and from data given in the previous section. As seen from the table all three devices show similar collection efficiencies for comparable dust particle sizes separated. Furthermore, the RFBF and the EP can be operated in a high temperature (1,000 ^{o}F) environment. The most significant difference among the three devices is the specific gas flow rate, i.e., the capacity of handling gas throughputs per unit surface area of filter. The value of the specific air flow rate of the RFBF is about 100 times larger than that of the EP and BF. Therefore, the required size of the RFBF is relatively very small. Compared with the EP and BF for handling 4,000 CFM (113 m^3/min) air, the RFBF needs only one small cylindrical distributor 2 ft (60 cm) high and 2 ft (60 cm) diameter while the BF needs 40 large tubes 20 ft (6.1 m) high and 8 in (20 cm) diameter and the EP needs 16 large plates 20 ft (6.1 m) high and 3 ft (91 cm) wide.

The RFBF also has the advantages of continuous operation and ease of cleaning over the other two devices. Although the pressure drop of the RFBF is higher than that of the BF and the EP, it can be kept constant (without increasing) during continuous operation by removing dirty granules and adding clean ones and by using the brush to clean the cake formed on the prefilter. Furthermore, the continuous operation with respect to granules and the maintenance of the RFBF does

Table 4: Comparison of the Rotating Fluidized Bed Filter with a Baghouse and an Electrostatic Precipitator

Filter Items	Rotating Fluidized Bed Filter	Baghouse	Electrostatic Precipitator
Dust Particle Size (μ)	above 1 μ	0.1 - 100 μ	0.1 - 200 μ
Collection Efficiency (%)	80 - 99.9	99.9 (Well-maintained Units)	80 - 99
Operating Temperature (^{o}F)	Limited by seals to 400 - 1,000	250 - 350	Up to 1,200
Specific Air Flow Rate (CFM/ft^2)	300	1.6 - 3	~4
Space Requirement for 4,000 CFM	1 cylinder 2 ft high/ 2 ft diameter	40 tubes 20 ft high/ 8 in diameter each	16 plates 20 ft high/ 3 ft wide each
Pressure Drop (cm H_2O)	50 - 70	10 - 15 (Initial, then increases with time)	~3
Operation	Continuous Operation	Batch (Stop for cleaning)	Continuous Operation
Cleaning	Fluidization: continuously fed and removed granules	Reverse gas or shaked/ cleaning	Periodic impact or rapping
Life (yrs)	Not known	2 - 3 (per bag)	20 - 30 (precipitator)
Operation and Maintenance Problems	Not known	Pressure drop, bag fly ash handling system	Particle resistivity, gas flow, corrosion

Table 4 (cont.)

Operating Cost (Power) [KW / 10.000 CFM]	2	Not known	0.5 - 1.5
Capital Cost ($/KW)	Not known	54 (Air-to-cloth ratio of 2)	35 (Specific collection area = 250)

not, at this point, appear to be a problem at temperatures up to 500 ^{o}F.

In addition, a detailed economic evaluation of the RFBF was performed by Prof. A. Squires from Virginia Polytechnic Institute and State University (Squires, 1987). Based on the data obtained previously during the present study, Prof. Squires provided a conceptual design of a RFBF for a coal-fired electricity station delivering 250 megawatts (electric). It shows that the RFBF may provide a means for significantly reducing the cost of fly ash removal at a coal-fired station.

Prof. Squires also points out that the most important advantage of the RFBF is its small "footprint." For a fully developed design of the RFBF, it may require on the order of one-tenth of the land area of an electrostatic precipitator or high-velocity fabric filter. A disadvantage is that the RFBF has a relatively high pressure drop compared to a precipitator and correspondingly high fan power. Nevertheless, the additional cost of the power does not seem to overcome the probable capital cost advantage that the RFBF appears to enjoy.

II.5.2. Conceptual design of the pilot size RFBF

In the design of the pilot size RFBF, Figure 21 shows that four fixed baffles will be introduced in the bed. These baffles will not only create better mixing but also, distribute the air throughout the bed more uniformly depending on their geometric configuration (see Section II.3.2). As seen in Figure 21, the rotating cylinder is divided into four equal sections where the air flow rate to each is one quarter of the total air flow rate, Q. If h is the height of the cylinder, the cross sectional area in each section is:

$$A(r) = hr\theta \qquad (28)$$

and the air velocity through the bed, U(r) is:

$$U(r) = \frac{Q}{4hr\theta} . \qquad (29)$$

The local pressure drop across a packed bed is:

$$dp/dr = \phi_1 U(r) + \phi_2 (U(r))^2 \qquad (30)$$

$$\phi_1 = \frac{1650\ (1-\epsilon)\ \mu}{d_g^2} \quad \text{and} \quad \phi_2 = \frac{24.5\ (1-\epsilon)\ \rho_f}{d_g} \qquad (31)$$

where the first term in equation (30) represents the viscous losses and the second, the kinetic energy losses. Substitution of the expression for U(r) in equation (29) into (30), yields:

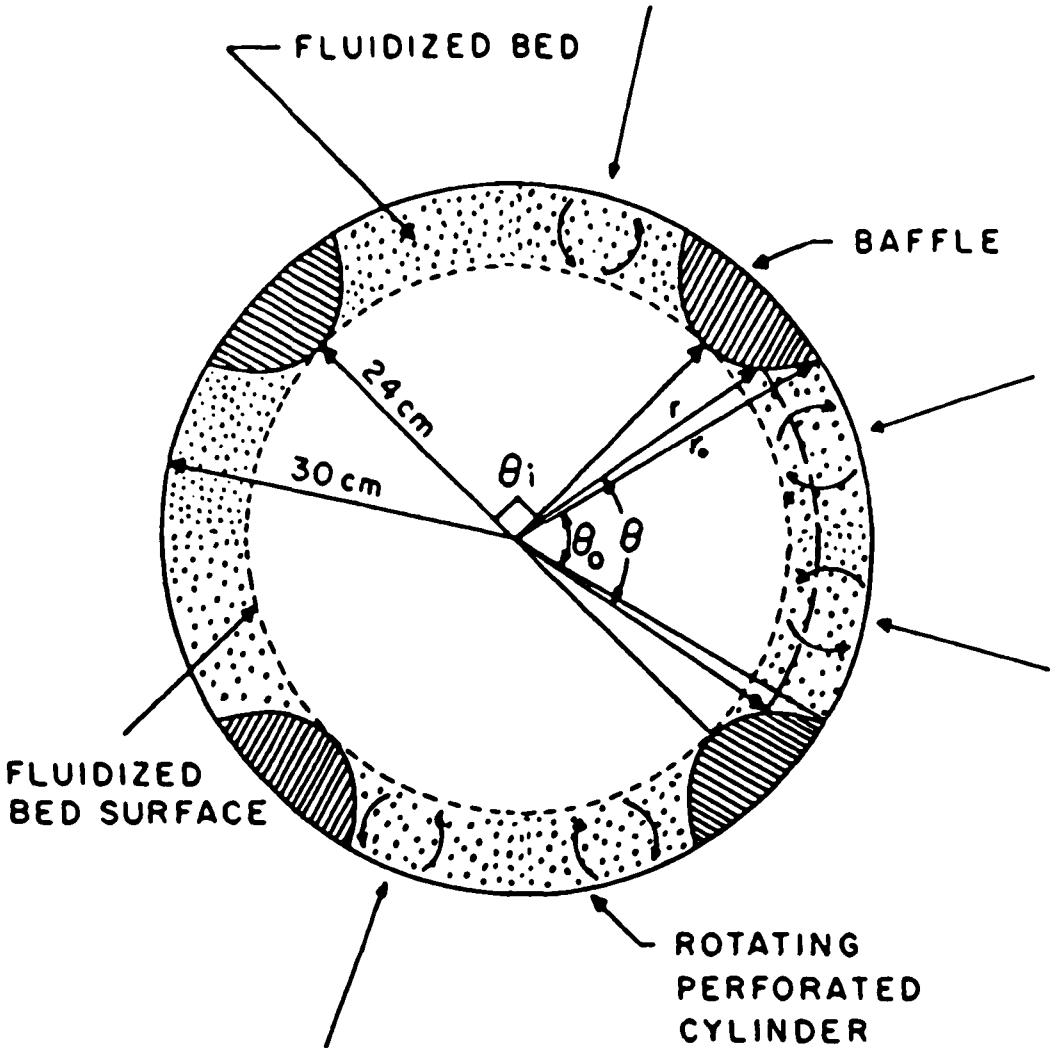

Figure 21. Proposed baffle design for the pilot size rotating fluidized bed filter. Top view.

$$dp/dr = \frac{\psi_1}{r\theta} + \frac{\psi_2}{(r\theta)^2} \qquad (32)$$

$$\psi_1 = \frac{1650(1-\epsilon)\mu Q}{4hd_g^2} \quad \text{and} \quad \psi_2 = \frac{24.5(1-\epsilon)\rho_f Q^2}{16h^2 d_g}. \qquad (33)$$

The local pressure drop across a fluidized bed, as given is:

$$dp/dr = (1-\epsilon)\,(\rho_g-\rho_f)\,W^2 r = \psi_3 r \qquad (34)$$

where

$$\psi_3 = (1-\epsilon)(\rho_g-\rho_f)W^2. \qquad (35)$$

At minimum fluidization, the local pressure drop in equations (32) and (34) is equal so that:

$$\frac{\psi_1}{r\theta} + \frac{\psi_2}{r^2\theta^2} = \psi_3 r. \qquad (36)$$

At low granule's Reynolds number, $Re_g \to 0$ ($Re_g = \frac{d_g \rho_f U_o}{\mu}$), the viscous losses dominate and equation (36) can be simplified to:

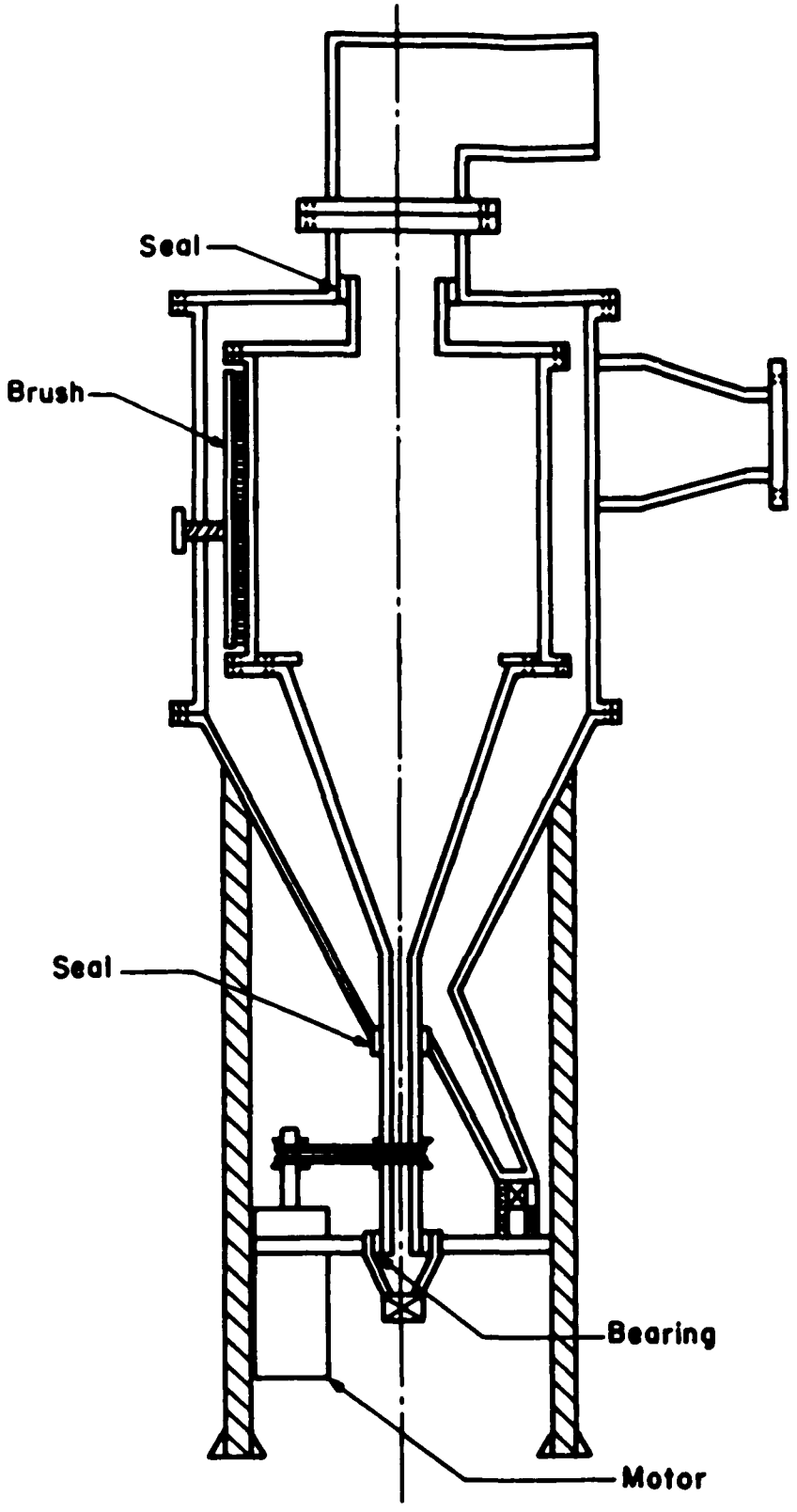

Figure 22. Conceptual design of the pilot size rotating fluidized bed filter. Side view.

$$\frac{\psi_1}{r\theta} = \psi_3 r \qquad (37)$$

so that

$$\frac{\theta}{\theta_o} = \left(\frac{r_o}{r}\right)^2 \qquad (38)$$

and at high granule's Reynolds number, $Re_g \rightarrow \infty$, the kinetic energy losses become dominant and the equation can be simplified to

$$\frac{\psi_2}{r^2\theta^2} = \psi_3 r \qquad (39)$$

so that

$$\frac{\theta}{\theta_o} = \left(\frac{r_o}{r}\right)^{1.5}. \qquad (40)$$

The fluidization in the RFBF will be accompanied by uniform mixing if the ratio between the radii as suggested by equation (38) for low Reynolds number, or equation (40) for high Reynolds number is used. In a rotating fluidized bed filter with a 60 cm (2.0 ft) diameter (r_o= 30 cm), a maximum bed thickness, L of 6 cm (r_i= 24 cm) and an opening angle of θ_i (at r_i= 24 cm) = 90^o, about 36% of the distributor will be

blocked (θ_o=58°) at $Re_g \rightarrow 0$. In contrast, at $Re_g \rightarrow \infty$ only 28% of the distributor will be blocked (θ_o=65°). Thus, it would be more difficult to control the RFBF when it is operated with small granules because the granule's Reynolds number, Re_g is small and the distributor will not allow high gas throughputs. At high Reynolds number, however, the 60 cm bed is easy to control and operate. Earlier (see Section II.3.2), it was stated that the proposed 60 cm diameter bed would alleviate the elutriation problem for the thicker bed because the air velocity through the bed is distributed uniformly. With the addition of the baffles, one provides not only a more uniform distribution of air velocity across the bed (because the cross sectional area of the bed is now more or less uniform depending on the angle θ) but also eliminates the dead volume which presently exists in the experimental RFBF.

An overall conceptual design of the scaled-up pilot size RFBF based on the results obtained to date and taking into account the above considerations is shown in Figure 22. The rotating cylinder is located in a cyclone which functions as a housing for the filter and will separate aerosol particles larger than about 10 μm. The rotating cylinder is supported inside the cyclone by two high temperature seals on the top and the bottom which can handle temperatures up to 500 °F and a specially constructed bearing at the bottom of the rotating shaft to support the weight of the cylinder as shown in Figure 22.

The rotating element is made out of a metal cylinder with holes to serve as the air distributor. The thickness of the granular bed inside the cylinder will be controlled by a circular ring located at the

bottom of the cylinder and supported by the conical section. The excess granules will fall down through the hollow shaft due to gravity forces. The granules, will then be collected at the bottom of the cyclone through a control valve. The rotating speed of the bed will be controlled by an adjustable speed motor and a set of pully and belts. A 400 mesh fine wire screen is placed outside the cylinder to serve as a prefilter to separate particles between 3 to 10 μm. An adjustable brush is used to remove the cake formed on the screen in order to keep the pressure drop across the system almost constant. The granule feeding system is similar to the one presently used and is based on an airlock to maintain a constant rate of feed.

The rotating cylinder inside the cyclone will be 60 cm (2 ft) high and 60 cm (2 ft) in diameter. This unit will handle an air flow rate of up to 4,000 CFM (113 m^3/min) as shown in Table 4 and, with a 6 cm (2.4 in) thick bed for particle collection should yield up to 99% efficiency for all aerosol particles larger than about 1 μm.

For a typical coal fired power plant, the boiler outlet contains high quantities of fly ash with sizes ranging from 0.05 to 20 microns as shown in Figure 23a. Among these particles, 92% of fly ash is larger than 2 μm and there is a very small amount of particles, about 1-2%, smaller than 1 μm (McElroy et al., 1982). Using the efficiency curve of the pilot size RFBF based on data recalculated from Figure 15 as shown in Figure 23a, the overall filtration efficiency of the bed can be computed from the equation

$$\eta_{overall} = \int_0^\infty \eta(d_p) M(d_p) dd_p \qquad (41)$$

where $\eta(d_p)$ is the filtration efficiency corresponding to the respective particle size and $M(d_p)$ is the particle size distribution at the boiler outlet. From equation (41), the overall filtration efficiency of the pilot size RFBF is determined to be about 97% for all particle sizes from 0.05 to 20 microns. The total amount of dust captured by the cyclone and the prefilter before the stream enters the granular bed is about 93%. Therefore, only about 4% of the dust particles are captured by the granules; these particles are mostly below 3 microns. Assuming that the concentration of fly ash from the boiler outlet is 1 g/m^3, the granules circulation rate in the RFBF can be computed from equation (27); for the pilot size RFBF which handles 4,000 CFM air this equals 1.7 liter per minute or 183 kg/hr of glass beads. At corresponding higher fly ash concentrations but identical dust particle size distributions the circulation rate will be proportionally higher.

a) Efficiency VS Fly ash size

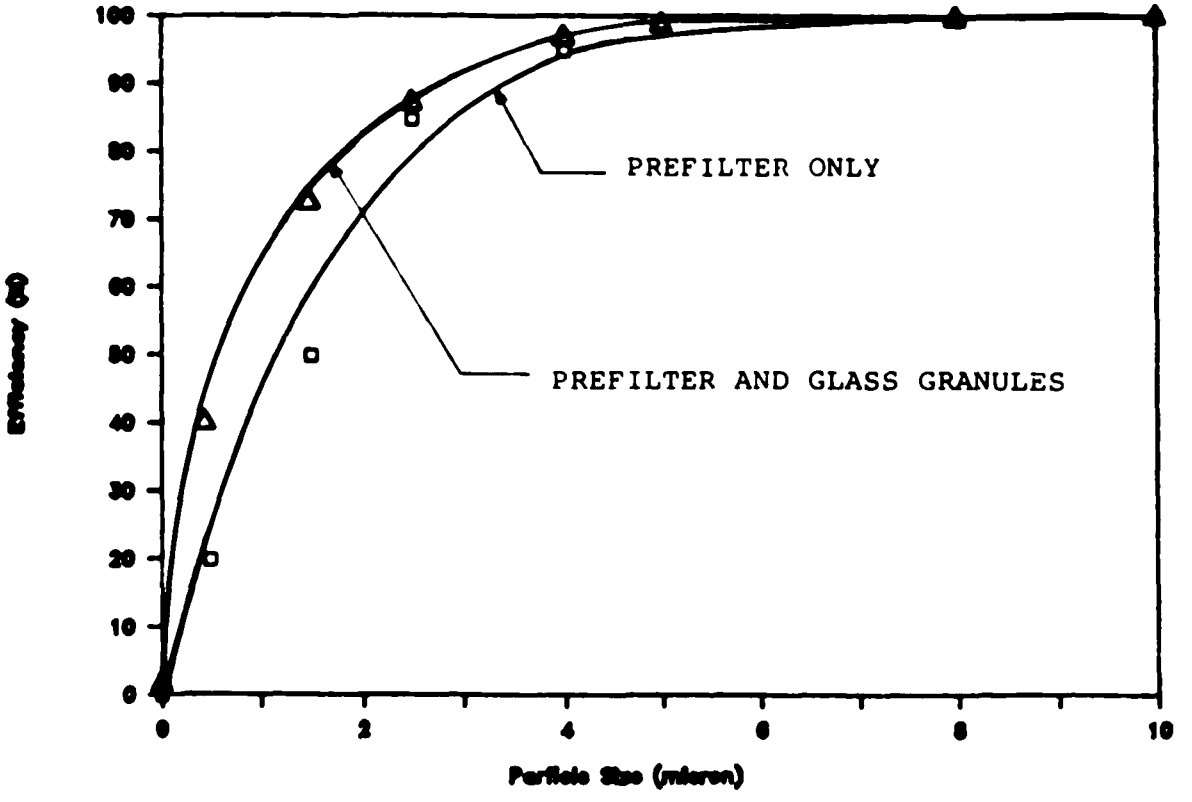

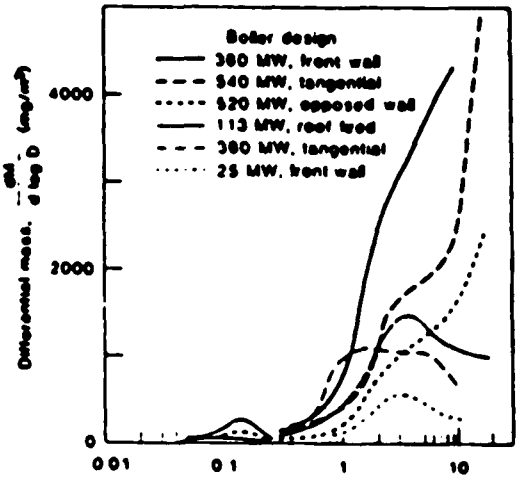

FLY ASH SIZE
92% LARGER THAN 2 MICRON
8% SMALLER THAN 2 MICRON
(McElroy et al., 1982)

b) Typical power plant boiler outlet fly ash distribution.

Figure 23. Typical power plant boiler outlet fly ash distribution and the corresponding filtration efficiency of the RFBF.

III. THE INFLUENCE OF ELECTROSTATIC EFFECTS IN FIBROUS AND GRANULAR BEDS WITH APPLICATIONS TO THE RFBF

In addition to diffusion, gravitation and inertial effects which all are purely mechanical filtration mechanisms, there exists another mechanism of capture process which results from the attraction or repulsion between electrostatic charges on particles and fibrous or granular beds. The filtration efficiency of these filters can be significantly increased by charging the aerosol particles and/or applying an external electric field across the filters (Kao et al., 1987).

During earlier experiments (see Appendix A2), it was shown that the filtration efficiency of the rotating fluidized bed filter increases due to the effects of triboelectrification. The electrostatic charge on the granules during this process depends on the composition of the granular material and the air humidity which determines the rate of charge relaxation. All electrostatic charges generated during the experiments described in Appendix A2 are due to triboelectrification and no external electric field was applied.

In order to further study the influence of the electrostatic effects and apply these results to the RFBF, external electric inputs are used to charge the aerosol particles and/or to create an electric field across the filter. Two series of experiments were performed:

(A) The experimental set-up shown in Figure 24 was used to study the influence of particle charge and the effect of the electrostatic field on the collection efficiency of both the prefilter (screen or pad) and the granular bed. This experimental unit can be operated under precisely controlled conditions such as air flow rate, air

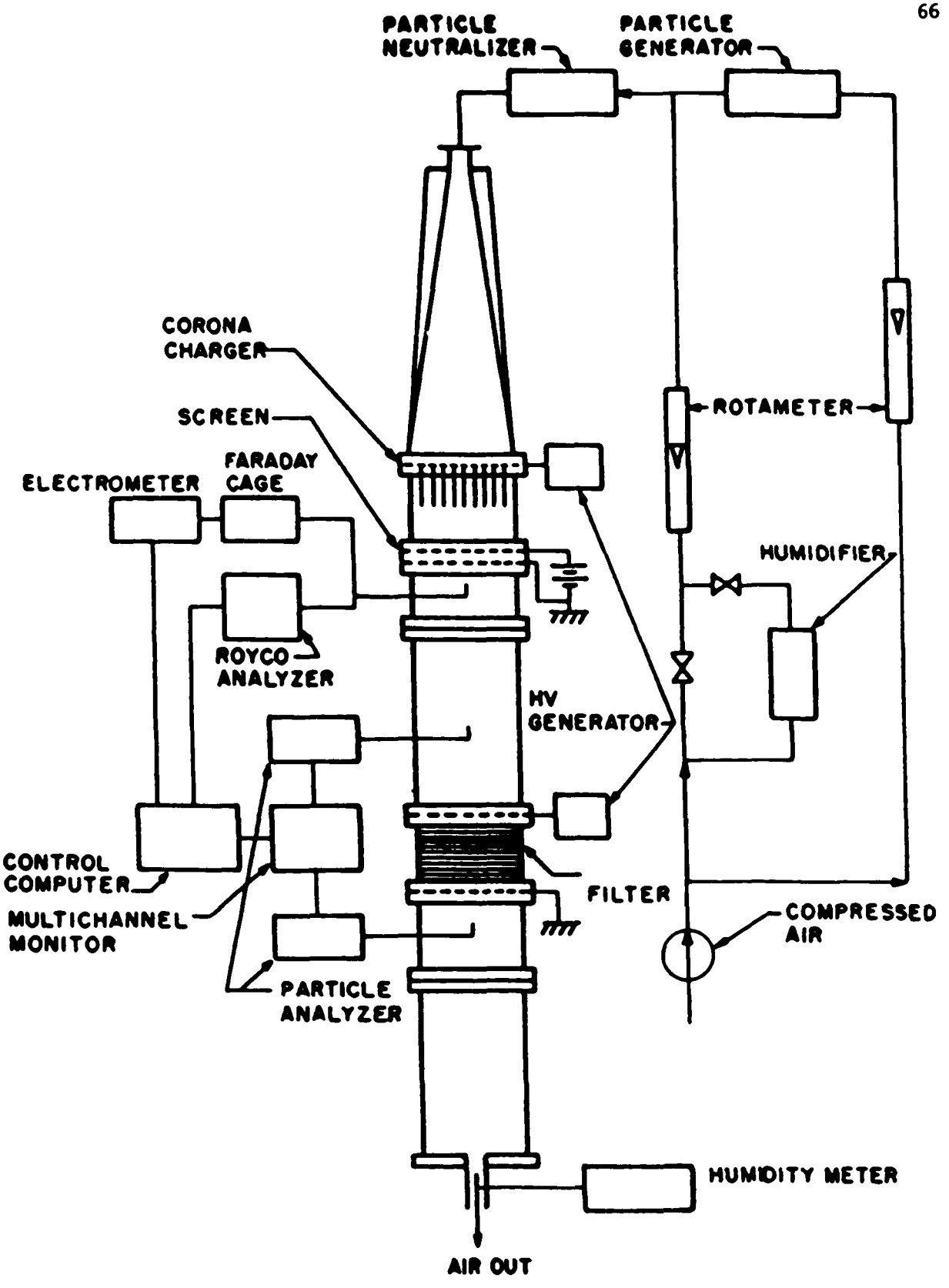

Figure 24. Schematic representation of the experimental set-up to test electrostatic phenomena in filters.

humidity, particle size and number, particle charge and electric field across the bed. Therefore the experimental results can be compared to theoretical models from previous work (Kao et al., 1987) (see Appendix B for details).

(B) Experiments were run using the existing RFBF and a newly constructed corona charger (shown in Figure 25) mounted at the entrance of the device. The charger can generate an electric field of up to 10 KV/cm using a 30 KV DC generator and is mounted on line between the dust generator and the rotating bed. Dust particles are pre-charged before they enter the bed. Therefore, the effect of electrically charging the dust particles by external means and the granules by triboelectrification on the filtration efficiency of the RFBF can be determined.

III.1. FILTER EFFICIENCY OF FIBROUS AND GRANULAR BEDS

III.1.1. Electrostatic fibrous filters

It was shown in Section II.4 that the filtration efficiency of the RFBF can be increased and the granules' circulation rate decreased by placing a screen or a fibrous pad prefilter outside the rotating cylinder. In this section the effect of using a 1 cm thickness fibrous filter (pad) with 0.9 porosity and 60 μm diameter fibers on the pressure drop and the filtration efficiency is described. The effect of charging the inlet aerosol particles and/or applying an electric field across it is also studied.

Assuming a steady state and incompressible fluid flow at low Reynolds number the flow field inside the fibers of the pad can be characterized by a stream function, ψ, given by

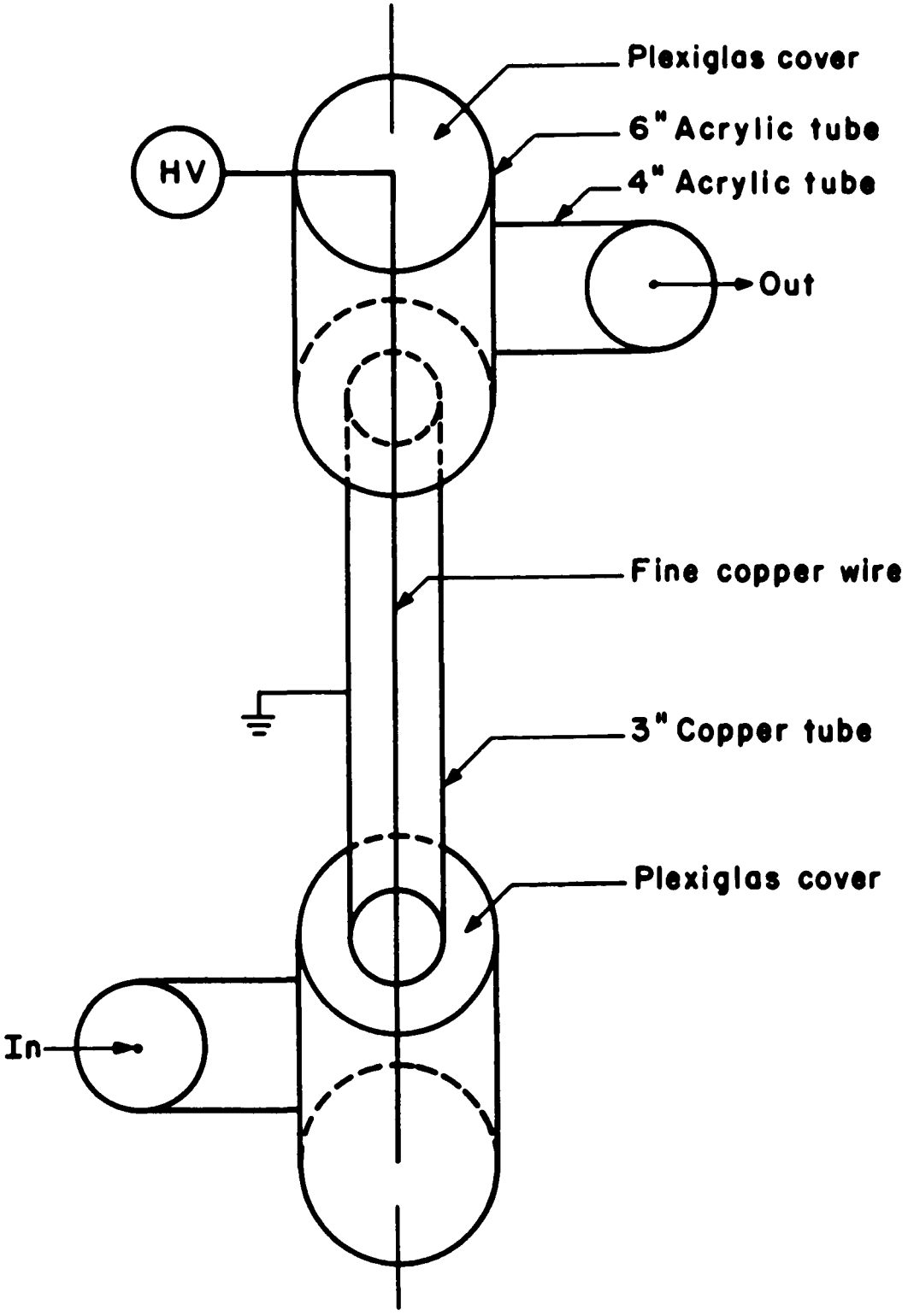

Figure 25. Design of the corona charger.

$$\psi = a_1[r^3 - \frac{4a^2 r\ln r}{2\ln a+1} + \frac{a^4(2\ln a-1)}{2\ln a+1}(\frac{1}{r})]\sin\theta + b_1[a^2 r - \frac{2a^2 r\ln r}{2\ln a+1} -$$

$$\frac{a^4}{2\ln a+1}(\frac{1}{r})]\sin\theta + \sum_{n=2}^{N}[a_n[r^{2n+1} - 2na^{4n-2}r^{3-2n} + (2n-1)a^{4n}r^{1-2n}] +$$

$$b_n[a^2 r^{2n-1} - (2n-1)a^{4n-2}r^{3-2n} + 2(n-1)a^{4n}r^{1-2n}]]\sin(2n-1)\theta \qquad (42)$$

where a is the radius of the fiber, a_1, b_1 ..... a_n, b_n are the coefficients determined from the configuration of the fibrous array and the boundary conditions and r and θ are cylindrical coordinates (see Appendix B2 for details). In these calculations it is necessary to assume that the fibers are made up of identical unit cells in series, each cell containing one fiber.

Once the coefficients in the series for ψ have been determined, the gas velocity at any point within the filter can be computed together with the drag force per unit length of a fiber in the array (pad). The force F per unit length on a cylinder exerted by the fluid moving with mean flow velocity U_o is given by: (Sangani and Acrivos, 1982)

$$F/\mu U_o = -\frac{8\pi a^2(2a_1+b_1)}{(2\ln a+1)} \qquad (43)$$

so that the pressure drop across the filter becomes

$$\Delta P = (F/\ell) \times m_b \qquad (44)$$

where ℓ is the length of a unit cell parallel to the flow direction, μ is the fluid viscosity and m_b is the number of unit cell layers in the bed in series (Kao et al., 1987).

Figure 26 shows the pressure drop across the pad as a function of the mean flow velocity (the Reynolds number, calculated using the fiber diameter and the mean gas velocity, is also given on the upper axis). The empty triangles were obtained from experimental measurements using a micromanometer which can read pressure drops as low as $1x10^{-3}$ mm H_2O which the solid line is computed from equation (44). As seen, the theoretical model predicts the experimental values very well up to a gas velocity of about 30 cm/sec but shows a deviation at higher velocities. One has to note here that the calculated values (solid line) were obtained for zero Reynolds number (creeping flow) while the Reynolds numbers at velocities higher than 30 cm/sec exceed 1.2; therefore discrepancy between theory and experiment is expected under these conditions.

The filtration efficiency of the filter (pad) can be increased by charging the aerosol particles and applying an electric field across the pad. In order to study the influence of the particle charge on the filtration efficiency, the aerosol particles are charged using a (point) needle-and-flat plate corona charger. As shown in Figure 24, dry clean compressed air is pumped in through the system at velocities up to 100 cm/sec. The humidity of the air in the system is controlled by a humidifer and can be adjusted to anywhere between 0 to 95%. The relative humidity is measured at the air outlet by a humidity meter. Monodispersed latex particles of known size are generated from a solution of methanol and then mixed with the inlet air. The particle

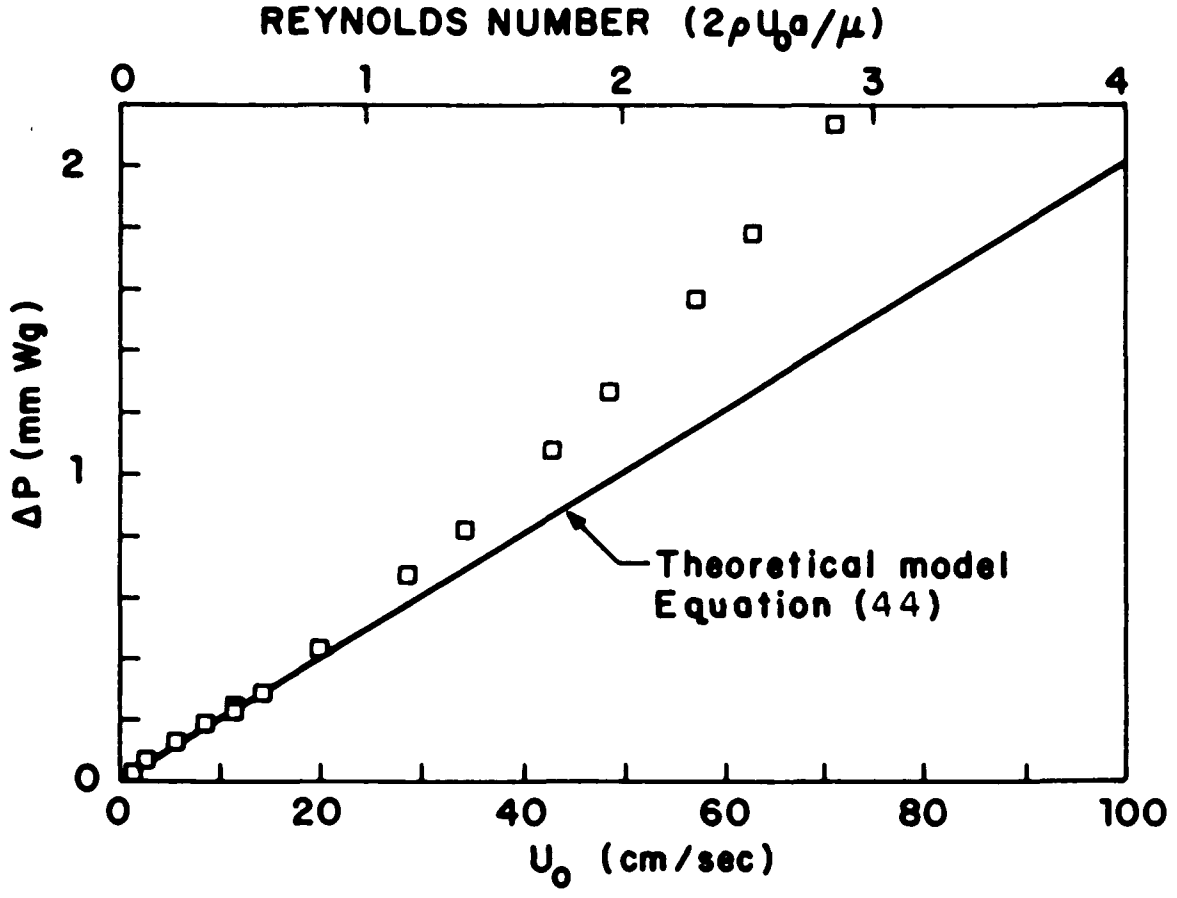

Figure 26. Pressure drop across an 1 cm thickness and 0.9 porosity fibrous pad as a function of superficial air velocity.

concentration is measured simultaneously at the inlet and outlet of the filter bed using two Royco particle analyzers. The particles are charged by the corona charger prior to entering the filter bed. The total charge on the particles is dependent on the current in the corona charger and the relative humidity of the inlet stream (see Appendix B3 for details). As shown in Figure 27, the current in the charger can be increased to up to 2.0 μA. The filtration efficiency of the pad increases from 0 to about 30% without applying an electric field across the pad and up to 95% with a 4.0 KV/cm electric field applied across the pad. There is a sharp increase in filtration efficiency when the current increases from 0 to about 0.2 μA and then levels off. This means that particles flowing through the corona charger have reached the saturation charge at a current of about 0.2 μA. Furthermore, the filtration efficiency increases with increasing humidity because of the increase in particle charge. (See Appendix B3 and Figure B4 for details.)

For further understanding the collection mechanisms governing a fibrous bed, a theoretical model has been developed (see Appendix B2). When an electric field is present the important dimensionless parameter is Kex, the electric number, and is defined as:

$$Kex = \omega_p E_o / U_o \qquad (45)$$

where ω_p is the electric mobility of the particle. For small particles where Stokes flow is applicable, particle mobility is related to the electrical charges on the particles Q_p, by

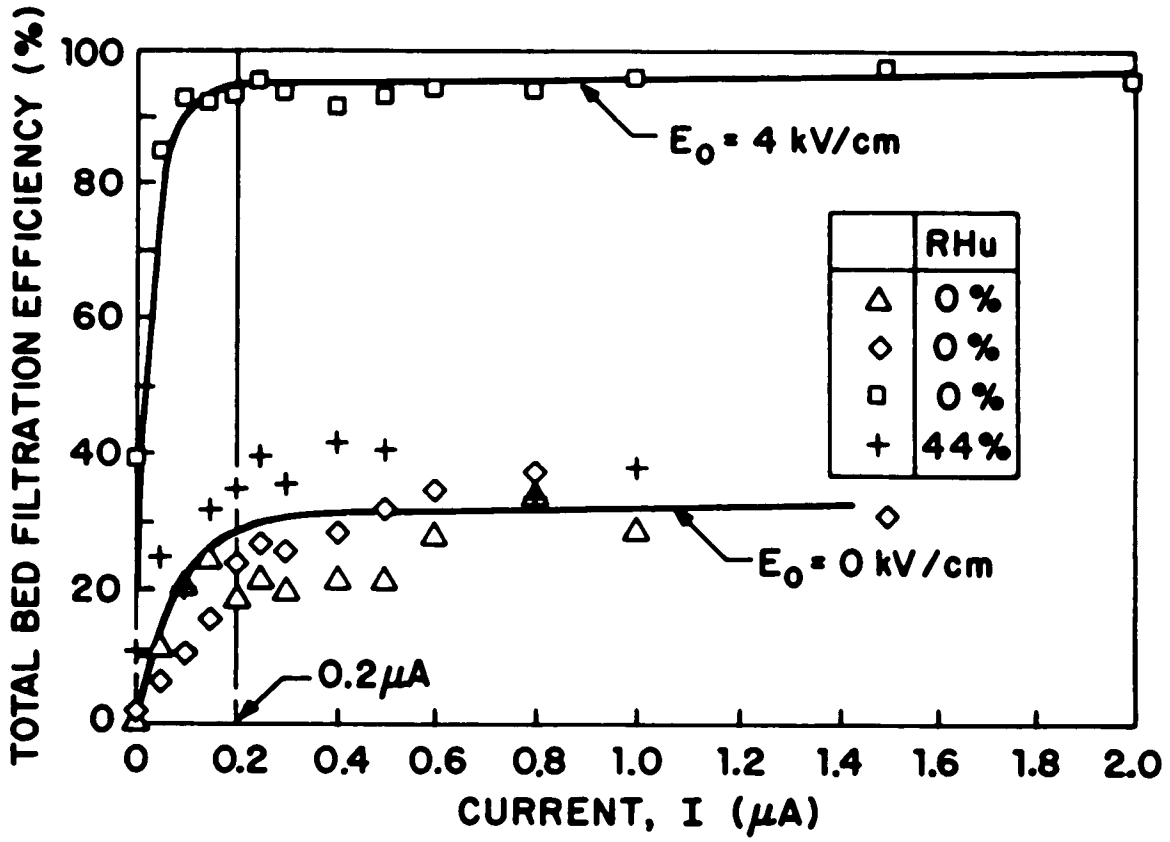

Figure 27. Filtration efficiency for an 1 cm thickness fibrous pad as a function of current through a corona charger.

$$\omega_p = CQ_p/3\pi\mu D_p \qquad (46)$$

where C is the Cunningham correlation factor and D_p is the diameter of the particle.

The theoretical model is based on the flow field developed in equation (42) and an electric potential field given by (Henry and Ariman, 1981)

$$\phi_o^e = -E_o x + \epsilon E_o a^2 \sum_{i=1}^{n} \frac{(x-x_i)}{(x-x_i)^2+(y-y_i)^2} \left[1 - \sum_{j=1}^{m} \epsilon \frac{a^2}{d_{ij}^2}\right] \qquad (47)$$

where (x_i, y_i) are the locations of the fibers, d_{ij} is the distance between fibers i and j and x and y are Cartesian coordinates. The polarization coefficient is given by $\epsilon = (\epsilon_f/\epsilon_o - 1)/(\epsilon_f/\epsilon_o + 1)$ where ϵ_f is the dielectric constant of the fiber and ϵ_o is the dielectric constant of air. (Kao et al., 1987)

The results of the filtration efficiency of the fibrous pad as a function of the dimensionless electric number Kex are shown in Figure 28. The solid lines are from theoretical computations while the symbols are from experimental data obtained in a similar way as described in Figure 27 with different velocities and gas humidities. Humidities are increased from 0 to up to 68% and velocities from 10 to 30 cm/sec. The model predicts values which are in vary good agreement with the experimental data.

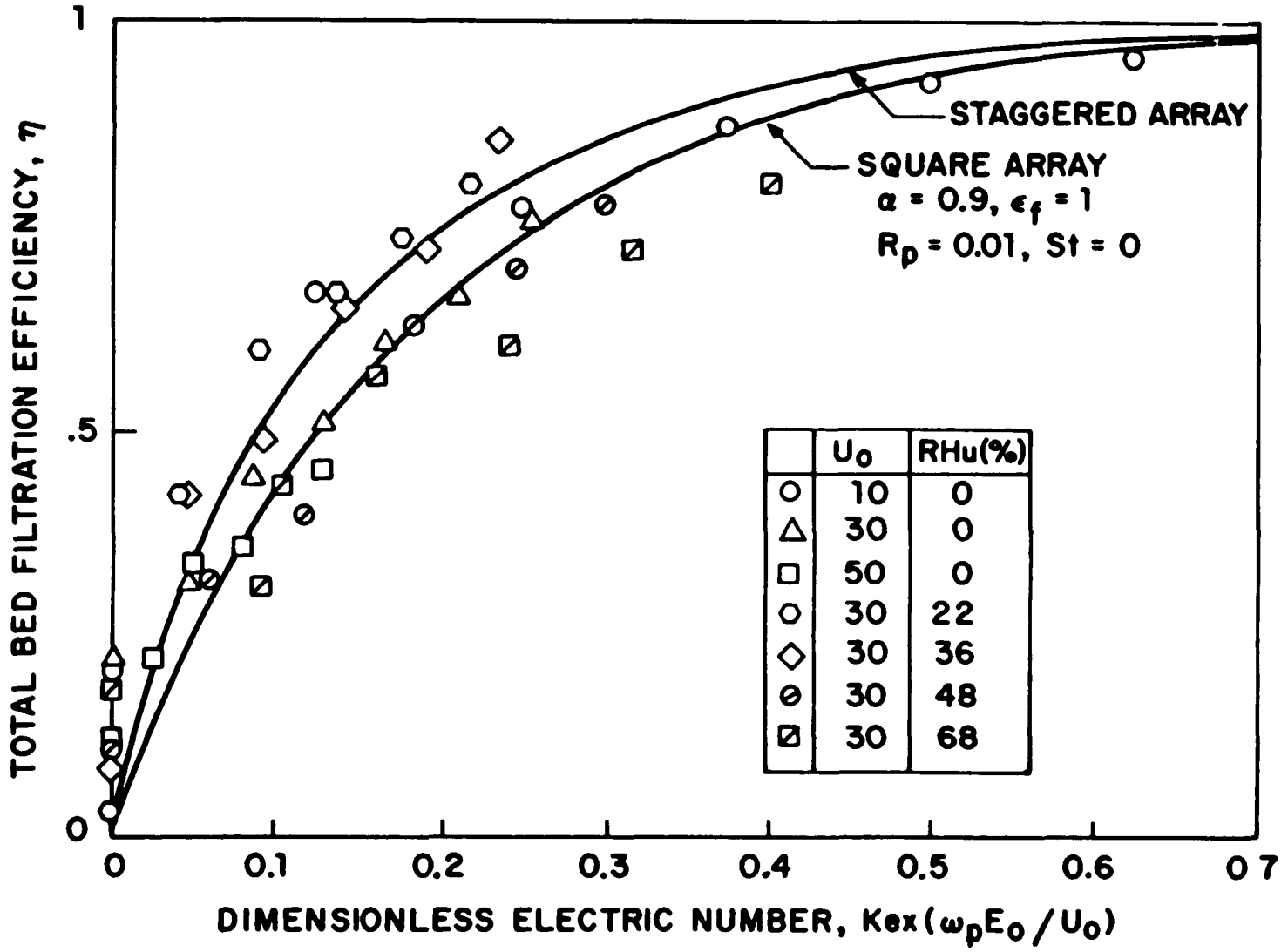

Figure 28. Filtration efficiency of an 1 cm thickness fibrous pad as a function of dimensionless electric number, Kex.

III.1.2. Charged aerosol separation in granular beds

In order to study the influence of the particle charge on the filtration efficiency in the RFBF, a granular bed was also tested in the electrostatic filter set-up shown in Figure 24 except that a 2 cm thick bed of glass beads replaced the fibrous pad. The aerosol particles were charged by the corona charger. The filtration efficiency of the granular bed as a function of the current through the corona charger is shown in Figure 29. As seen in this figure, the filtration efficiency of the granular bed without applying electric fields across the bed increases from 10% to about 30% when the current of the charger increases from 0 to 0.2 μA. When an additional 2 KV/cm electric field is applied to the bed, the filtration efficiency jumps to 99% when the particles are also charged. Here, particle deposition is similar to the process taking place in the fibrous bed as shown in Figure 27. These results can be used to predict the behavior of the RFBF in which electrically charged particles are introduced.

III.2. APPLICATION OF ELECTROSTATIC EFFECTS TO THE RFBF

The results of electrostatic charge measurements for fibrous and granular beds could now be applied to the RFBF. To this end a corona charger was built (see Figure 25) and mounted on line between the dust generator and the rotating bed. Experiments to determined the effect of electrically charging the dust particles by external means and the granules by triboelectrification on the filtration efficiency of the RFBF were performed.

The filtration efficiency of the RFBF under fluidization as a function of the corona charger current is shown in Figure 30 for DOP aerosols in a 3 cm thickness granular bed made of 1.5 mm glass beads.

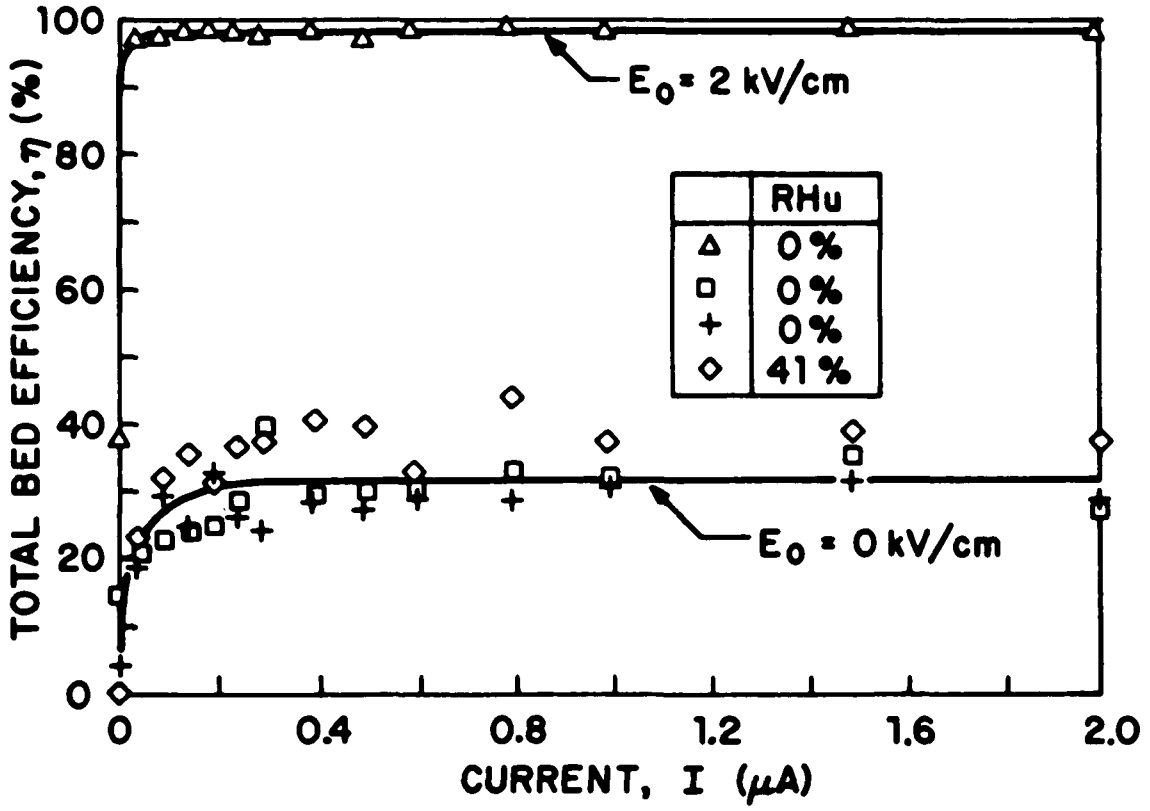

Figure 29. Filtration efficiency for a 2 cm thickness granular bed containing 0.15 cm glass beads as a function of current through the corona charger.

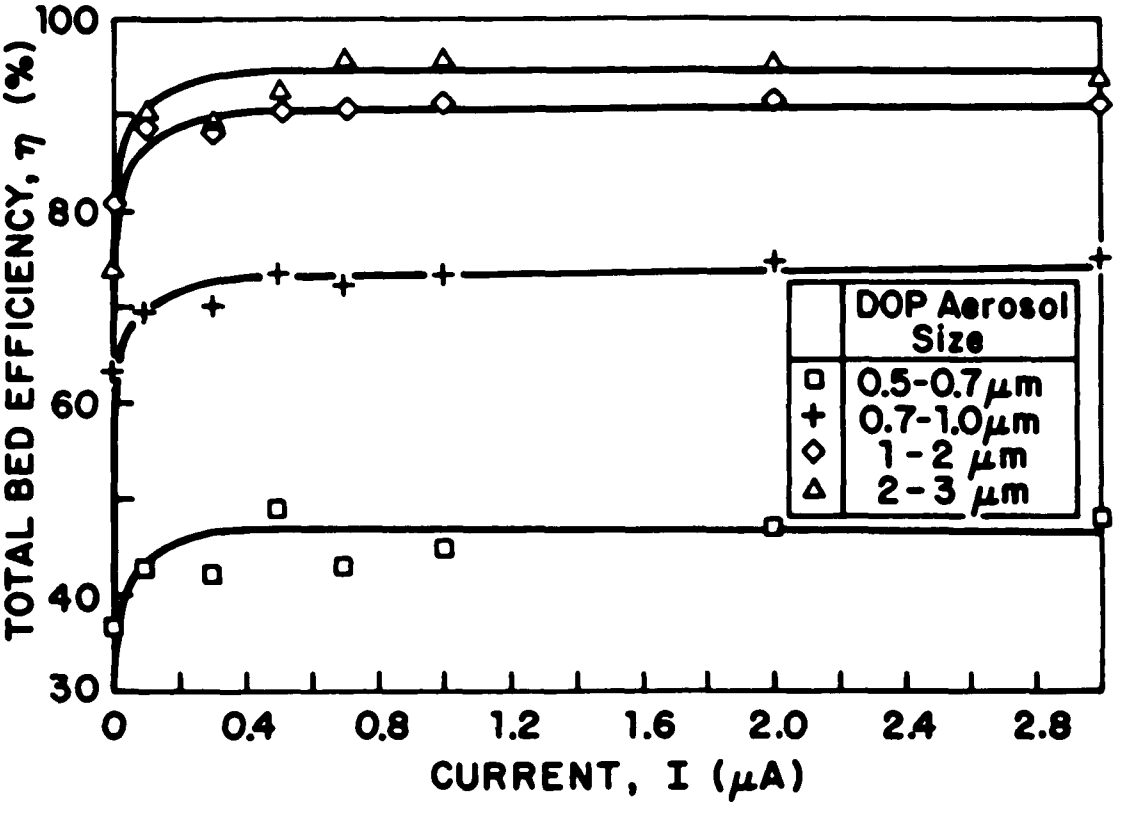

Figure 30. Total filtration efficiency as a function of current through the corona charger for DOP aerosols in a 3 cm thick bed in the RFBF containing 0.15 cm diameter glass beads and a fine screen around the cylinder. Rotating speed, W=220 RPM; Air velocity, U_o=150 cm/sec; Relative humidity, RHu=0%.

The filtration efficiency of DOP aerosols increases about 10 to 20% for all sizes when the aerosols are charged by the corona charger. Shown in Figure 31 are results for fly ash under the same operating conditions. The filtration efficiency of fly ash increases significantly for small particles when they are charged: from about 10% to close to 50% for particles in the range 0.5-1 μm. However, for larger particles, the influence of electric charge is not as strong; there is only a slight increase in filtration efficiency for fly ash for particles larger than about 1 μm. It is concluded therefore that using precharged particles can enhance the filtration efficiency of the RFBF without an increase in pressure drop through the bed and with only a minor complication in the construction of the device.

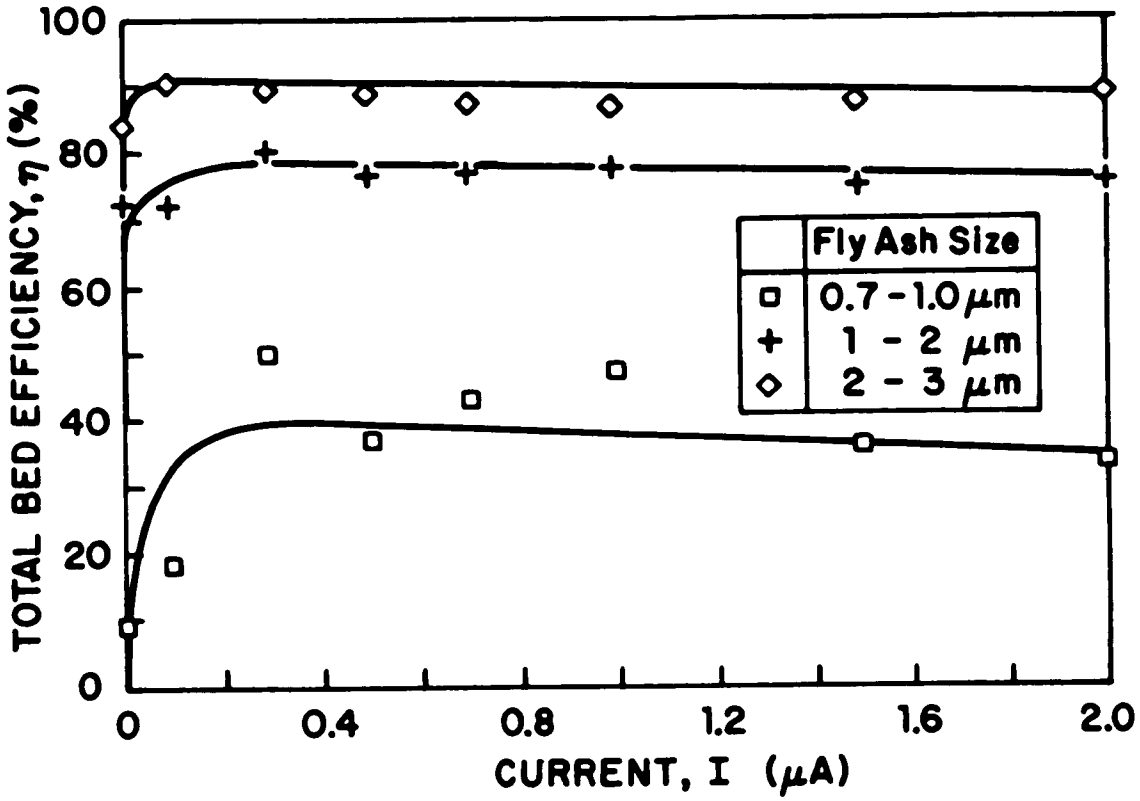

Figure 31. Total filtration efficiency as a function of current through the corona charger for fly ash dust particles in a 3 cm thick bed in the RFBF containing 0.15 cm diameter glass beads and a fine screen around the cylinder. Rotating speed, W=220 RPM; Air velocity, U_o=150 cm/sec; Relative humidity, RHu=0%.

IV. CONCLUSIONS

IV.1. CONCLUSIONS

The performance of a rotating fluidized bed filter (RFBF) as a dust or aerosol collector operating continuously so that the filter media (granules) is continuously replaced as it becomes loaded with dust was studied. A thorough optimization of the device with respect to rotational speed, gas velocity, pressure drop, aerosol size, type, and concentration, granule size and type and bed thickness was also undertaken. The optimization showed that if the dimensionless Stokes number (St) is larger than 0.03 a minimum filtration efficiency of about 90% is reached. This value can be obtained by adjusting parameters in the Stokes number such as the average air velocity, aerosol and granule size, etc.

In addition, it was found that if a fine wire cloth is mounted outside the rotating cylinder to serve as a prefilter the efficiency of the device is further increased. The prefilter is especially useful for streams with high dust concentration to prolong saturation time of the granules inside the bed and reduce the granules circulation rate. By using the prefilter this rate can be reduced by about an order of magnitude for operation in a typical commercial power plant boiler outlet; however the pressure drop across the bed increases because of cake formation on the screen's surface. A stationary brush to cut cake formation from the screen surface will be necessary to keep the pressure drop within acceptable limits.

During the study of the rotating fluidized bed, the occurrence of partial fluidization was discussed. This phenomenon is due to the curvature of the rotating cylinder which contains the bed and causes

the air velocity inside the bed to become non-uniform and to the centrifugal forces which are dependent on the radius of the bed. As a result, fluidization inside the bed occurs layer by layer from the inside surface outward as the inlet air velocity increases. It was also found that there is a diminished internal circulation of granules inside the bed probably due to reduced bubble motion.

Both problems mentioned above can be solved by mounting inserts inside the bed. By correctly designing the shape of these inserts (as shown in Figure 21), the velocities through the bed become more uniform and some internal circulation is created due to increased and more stable bubble circulation.

The conceptual design of the pilot size rotating fluidized bed incorporates all the findings described above. It is housed in a cyclone so that dust particles larger than about 10 μm are separated by the cyclone; the screen (prefilter) on the rotating cylinder captures most particles between 2 and 10 μm while the remainder of the dust particles are collected by the granules. The unit was designed to handle gas flow rates up to 4,000 CFM and to withstand temperatures up to 500 ^{o}F. It is planned to install a pilot size RFBF, constructed based on the conceptual design, in a power plant boiler outlet to replace the electrostatic precipitator. The collection efficiency of both devices should be comparable. However, the size of the RFBF would be only one tenth of that of the electrostatic precipitator due to the ability of the RFBF to handle much higher gas velocity.

In the second part of this work, the influence of electrostatic effects in fibrous and granular bed with applications to the RFBF was studied. A theoretical model predicting both pressure drop and

filtration efficiency of dust particles through a fibrous bed was developed and careful experiments were carried out to verify the model. The filtration efficiency due to the influence of electrostatic effects was found to depend on the particle charge, electric fields, air humidity and gas velocity. The results show that the filtration efficiency of fine dust particles can be significantly increased by charging the particles even though no electric field is applied across the bed. Similar experiments were also performed with a granular bed which yielded an even better performance. The results of the experiments with charged particles for fibrous and granular filters were used to improve the filtration efficiency of the RFBF for fine dust particles in the size range of 0.1 to 1 μm by passing the dusty gas through a corona charger placed at the entrance of the filter.

IV.2. RECOMMENDATION FOR FUTURE WORK

An *in situ* test will be necessary on a pilot size RFBF to obtain a more realistic evaluation of its capabilities in an industrial environment. Also, a thorough economic evaluation of the RFBF as an industrial filter regarding operating costs, capital costs, space requirement and plant design will be necessary based on the results of the in situ test. Furthermore, the RFBF has potential to remove gaseous pollutants in the exhaust gases of power plant boiler such as NO_x, SO_2 and SO_3 using chemically active granules which can react with those pollutants.

Lastly, by applying the results of electrostatic experiments from the granular and fibrous beds to the RFBF, a theoretical model taking into account the electrostatic effects of particle charges and electric fields across the RFBF in the fluidized condition should be developed. This model can be used to predict the exact motions of the dust particles inside a rotating fluidized bed and the influence of the electrostatic effects on the filtration efficiency of the bed. Also a careful design of applying an electric field across the RFBF should be considered so that a 99% filtration efficiency can be reached even for very fine dust particles.

V. APPENDICES

V.1. APPENDIX A: DETAILED DESCRIPTION OF RESEARCH PERFORMED ON THE RFBF

CONTENTS

A.1. FILTRATION EFFICIENCY OF THE RFBF

In a granular bed, an aerosol particle is captured if it collides with the granule's surface and if it sticks to it. A particle reaches the granule's surface due to one or more filtration mechanisms which include inertia, interception, diffusion, gravity settling and electrostatic attraction. In the rotating fluidized bed filter which operates at high gas velocity the main filtration mechanism is inertial impaction. Also, if the aerosol and granules are electrically charged, electrostatic effects may become important. The effect of diffusion and gravitation in the RFBF is small except for really small aerosol particles where diffusion may become important or very large particles where gravitation may become significant.

The measured experimental total bed efficiency for a certain size of dust particle is defined as:

$$\eta = 1 - n_{out}/n_{in} \qquad (A1)$$

where n_{in} and n_{out} are the number concentration of dust particles of a certain size in a unit volume of gas before and after passing through the filter, respectively.

The concentrations n_{in} and n_{out} are measured simultaneously by the Climet CI-225 and CI-208S dust particle counters. The Climet dust particle counter is an optical device which measures the number and size of dust particles by light scattering. The results are given in terms of number of particles of a certain size range per unit volume of gas. The instrument can detect particles with diameters larger than 0.3 μm and it has 7 channels for particles in the size range of 0.3 - 10 μm. The simultaneous reading of inlet and outlet concentrations enable accurate measurements of filtration efficiency even when the

dust concentration varies as a function of time. The data are collected and analyzed by a microcomputer.

The Effect of Air Velocity

The effect of velocity on filtration efficiency in the rotating fluidized bed filter is shown in Figures A1 and A2. As the velocity increases from 60 cm/sec (2.0 ft/sec) to 230 cm/sec (7.5 ft/sec) using polypropylene granules (Figure A1), filtration efficiency increases from 20% to 95% for the 1-2 μm DOP particles. For larger size dust particles (2-3 μm), the filtration efficiency stays at 99% for velocities from 100 cm/sec (3.3 ft/sec) to 250 cm/sec (8.2 ft/sec). A similar trend is shown in Figure A2 using polyethylene granules. Therefore, a granular bed acts almost as an absolute filter for aerosol particles larger than 2 μm. However when the particles are smaller, penetration occurs and the filtration efficiency drops very rapidly when the average air velocity decreases.

In order to test the potential application of the RFBF in a high temperature environment, sand and alumina granules which can withstand high temperatures were used. As previously reported, the efficiency of the RFBF increases with increasing air velocity in the fixed bed region with polypropylene and polyethylene granules used as filter media. Similarly, for sand, it is observed that the filtration efficiency for DOP aerosol particles (1-2 μm) increases from 47% to 98% as the air velocity increases from 60 to 180 cm/sec (2.0 to 5.9 ft/sec). For larger size particles (2-3 μm), the efficiency remains steady at above 95% in this range of velocities (Figure A3). As the velocity is increased further and the bed becomes fluidized the efficiency drops significantly. We believe the drop in efficiency results mainly

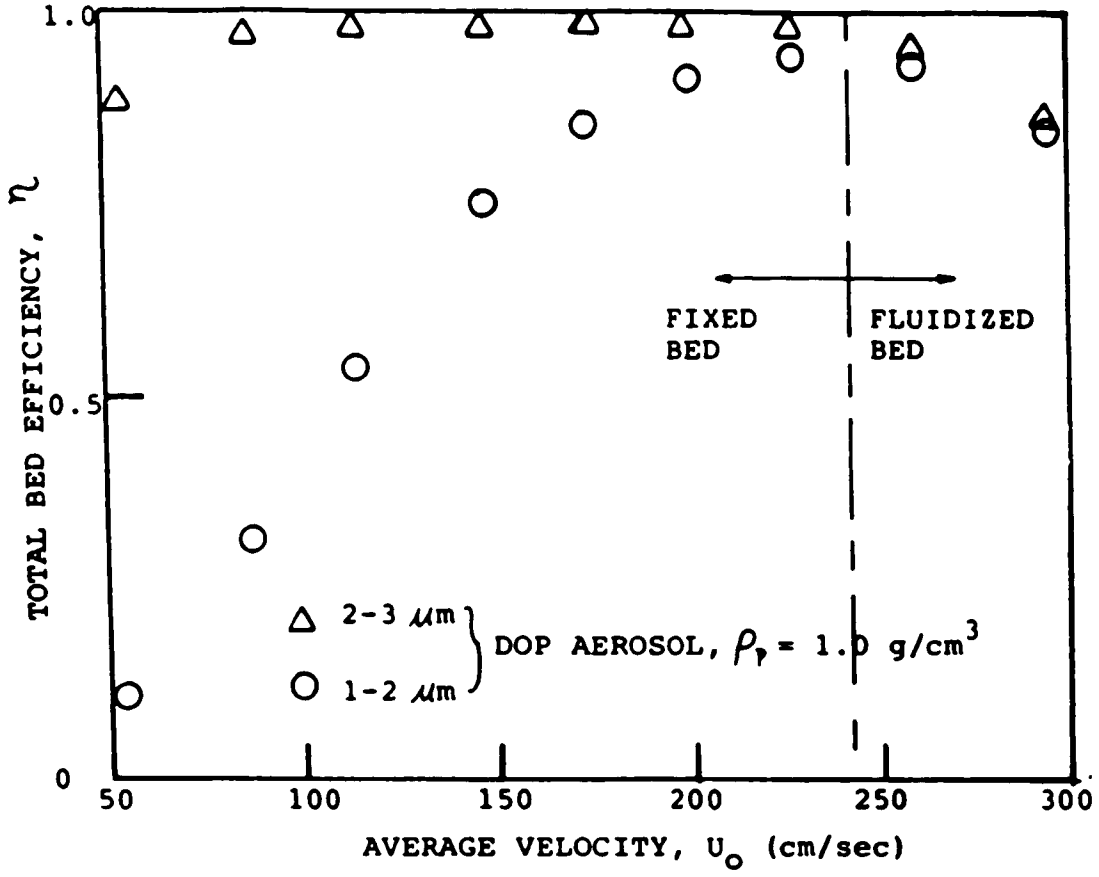

Figure A1. Total bed efficiency as a function of air velocity for dust particles in a RFBF containing 0.3 cm diameter polypropylene granules.
Bed thickness, L = 3 cm;
Bed porosity, ε = 0.4;
Rotating speed, W = 455 RPM;
Relative humidity, RHu = 40%.

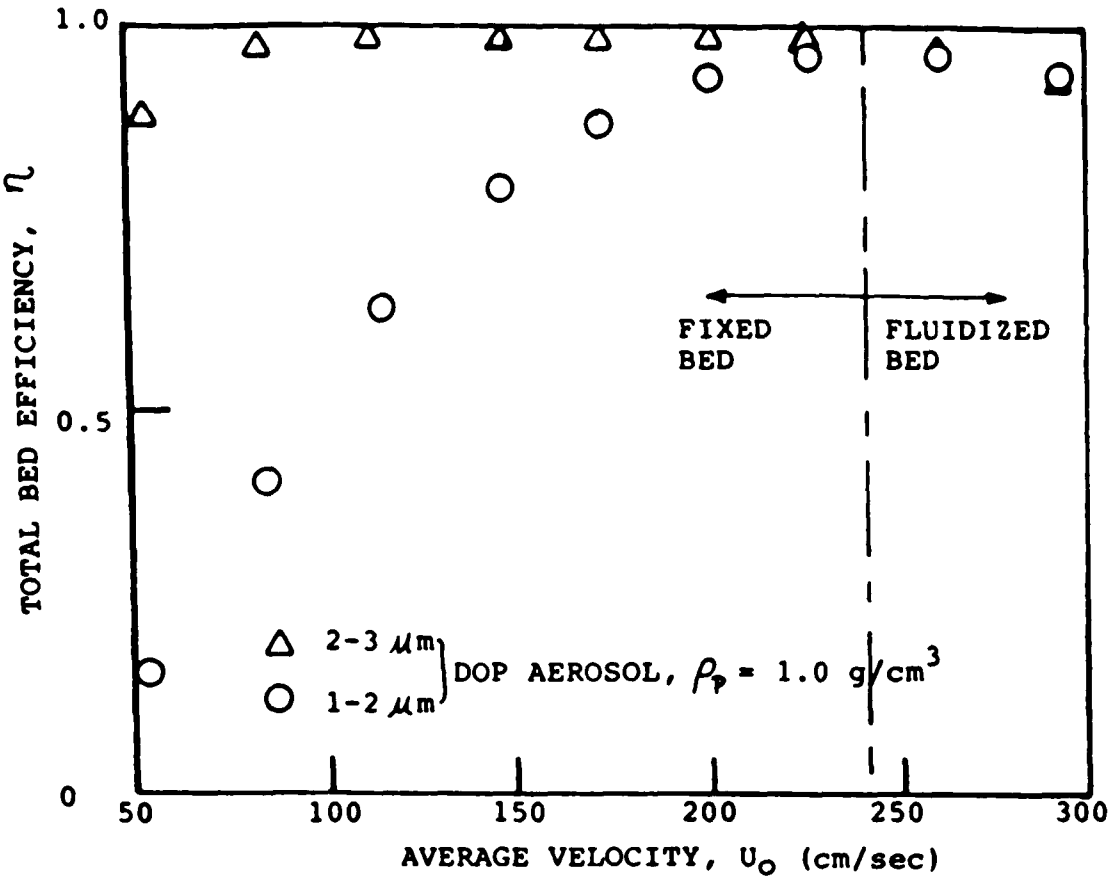

Figure A2. Total bed efficiency as a function of air velocity for dust particles in a RFBF containing 0.3 cm diameter polyethylene granules.
Bed thickness, L = 3 cm;
Bed porosity, ε = 0.4;
Rotating speed, W = 455 RPM;
Relative humidity, RHu = 40%.

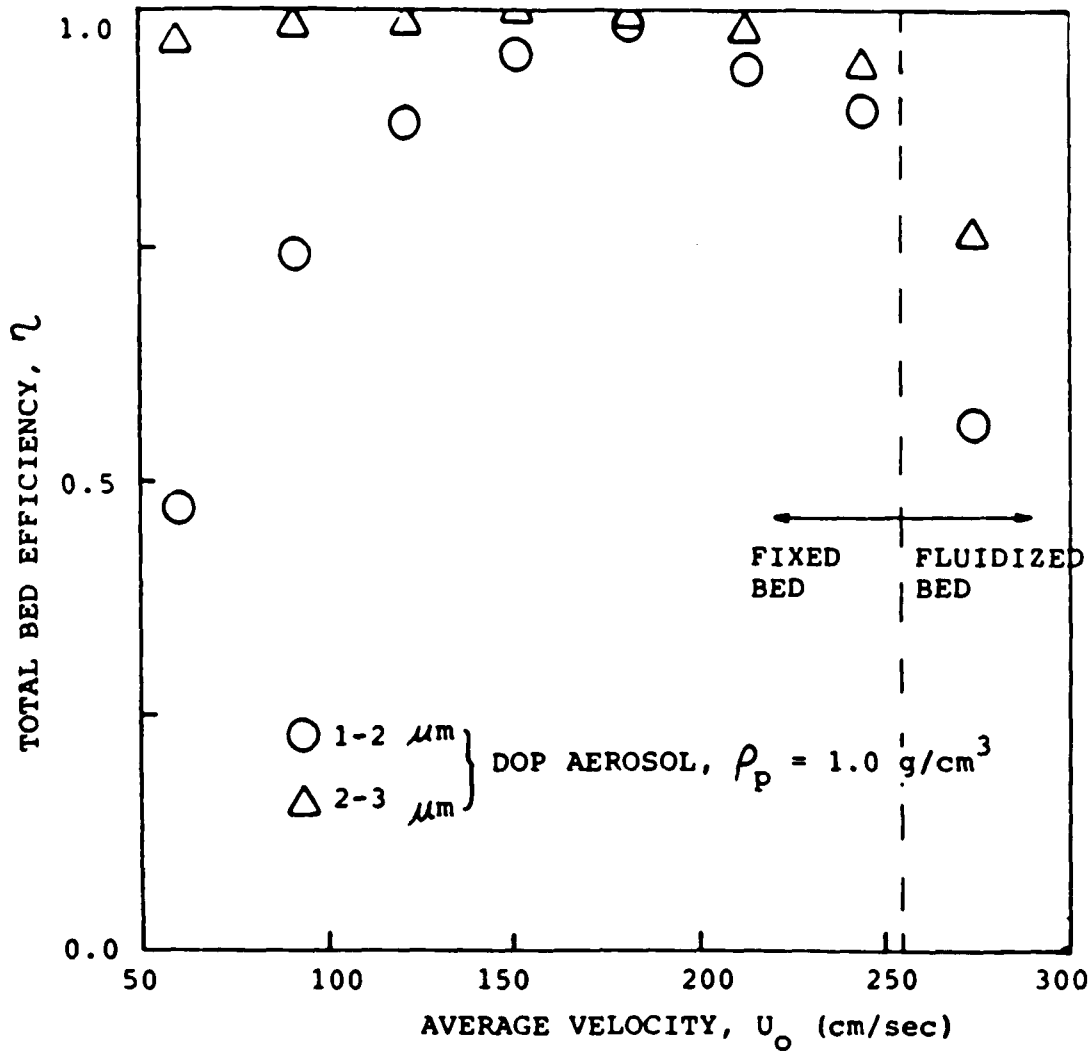

Figure A3. Total bed efficiency as a function of air velocity for dust particles in a RFBF containing 0.1 cm diameter sand granules.
Bed thickness, L = 1.3 cm;
Bed porosity, ε = 0.46;
Rotating speed, W = 455 RPM;
Relative humidity, RHu = 0 %.

because of reentrainment of dust particles by the high velocity air already captured on the granules and possibly also because of bubble formation in the bed when the gas velocity exceeds minimum fluidization.

Experiments using small alumina granules (150 μm in diameter) required placing a very fine layer of 400 mesh screen (37 μm opening) around the inside wall of the rotating cylinder to hold the alumina granules inside the bed. From Figure A4, it is seen that the behavior of the total bed efficiency is completely different from what we have observed with the plastic and sand granules. Using DOP particles, the total bed efficiency drops rapidly to zero as the velocity is increased from 150 cm/sec (4.9 ft/sec) and higher and using alumina dust particles, the efficiency drops to zero when the velocity exceeds 70 cm/sec (2.3 ft/sec). The large difference in total bed efficiency observed using the DOP and alumina dust particles in the low air velocity region is probably due to the surface characteristics of the alumina granules. The alumina dust particles which hit the surface of the alumina granules, bounce off without being captured, and then are carried away in the outlet air whereas the DOP aerosol particles, being sticky, will tend to adhere to the surface of the alumina granules. At higher velocities, in the fluidized bed mode, the total bed efficiency drops very rapidly even for the DOP particles indicating either reentrainment of aerosol due to the high velocity air or aerosol by-passing the granules because of bubble formation or even generation of dust due to granule attrition.

In order to further study the effect of using the small alumina granules, additional experiments were performed using the following configurations: empty bed (no granules) with screen only; 0.6 cm thick

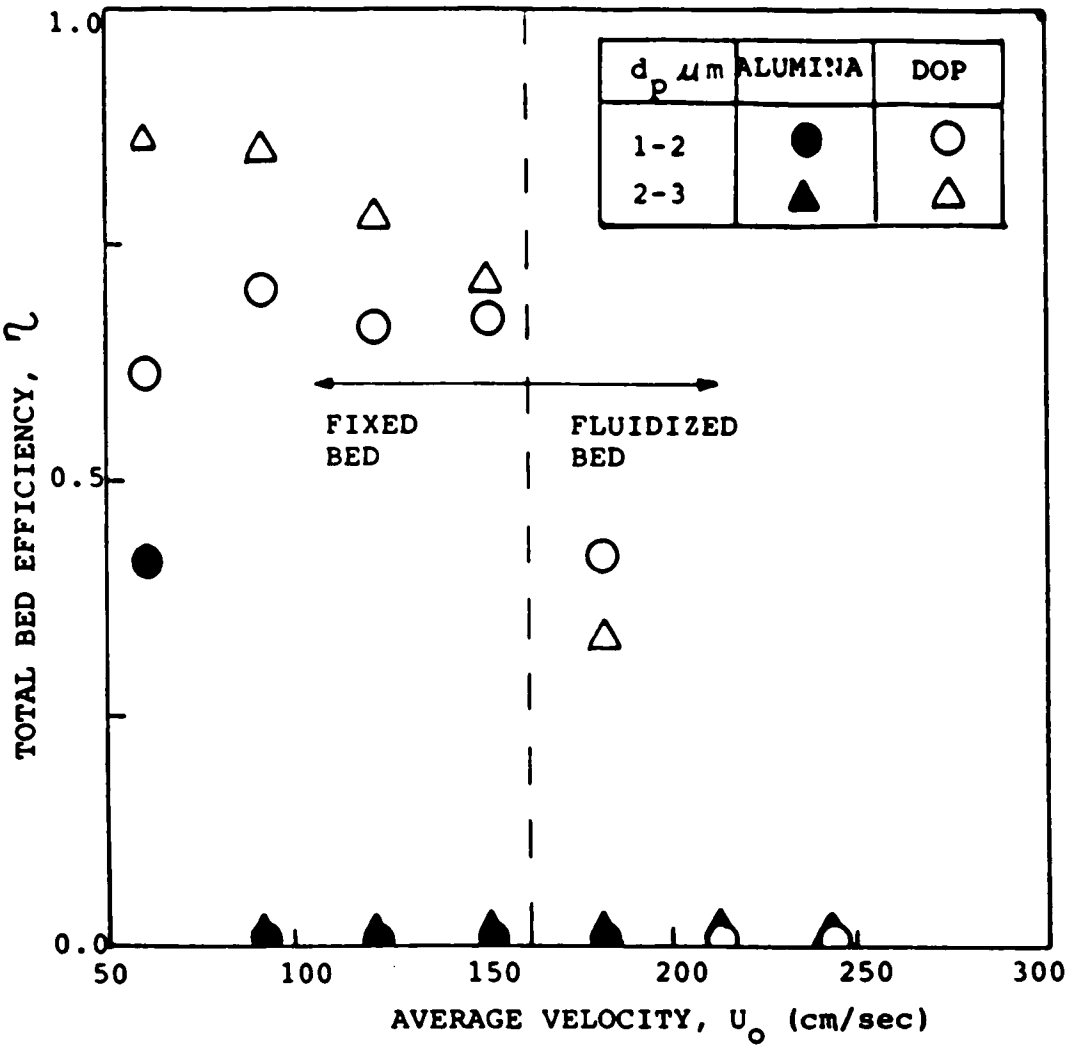

Figure A4. Total bed efficiency as a function of air velocity for dust particles in a RFBF containing 150 μm diameter alumina granules.
Bed thickness, L = 0.6 cm;
Bed porosity, ε = 0.40;
Rotating speed, W = 455 RPM;
Relative humidity, RHu = 17 %.

alumina granule bed with screen; 0.6 cm thick alumina granule bed precoated with DOP and with screen. The results are shown in Figure A5. The full solid circles show the collection efficiency of the fine screen: it serves as a prefilter with about a 30% collection efficiency. When the alumina granules are added up to a bed thickness of 0.6 cm the efficiency drops to zero as shown by the empty triangles. The only explanation of these results is that the outlet air actually carries out some dust particles which are present on the granules' surface and consequently the alumina granules serve as a dust generator. Therefore, the efficiency is even lower than that of the empty bed with the screen. Nevertheless, from the same figure a 90% collection efficiency (empty circles) for 1-2 μm in diameter solid dust particles in the velocity range of 70 to 180 cm/sec (2.3 to 5.9 ft/sec) can be seen for the same 0.6 cm thick alumina granule bed. This is achieved by first coating the granules with DOP aerosols for about 2 hours, then introducing fresh air for 40 minutes to clean the granules from any excess DOP deposit. Thus we use the DOP as a filter-aid to coat the granules' surface so as to minimize attrition and bouncing (reentrainment). However, this cannot be done in a high temperature environment because the DOP coating will vaporize and lose its filter-aid effect. Nevertheless the results using the DOP coated alumina granules are in agreement with the theory that the smaller the granules the higher the collection efficiency will be because of the larger surface area and the greater numbers of layers of granules per unit volume provided that there is no bouncing of aerosol off the granules' surface.

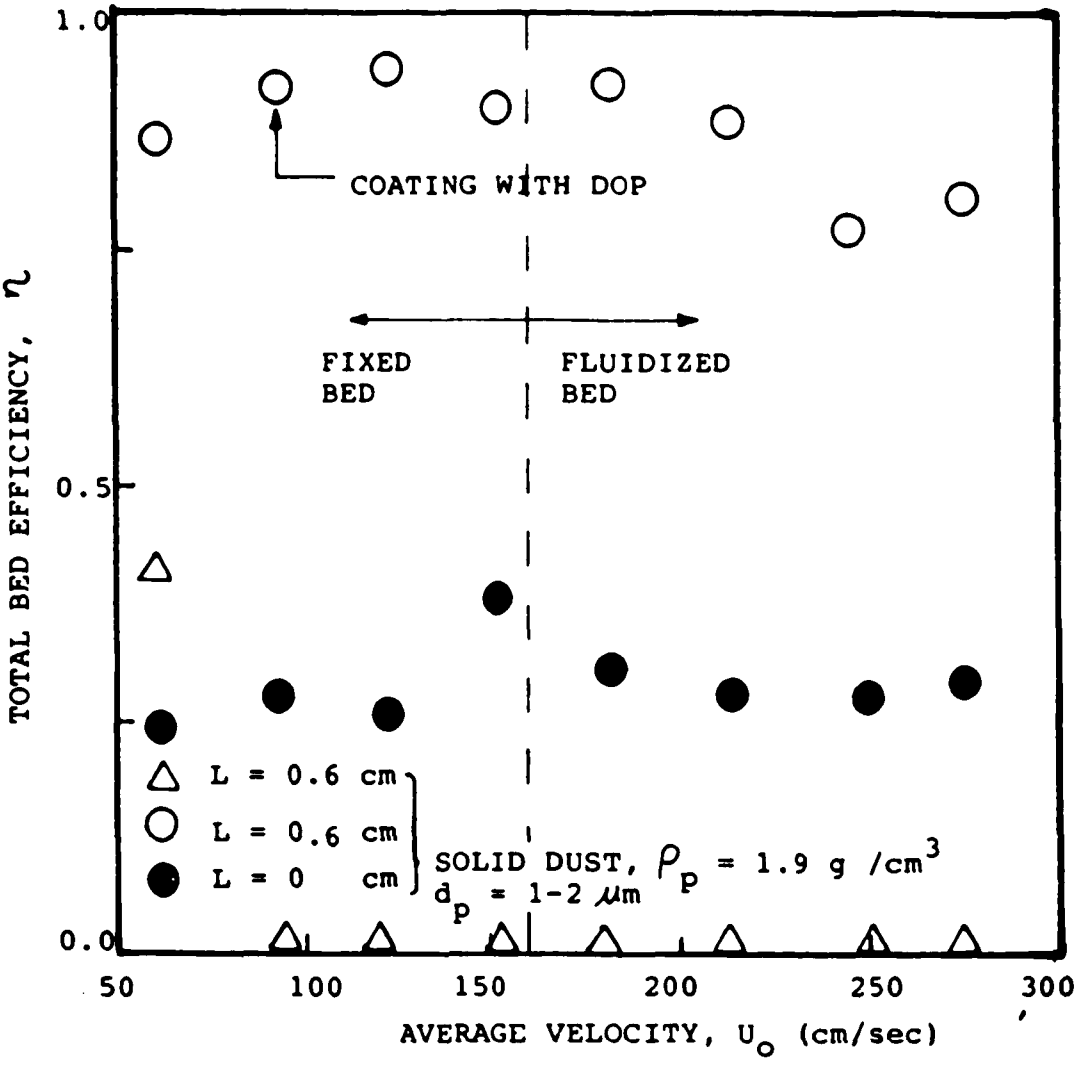

Figure A5. Total bed efficiency as a function of air velocity for dust particles in a RFBF containing 150 μm diameter alumina granules with a thin layer of DOP coating on the surface and a very fine screen (400 mesh) around the cylinder.
Bed porosity, $\varepsilon = 0.40$;
Rotating speed, W = 455 RPM;
Relative humidity, RHu = 18 %.

The Effect of Rotating Speed

In the rotating fluidized bed minimum fluidization can be obtained at almost any given velocity by adjusting the rotating speed of the bed within the mechanical limitations of the system. the effect of rotating speed on filtration efficiency is shown in Figures A6 and A7 using polypropylene and polyethylene granules. In the fixed bed region filtration efficiency is not affected by the rotation. As the rotating speed decreases at a given air velocity the bed changes from a fixed to a fluidized bed. the filtration efficiency at minimum fluidization conditions is about the same as the efficiency in the fixed bed region and drops slightly as the rotating speed decreases. Further decrease in the rotating speed results in bubble formation which reduces filtration efficiency very rapidly. It is advantageous to operate the bed just above minimum fluidization velocity where the filtration efficiency is high and the bed material can easily be continuously introduced and discharged from the bed because of the fluidized state.

The effect of rotating speed on filtration efficiency using sand and alumina granules is shown in Figures A8 and A9. Figure A8 shows that the total bed filtration efficiency of sand behaves slightly different from that of the polypropylene and polyethylene granules reported previously. The filtration efficiency decreases as the rotating speed is reduced in the fixed bed region. This might be due to the characteristics of the sand's surface. As the rotating speed is reduced even further so that the gas velocity becomes higher than minimum fluidization, the bouncing and bubble effects become more and more significant and the filtration efficiency drops rapidly to zero in the fully fluidized state in tremendous reduction in the collection efficiency. In contrast, using alumina granules as the filter medium,

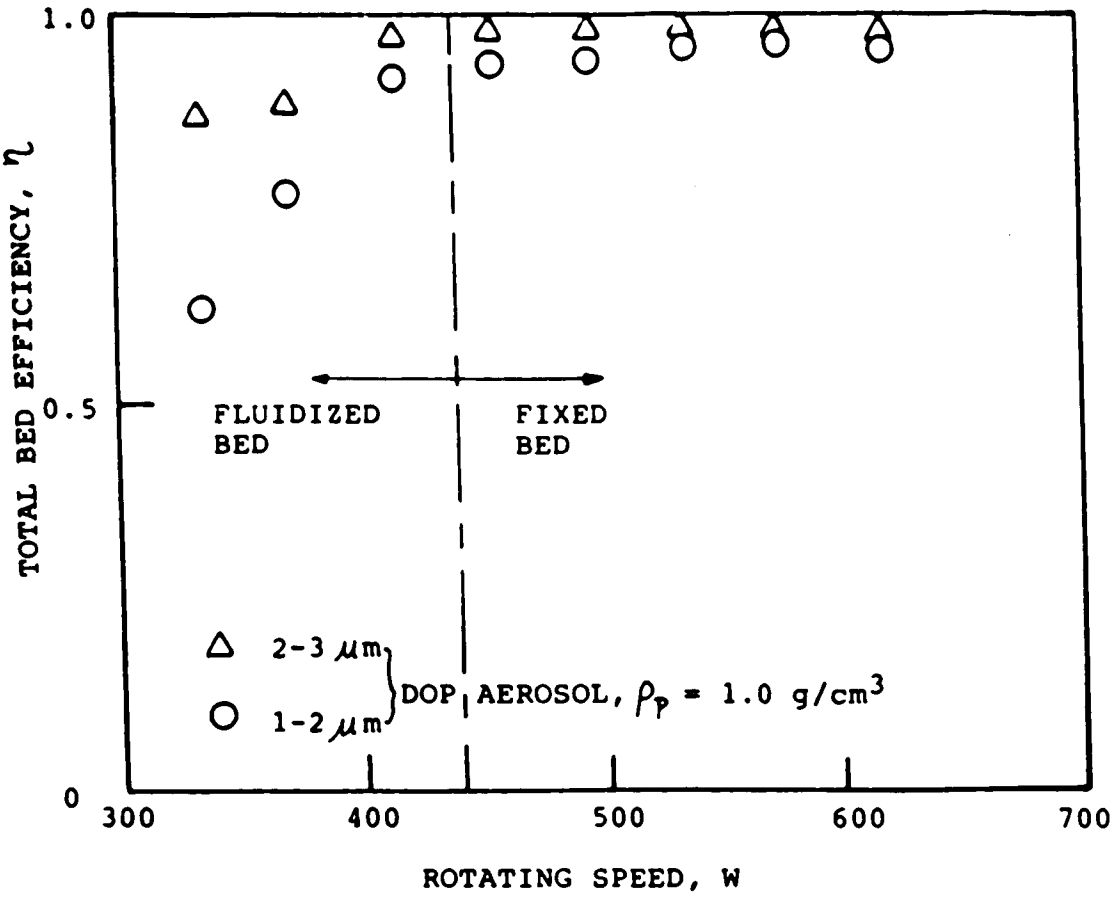

Figure A6. Total bed efficiency as a functional speed of the RFBF containing polypropylene granules.
Bed thickness, L = 3 cm;
Bed porosity, ε = 0.4;
Granule diameter, d_g = 0.3 cm;
Relative humidity, RHu = 40%;
Average velocity, U_o = 230 cm/sec.

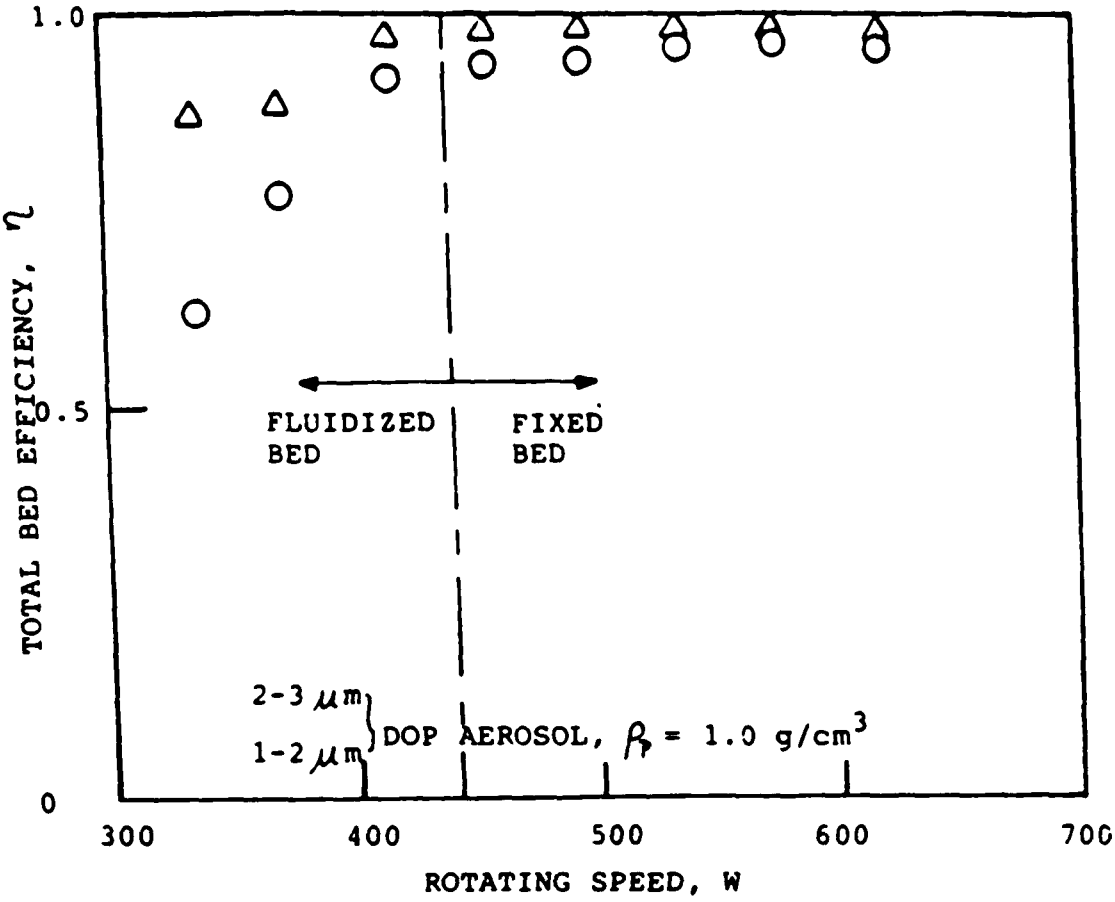

Figure A7. Total bed efficiency as a functional speed of the RFBF containing polyethylene granules.
Bed thickness, L = 3 cm;
Bed porosity, ε = 0.4;
Granule diameter, d_g = 0.3 cm;
Relative humidity, RHu = 40%;
Average velocity, U_o = 230 cm/sec.

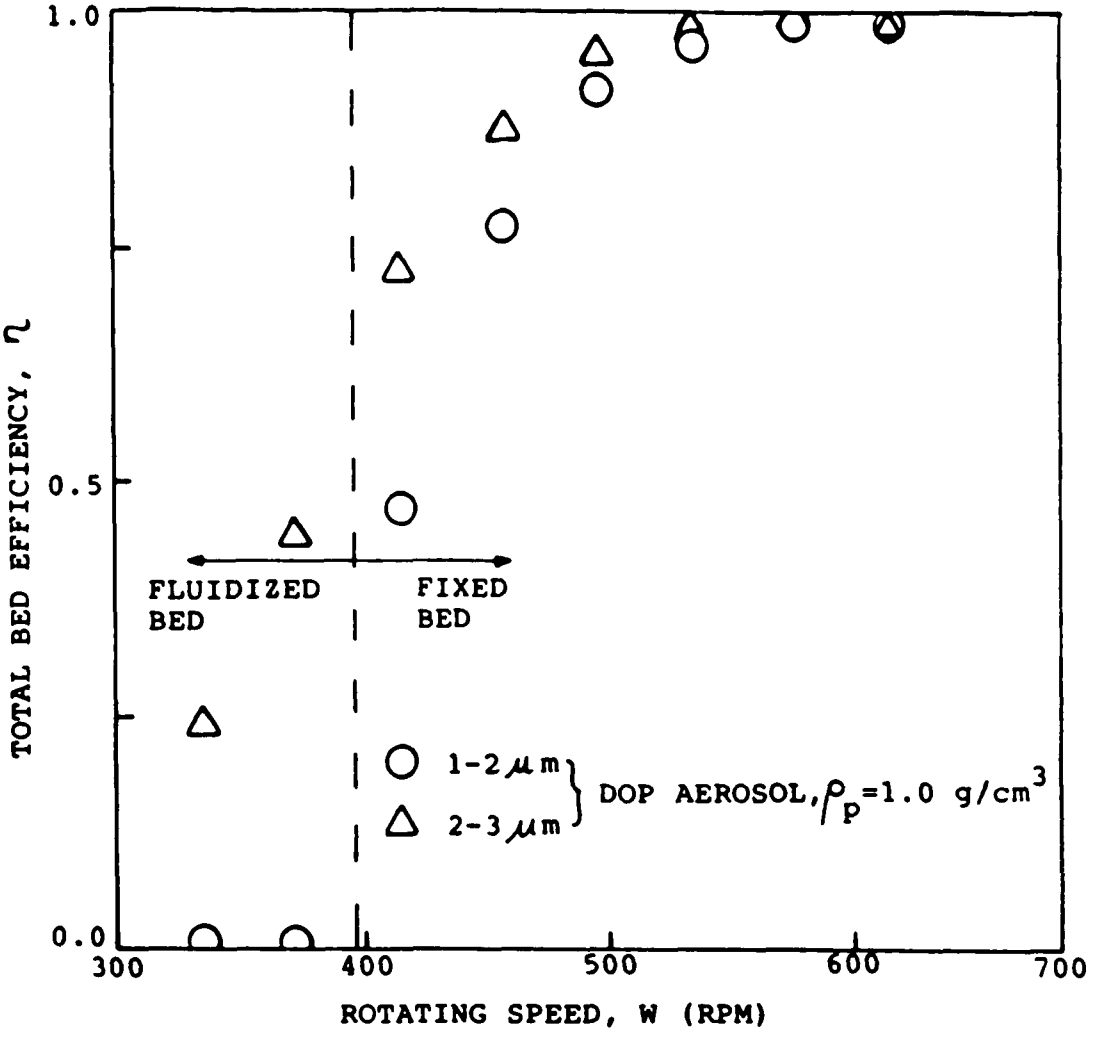

Figure A8. Total bed efficiency as a functional speed of the RFBF containing sand granules.
Bed thickness, L = 1.3 cm;
Bed porosity, ε = 0.46;
Granule diameter, d_g = 0.1 cm;
Relative humidity, RHu = 0 %;
Average velocity, U_o = 240 cm/sec.

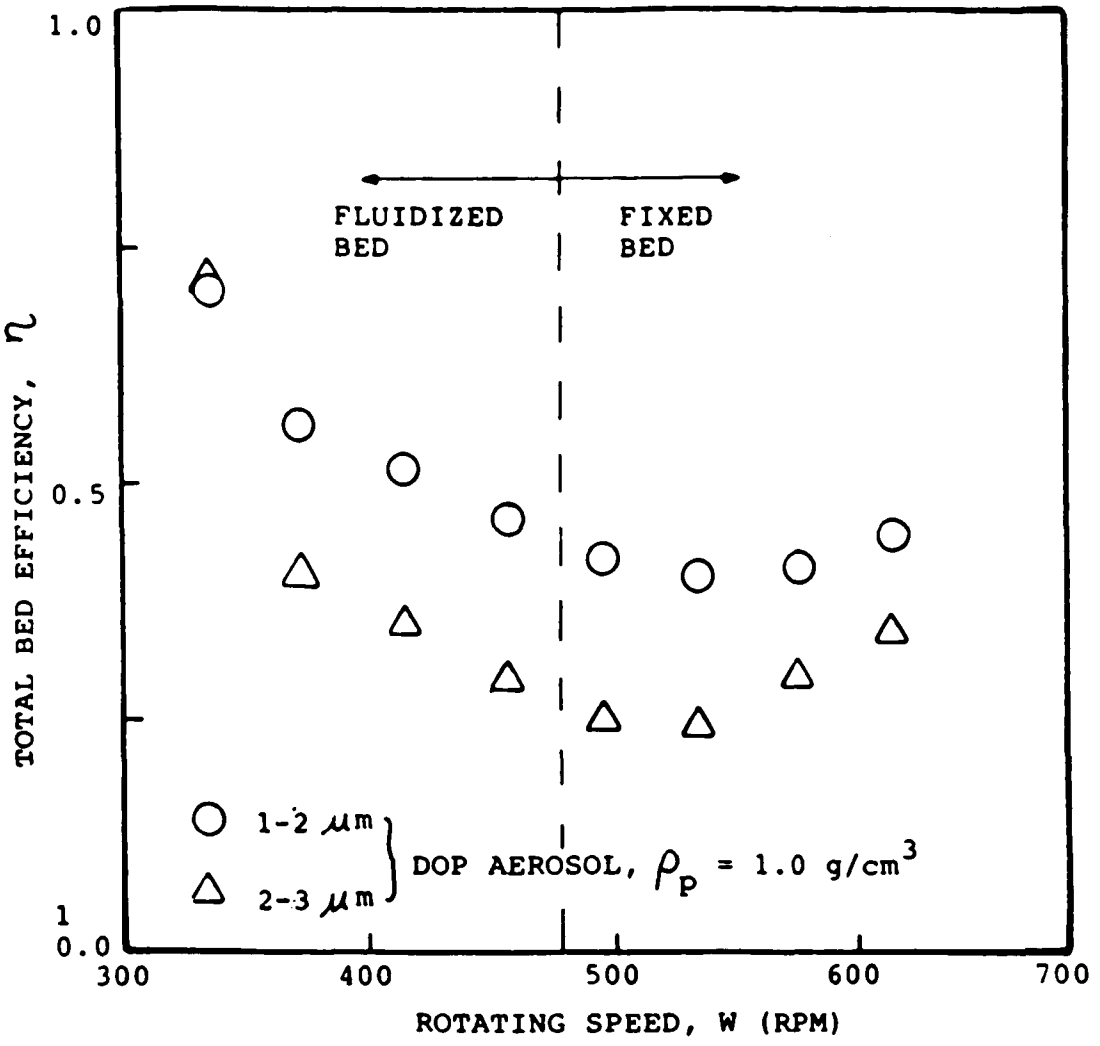

Figure A9. Total bed efficiency as a functional speed of the RFBF containing alumina granules.
Bed thickness, L = 0.6 cm;
Bed porosity, ε = 0.40;
Granule diameter, d_g = 150 μm;
Relative humidity, ^{g}RHu = 17 %;
Average velocity, U_o = 180 cm/sec.

we observed a completely different behavior (Figure A9) as compared to sand, polypropylene and polyethylene. This figure indicates that the efficiency for DOP aerosol particles in the range of 1-2 μm in diameter is higher than that of the 2-3 μm in diameter particles even though the filtration efficiencies for both size ranges are fairly constant over the entire range of rotating speed. This tendency can also be seen in Figure A4 at an average velocity of 180 cm/sec (5.9 ft/sec).

The Effect of Granule Size

Figure A5 shows that for a bed thickness, L=0.6 cm, the filtration efficiency (for 1-2 μm aerosols) obtained is much higher for the DOP coated alumina silicate granules than that of sand or polypropylene. At an average velocity of 120 cm/sec (3.9 ft/sec), the efficiency for alumina silicate, sand and polypropylene granules is 94%, 56% and 51% respectively (Figure A10). This is due to the fact that the alumina silicate granules have an average diameter of 0.015 cm as compared to sand of average diameter of 0.1 cm and to polypropylene of average diameter of 0.3 cm. Thus the alumina silicate granules have a much greater surface area in a given volume for the aerosol particles to come in contact with.

The Effect of Bed Thickness

As the the bed thickness increases, aerosol particles pass through more layers of bed material and the probability of them being captured also increases. Assuming that each granule experiences similar filtration phenomena, one can predict an exponential relationship between the total bed efficiency and the bed thickness based on the

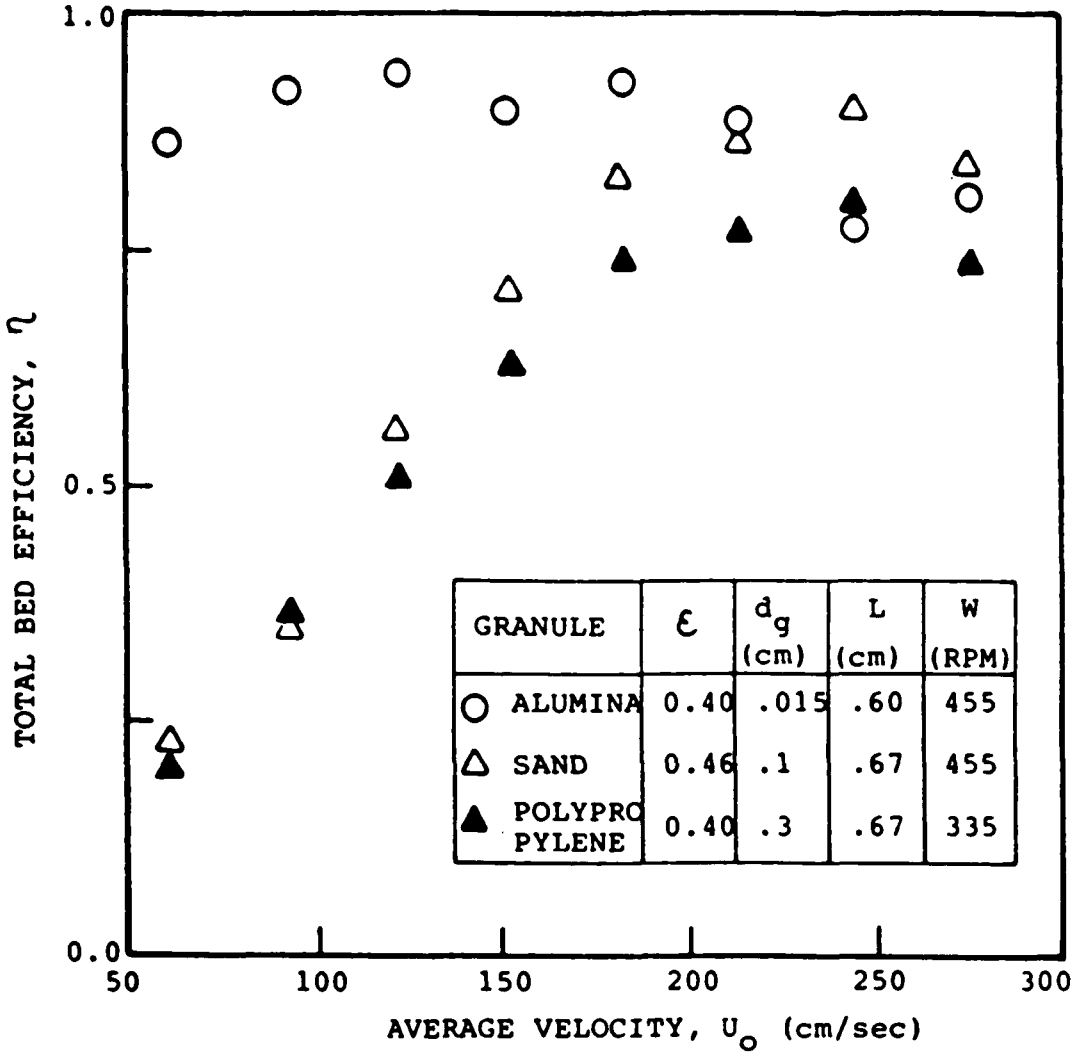

Figure A10. Total bed efficiency as a function of air velocity for different filter granules.
Relative humidity, RHu = 0-17 %;
Dust particle size, d_p = 1-2μm.

semi-empirical expression commonly used for the total bed efficiency, η, which is given as:

$$\eta = 1 - \exp [-K_1 (1 - \epsilon) (L/d_g)E] \qquad (A2)$$

where E is the single sphere efficiency, defined as the ratio of the number of dust particles in the gas reaching and sticking to a single granule to the number of dust particles approaching it, ϵ is the bed porosity, K_1 is a constant, L is the bed thickness and d_g is the granular diameter. In Figures A11 and A12, total bed penetration, which is defined as $1-\eta$, is shown as a function of bed thickness for sand and polypropylene granules. The curves in Figure A11 are linear as expected from equation (A2) up to a bed thickness of about 1-1.5 cm. However, the slope changes somewhat as the thickness increases.

This phenomenon of lower than expected efficiency especially near the free surface of a thicker bed and at high velocities, can be explained by the non-uniformity of the fluidization in the rotating fluidized bed. As the air flows radially inward through the distributor and into the bed of granules, the cross-sectional area becomes smaller and the average gas velocity increases. In addition, radial acceleration and centrifugal forces close to the free surface are smaller than those close to the distributor adding to the non-uniformity of fluidization. Thus while the bed operates, on the average, near minimum fluidization velocity or even in the fixed bed region, the surface may, in fact, be in bubbling fluidization with a much lower efficiency than the rest of the bed. The deviation from

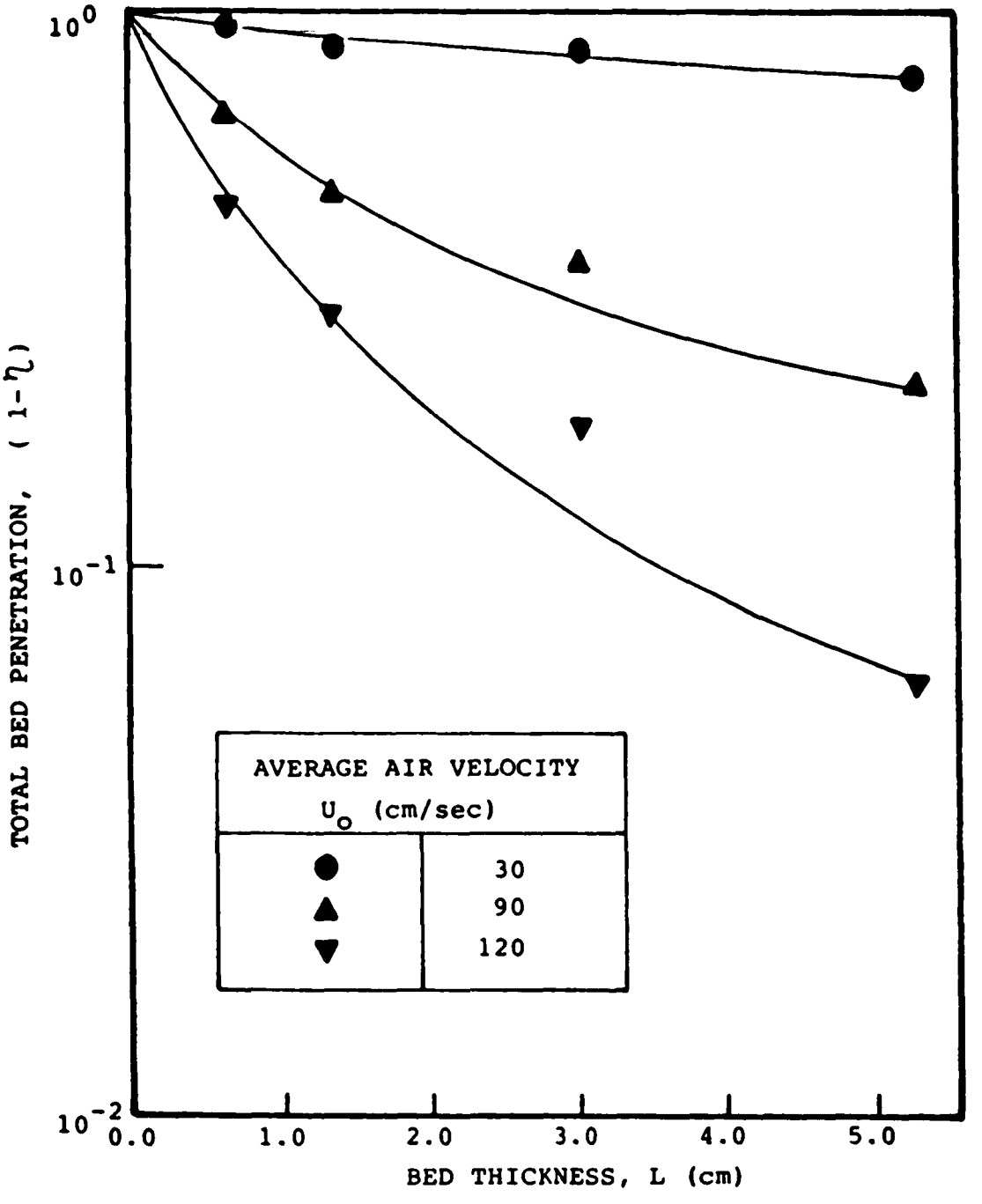

Figure A11. Total bed penetration as a function of bed thickness at different velocities in the RFBF containing sand granules.
Granule diameter, d_g = 0.1 cm;
Bed porosity, ϵ = 0.4;
Relative humidity, RHu = 0-10 %;
Rotating speed, W = 455 RPM;
DOP particle diameter, d_p = 1-2μm.

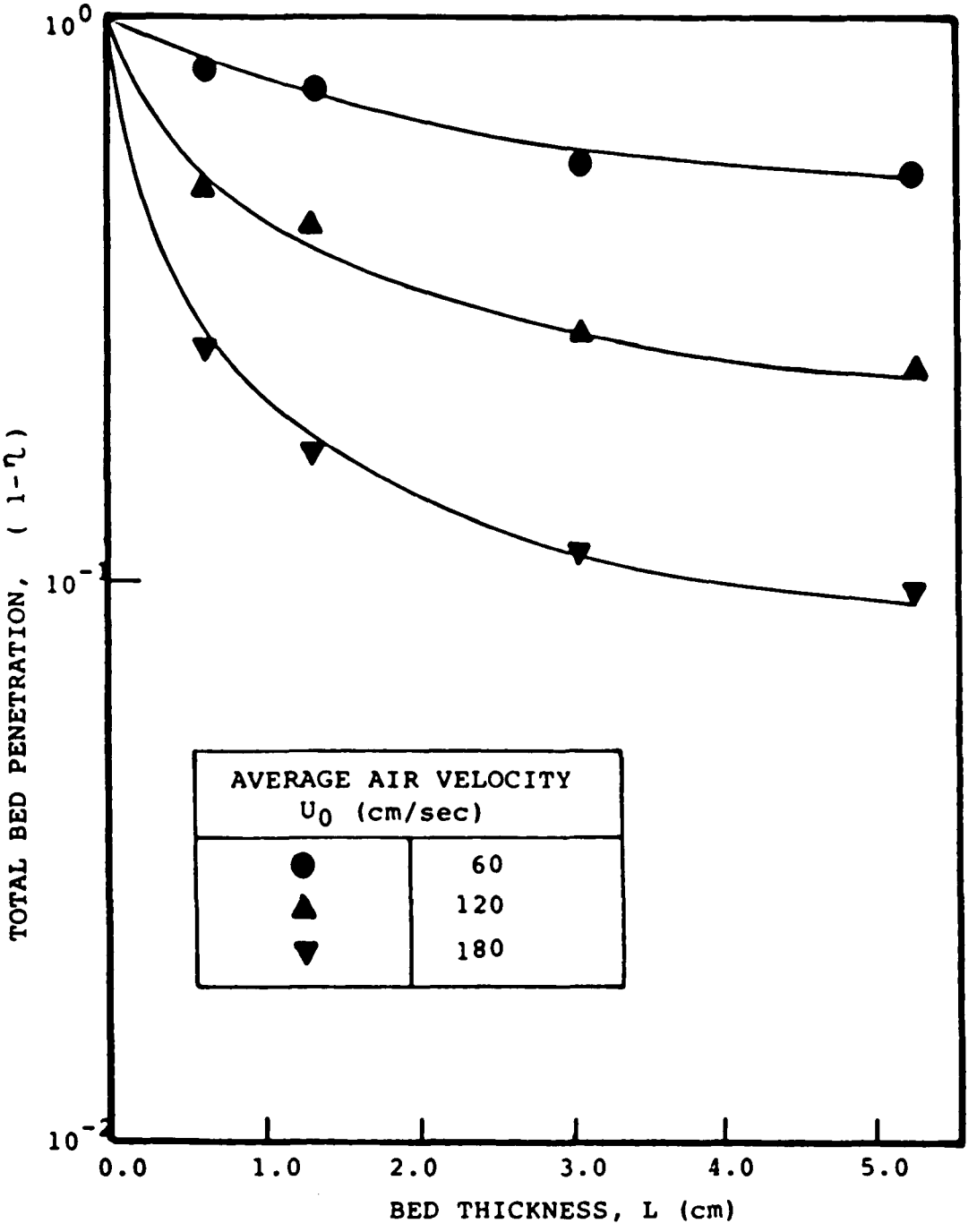

Figure A12. Total bed penetration as a function of bed thickness at different velocities in the RFBF containing polypropylene granules.
Granule diameter, d_g = 0.3 cm;
Bed porosity, ε = 0.4;
Relative humidity, RHu = 0-10 %;
Rotating speed, W = 335 RPM;
DOP particles diameter, d_p = 1-2μm.

linearity is even more pronounced in Figure A12 using polypropylene granules.

The effect of bed thickness on the pressure drop across the granular bed for 0.1 cm diameter sand granules is very large and is shown in Figure A13. At an average velocity of 90 cm/sec (3.0 ft/sec), the pressure drop across the bed thickness of 1.39 and 3.05 cm is 2.0 and 4.7 gr/cm^2, respectively, or an increase of 135% whereas the total filtration efficiencies at this velocity are 53 and 63% for 1-2 μm in diameter DOP particles, or an increase of 19% (Figure A14). However at 150 cm/sec (4.9 ft/sec), there is a 171% increase in pressure drop (from 5.5 to 14.9 gr/cm^2) while there is virtually no increase in overall efficiency. At still higher velocity, at constant rotational speed, it is observed that the efficiency for the thicker beds (3-5 cm) drops quickly to zero because it now has exceeded the minimum fluidization velocity. At a velocity of 210 cm/sec (6.9 ft/sec), the filtration efficiency of the 1.39 cm thick bed yields the highest efficiency of 96% as compared with 86% for the 0.67 cm thick bed (or an increase of 12% in efficiency) coupled with a 190% increase in pressure drop (from 4.0 to 11.6 gr/cm^2).

The Effect of Aerosol Size

Lexan granules were used as the filter medium in these experiments in order to gather data on the performance of a wide range of materials. Previously we have tested the following types of granules: polyethylene, polypropylene, sand and alumina. With the exception of the alumina, we have found that the efficiency of the RFBF increases with increasing air velocity in the fixed bed region, reaches a value

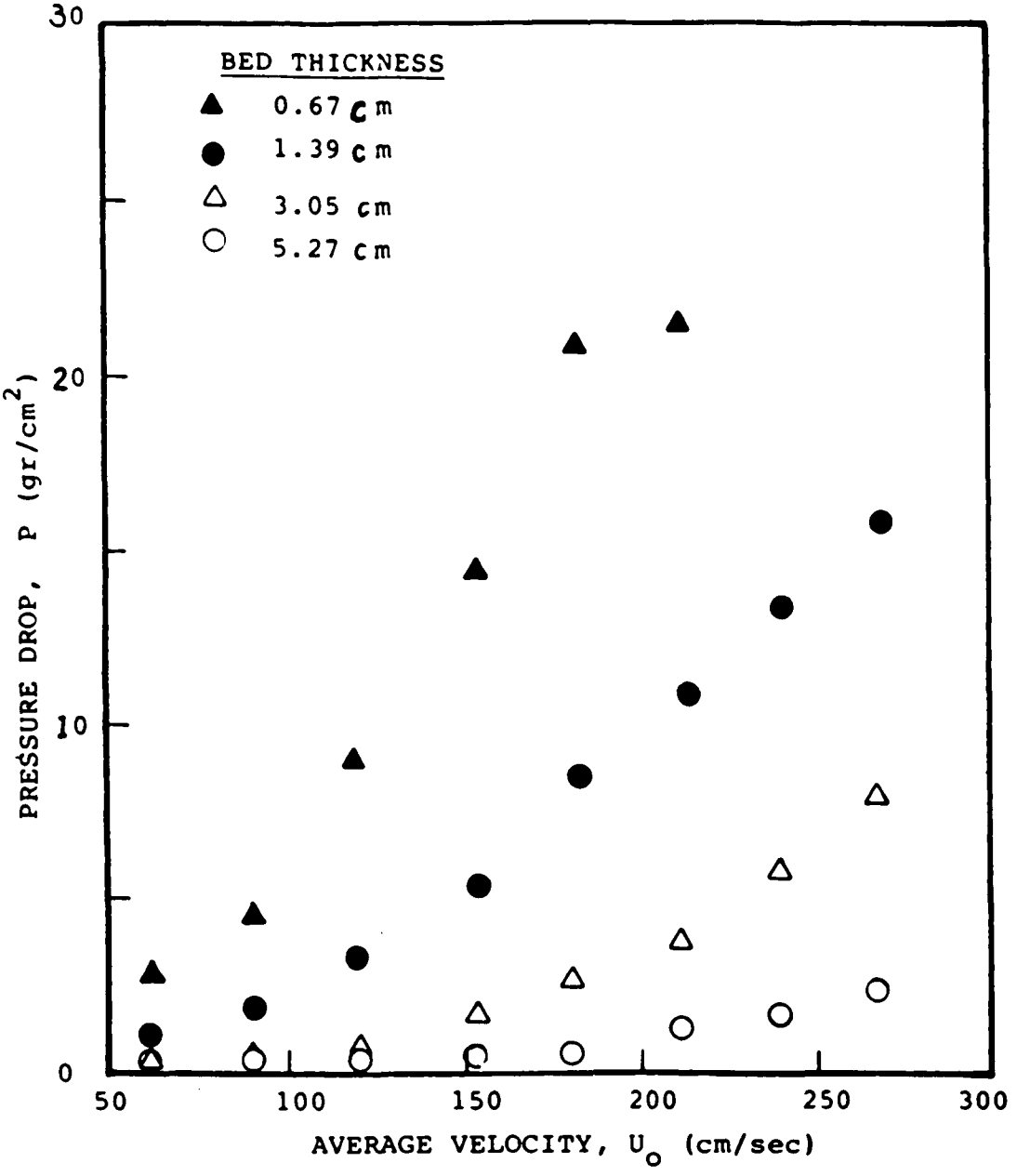

Figure A13. Pressure drop in the RFBF containing 0.1 cm in diameter sand granules as a function of air velocity. Bed porosity, $\varepsilon = 0.46$; Rotating speed, W = 455 RPM.

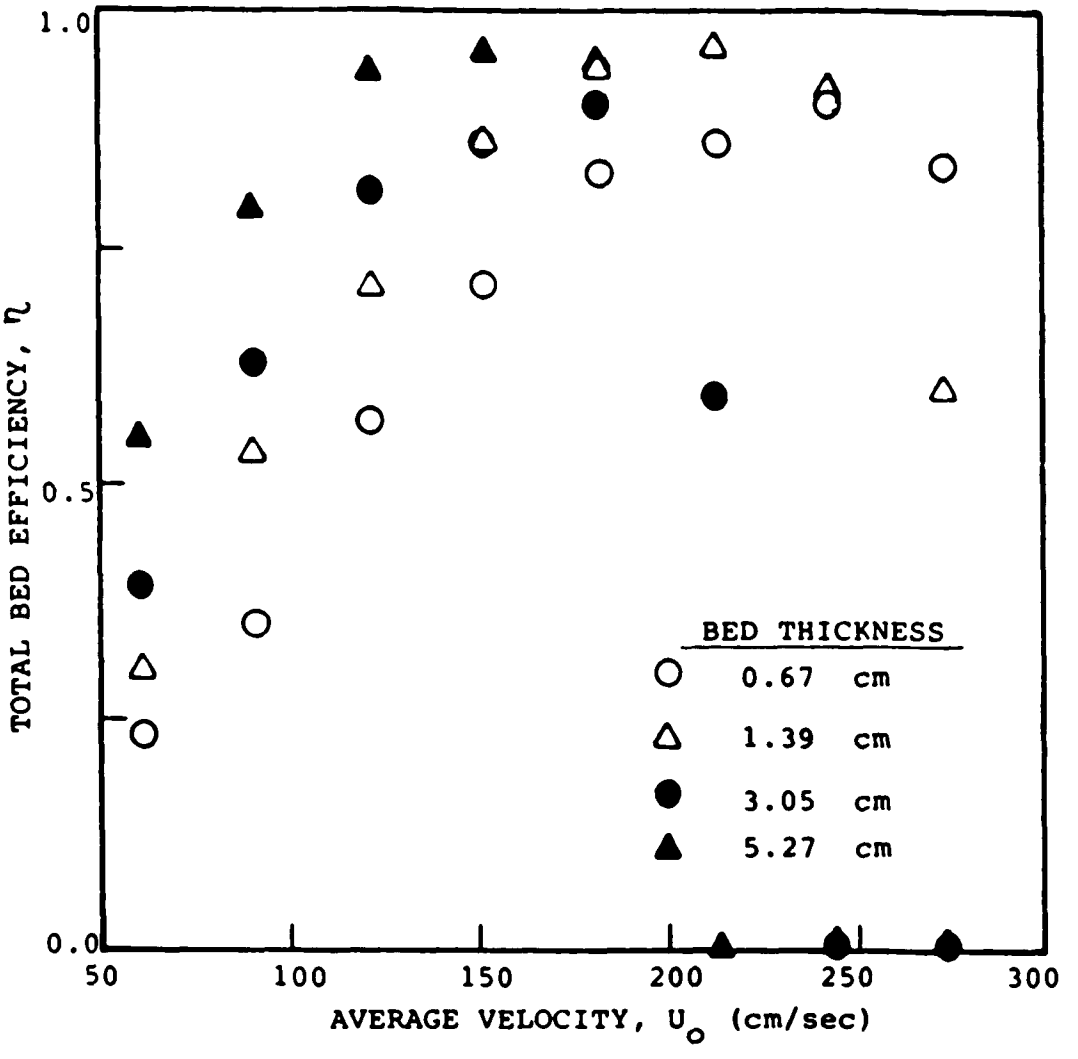

Figure A14. Total bed efficiency of the RFBF containing 0.1 cm in diameter sand granules as a function of air velocity.
Bed porosity, ε = 0.46;
Rotating speed, W = 455 RPM;
Dust particle size, d_p = 1-2 μm.

very close to the maximum efficiency at minimum fluidization conditions and then decreases when the bed becomes fluidized. Further increase in air velocity in the fluidized bed region reduces the filtration efficiency sharply due to aerosol by-passing the bed granules and/or reentrainment of aerosol due to the high velocity gas stream.

Using the Lexan granules (Figure A15), it is observed that the filtration efficiency for DOP aerosol particles increases with increasing air velocity and attains an efficiency of over 90% for particles larger than 1 μm at minimum fluidization conditions. Notably for 1-2 μm DOP particles, the efficiency increases from 44% to 95% as the air velocity increases from 90 to 230 cm/sec (3.0 to 7.5 ft/sec). For larger aerosol particles, the efficiency remains over 90% in this range of air velocity. Therefore the granular bed operating at minimum fluidization conditions, can be assumed to act almost as an absolute filter for particles larger than 1 μm. However for smaller particles, the efficiency remains relatively low even at high air velocity. This is due to the low inertia of the smaller particles and will be discussed in the later section. It can also be observed that as the air velocity is reduced, the filtration efficiency drops rapidly for particles smaller than 2 μm.

Figure A16 shows the filtration efficiency as a function of the rotating speed. In the fixed bed region, the filtration efficiency is independent of bed rotation for all aerosol sizes. However, at the given air velocity, the bed changes from a fixed to a fluidized bed as rotating speed decreases. It is again observed as previously reported that at minimum fluidization conditions, the total bed filtration efficiency is about the same as the efficiency obtained in the fixed bed region. The filtration efficiency decreases slightly as the

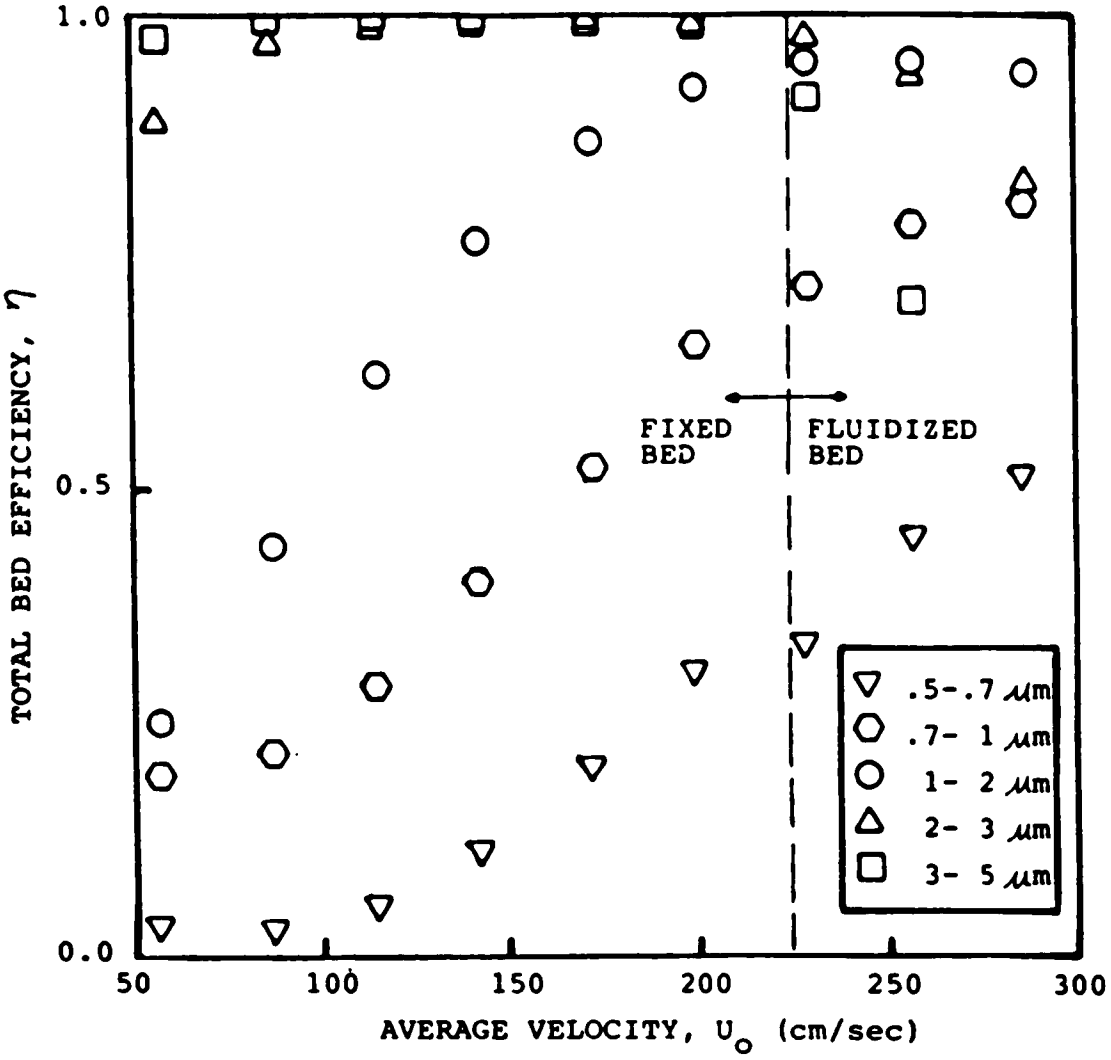

Figure A15. Total bed efficiency as a function of air velocity for DOP aerosol (ρ_p = 1.0 g/cm3) in a RFBF containing 0.3 cm diameter LEXAN granules.
Bed thickness, L = 3 cm;
Bed porosity, ϵ = 0.4;
Rotating speed, W = 370 RPM;
Relative humidity, RHu = 30%.

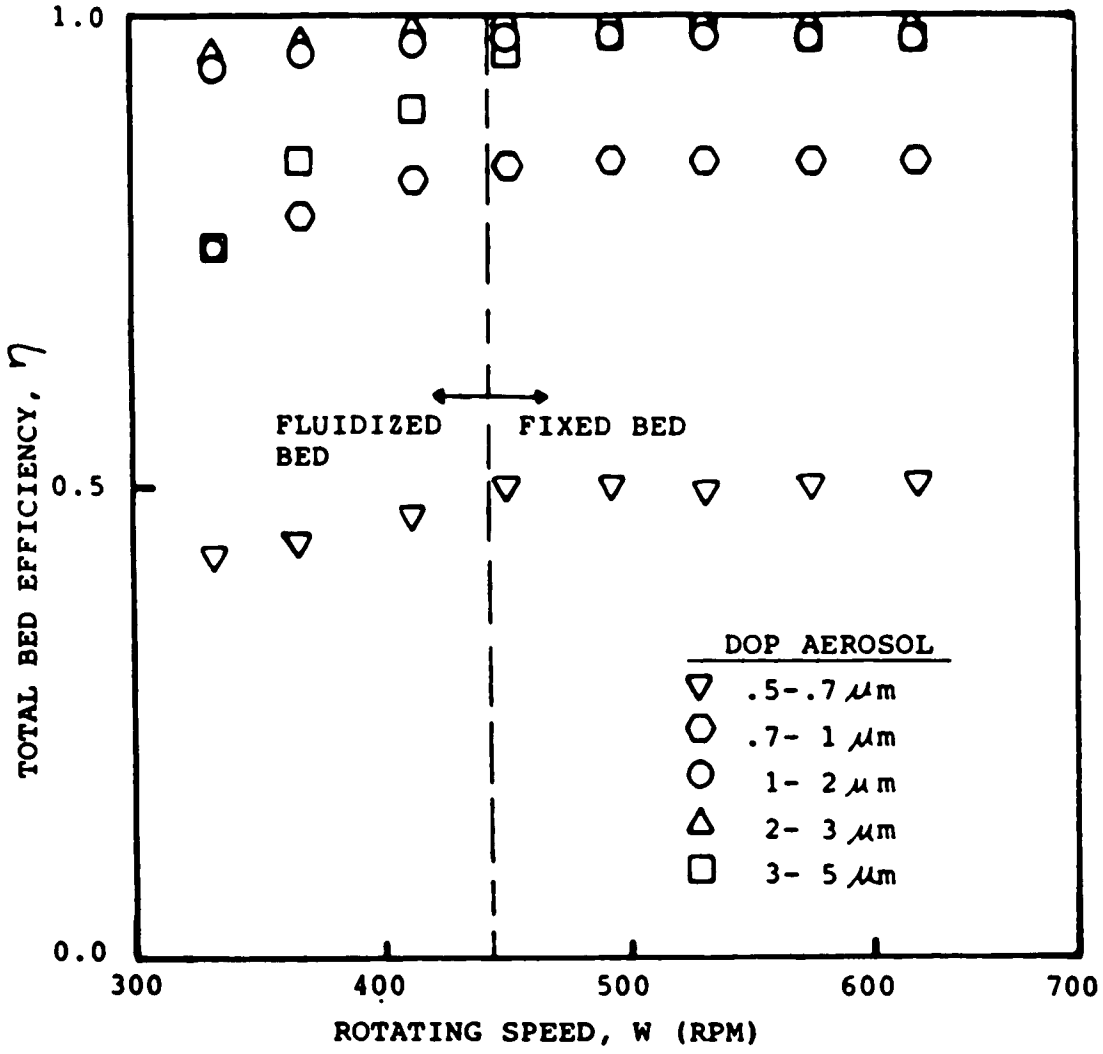

Figure A16. Total bed efficiency as a functional speed of the RFBF containing 0.3 cm diameter LEXAN granules.
Bed thickness, L = 3 cm;
Bed porosity, ϵ = 0.4;
Relative humidity, RHu = 30%;
Average velocity, U_o = 260 cm/sec.

rotation is further reduced; however any further reduction in the rotating speed will result in some bubble formation which in turn will reduce the efficiency significantly. Therefore, in a continuous process, it is advantageous to operate the bed at just above the minimum fluidization where the efficiency is about the same as in a packed bed but the filter granules can be continuously introduced and discharged from the bed because of the fluidized state.

The Effect of Particle Concentrations

Figure A17 shows that the total bed filtration efficiency of DOP aerosol particles of size range 1-2 μm and 2-3 μm remains constant as the DOP aerosol concentration is varied by about 2-3 orders of magnitude. This can be attributed to the fact that DOP aerosol, being sticky, forms a strong adhesion with the granules' surface and consequently no bouncing, which causes a reduction in the filtration efficiency, is observed.

The Effect of Inertia

Inertial effects in a regular fluidized bed are similar to those in a fixed bed and both types of filters are governed by the same set of parameters which control the filtration efficiency. Those parameters are: air velocity, granule size, Reynolds number, aerosol density and the size of the aerosol particles. Using the same set of parameters, experiments were performed to study the filtration efficiency in the RFBF; electrostatic effects are considered negligible at a relative humidity of 30% or higher. Furthermore, DOP was used in the experiments so that bouncing is not a major factor in determining filtration efficiency. Consequently, the efficiency

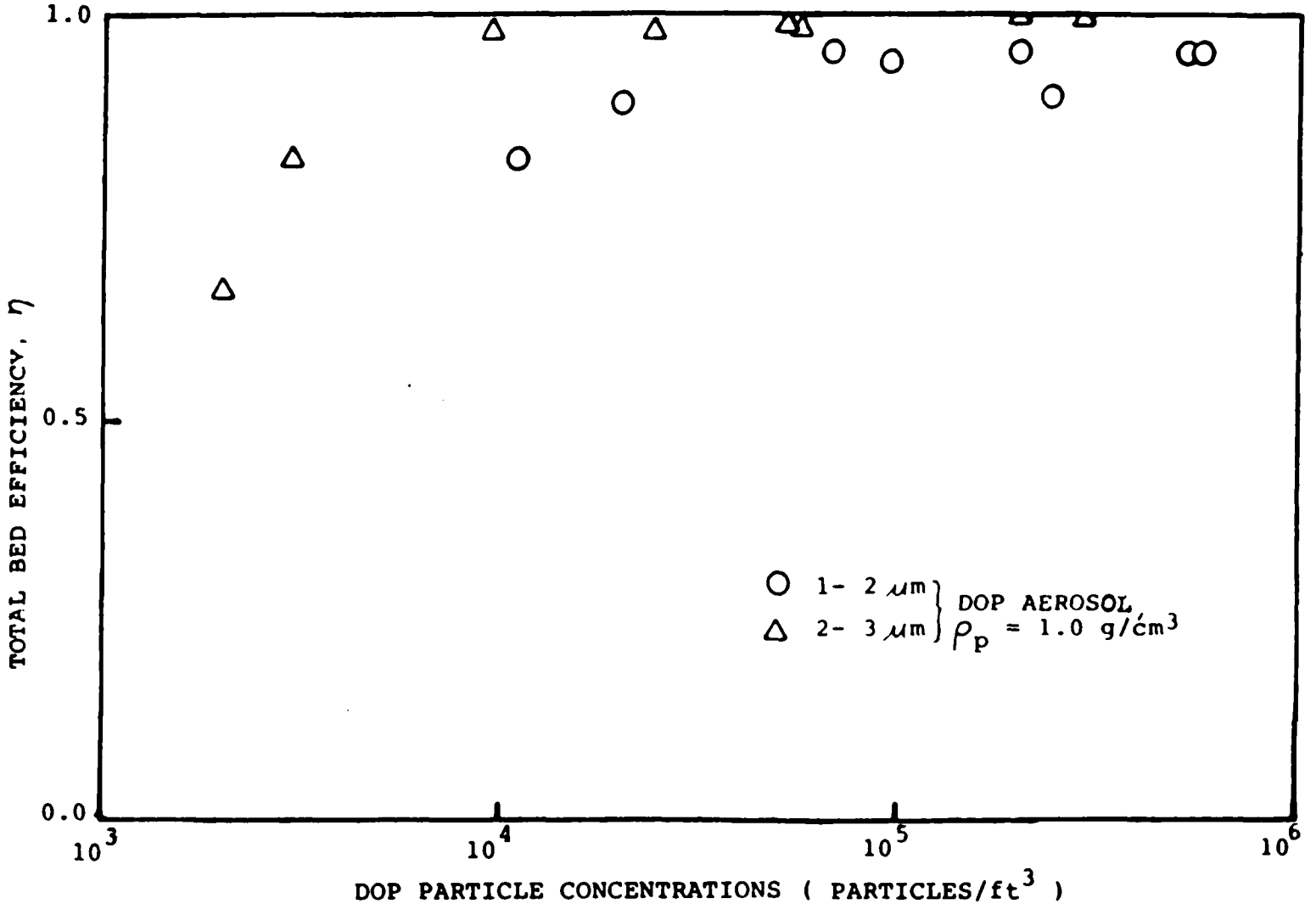

Figure A17. Total bed efficiency as a function of aerosol concentration in the RFBF containing 0.3 cm diameter LEXAN granules. Bed thickness, L = 3 cm; Bed porosity, ϵ = 0.4; Rotating speed, W = 370 RPM.

observed is largely due to the effects of inertia. Figure A18 shows the filtration efficiency as a function of the Stokes number, St. This is a dimensionless parameter which characterizes inertial effects and is given as:

$$St = \frac{2 \rho_p r_p^2 U_o C}{9 \mu a} \qquad (A3)$$

where ρ_p is the density of DOP, r_p is the radius of the aerosol particle, U_o is the average air velocity, C is the Cunningham correction factor, μ is the air viscosity, and a is the radius of the filter granule. The filtration efficiency shown in Figure A18 is caused mainly by inertial effects which are dominant in these experiments. It is clear that particles smaller than 1 μm have a very low Stokes number which verifies our conclusion that the low filtration efficiency observed is due to the small inertia of these particles. The apparent "tails" to the left of Figure A18 is due to the contribution of other filtration mechanisms, such as diffusion rather than inertia, which becomes dominant at the low end of the Stokes number. Thus, it is clear that in order to obtain a higher filtration efficiency in granular bed filters for particles smaller than 1 μm, mechanisms other than inertial effects must be utilized.

In the granular bed filtration process, the dusty gas flows through a bed of granules on which dust particles are captured. The total bed filtration efficiency can thus, in principle, be predicted if the trajectories of all aerosol particles travelling inside the bed are known assuming that aerosol particles deposited on the granule's

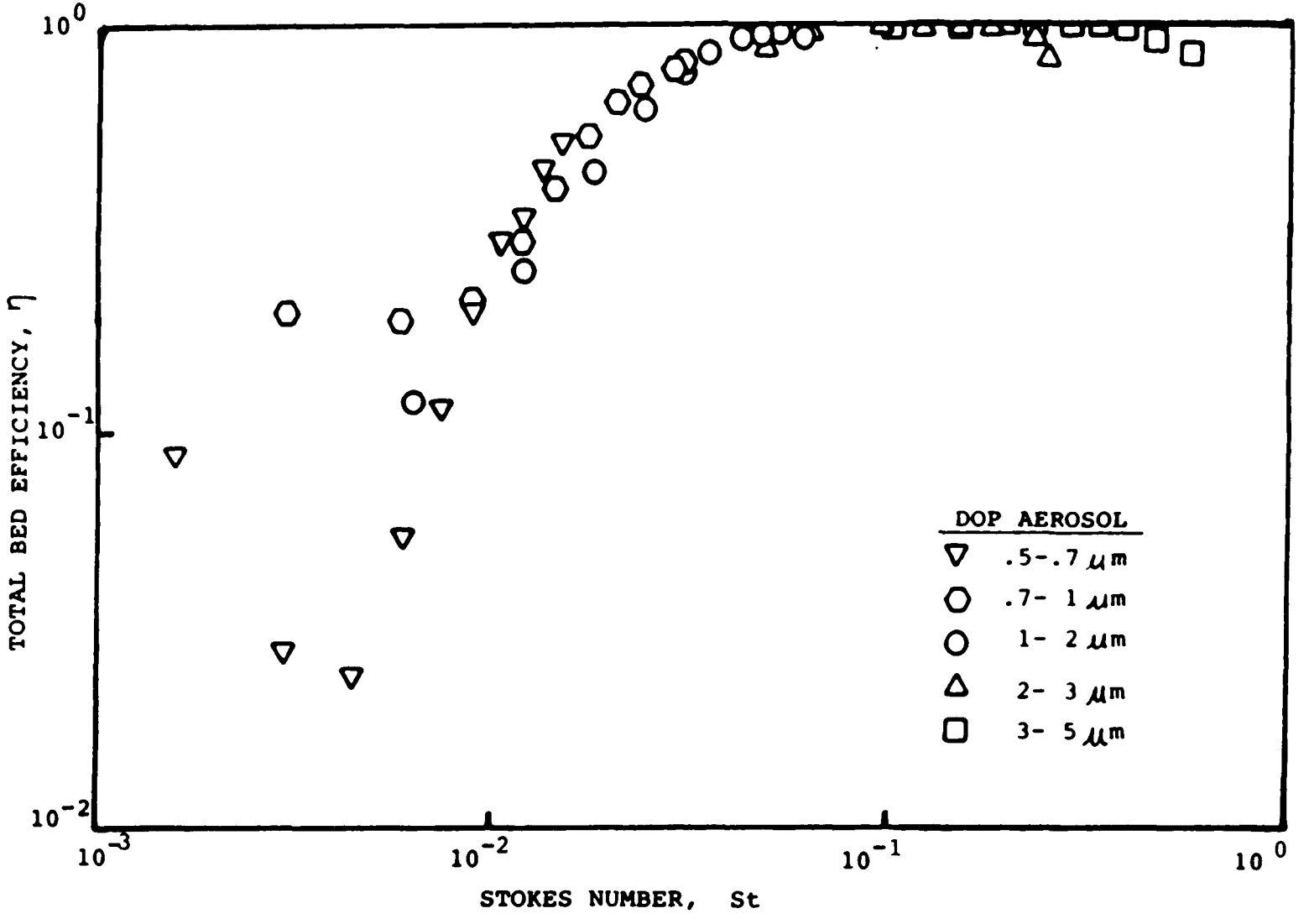

Figure A18. Total bed efficiency as a function of the Stokes number, St, in the RFBF containing 0.3 cm diameter LEXAN granules. Bed thickness, L = 3 cm; Bed porosity, ϵ = 0.4; Rotating speed, W = 370 RPM; Relative humidity, RHu = 30%.

surface do not bounce off. Therefore, the prediction of filtration efficiency is basically the prediction of the trajectories of aerosol particles in the bed; an aerosol particle whose center approaches the surface of a granule to within a distance equal to its radius is said to be collected.

The general equation of motion of a small particle of radius, r_p in a velocity field can be obtained simply from Newton's law by assuming Stokesian drag on the particle (Paretsky et al., 1971):

$$m_p \frac{d^2\vec{x}}{dt^2} = \frac{6\pi\mu r_p}{C} \left(\vec{u} - \frac{d\vec{x}}{dt} \right) + \vec{F}_{ext} \qquad (A4)$$

where $\vec{x}$ is the position vector, $\vec{u}$ is the air velocity, μ is the air viscosity, r_p and m_p are the particle's radius and mass respectively, C is the Cunningham correction factor and $d^2\vec{x}/dt^2$ and $d\vec{x}/dt$ are the particle's acceleration and velocity, respectively. In equation (A4), the first term on the right-hand side is the drag force, while $\vec{F}_{ext}$ is the sum of all other forces acting on the particle travelling inside the bed such as gravitational and electric forces. The motion of an aerosol particle in a granular bed depends on its shape and size, its initial velocity, the flow field in which it travels, the external forces acting on it, and the obstacles in its path. When these parameters are known, the trajectories of the particles travelling inside the bed can, in principle, be computed.

When the bed and aerosol particles are electrically neutral and diffusional and gravitational effects are negligible, inertia becomes the dominant mechanism of filtration and equation (A4) is reduced to:

$$\frac{d^2\vec{x}}{dt^2} = \frac{6\pi\mu r_p}{m_p C}\left(\vec{u} - \frac{d\vec{x}}{dt}\right) . \qquad (A5)$$

In dimensionless form, the equation of motion is:

$$\frac{d^2\vec{X}}{dT^2} = \frac{1}{St}\left(\vec{U} - \frac{d\vec{X}}{dT}\right) \qquad (A6)$$

where the dimensionless parameters are:

$$\vec{X} = \frac{\vec{x}}{a} \quad , \quad T = \frac{tU_o}{a} \quad , \quad \vec{U} = \frac{\vec{u}}{U_o}$$

and the Stokes number, $St = \dfrac{2\rho_p r_p^2 U_o C}{9\mu a}$

where a is the radius of the granule and U_o is the air superficial velocity.

The trajectory of a particle through an entire granular bed is still very difficult to compute from equation (A6) even if only inertia is considered. To simplify the problem further, it is assumed that every filter element experiences similar filtration phenomena and therefore a single particle efficiency, E, can be defined. This quantity is the ratio of the number of aerosol particles in the air stream captured by a filter element of radius, a, to the number of

aerosol particles approaching the element. Using this approach the filtration efficiency of the entire bed of granules, η, can be computed by summing the effect of all the elements in the filter. The semi-empirical expression commonly used for η is (Snaddon and Dietz, 1980):

$$\eta = 1 - \exp(-1.5 (1-\epsilon) (\frac{L}{2a}) E) \qquad (A7)$$

where ϵ is the bed porosity, L is the bed thickness, a is the filter element's radius and E is the single sphere efficiency.

Lately, a number of researchers have developed empirical correlations for the single sphere efficiency for packed bed conditions especially for the region where inertial effects are dominant; some of these correlations are given in Table A1. Comparisons between the various models predicting the single sphere efficiency in the RFBF containing 0.3 cm diameter polyethylene granules with experimental data recomputed from Figure 8 in section (II.3) using equation (A7) are shown in Figure A19 for DOP aerosols and Figure A20 for alumina dust.

Figure A19 indicates that Gal, Tardos and Pfeffer's filtration model (1985) agrees well with the experimental data in the range of modified Stokes numbers from 0.01 to 0.03. At larger modified Stokes numbers, Gal, Tardos and Pfeffer's theoretical correlations overestimate the filtration efficiency. There are various factors that contribute to this difference: a) at higher Stokes numbers, the Reynolds numbers are also higher due to the larger air velocities and the flow field assumed in the model becomes less accurate; b) bouncing may also contribute to the lower filtration efficiency observed. Bouncing increases as the kinetic energy of the aerosol increases

TableA1: Empirical correlations for Single Sphere Efficiency, E

Authors	E	Range
Thambimuthu et al. (1978)	$10^5 \times St^3$	$0.001 < St < 0.01$
D'Ottavio and Goren (1983)*	$\frac{St_{eff.}^{3.55}}{1.67 + St_{eff.}^{3.55}}$	$13 < Re < 1650$ $0.33 < \epsilon < 0.38$
Gal, Tardos and Pfeffer (1985)#	$\frac{2St'^{3.9}}{4.3\times10^{-6} + St'^{3.9}}$	$0.01 < St' < 0.03$

$$St = \frac{2\rho_p r_p^2 U_o C}{9\mu a}$$

* $St_{eff.} = f(Re,\epsilon) \times St$

$f(Re,\epsilon) = (1-a^{5/3})/(1-1.5a^{1/3}+1.5^{5/3}-a^3) + 1.14Re^{0.5}(1-a)^{-3/2}$

where $a = 1-\epsilon$

$St' = f(Re,\epsilon) \times St$

$f(Re,\epsilon) = 1 + 1.75Re/150(1-\epsilon)$

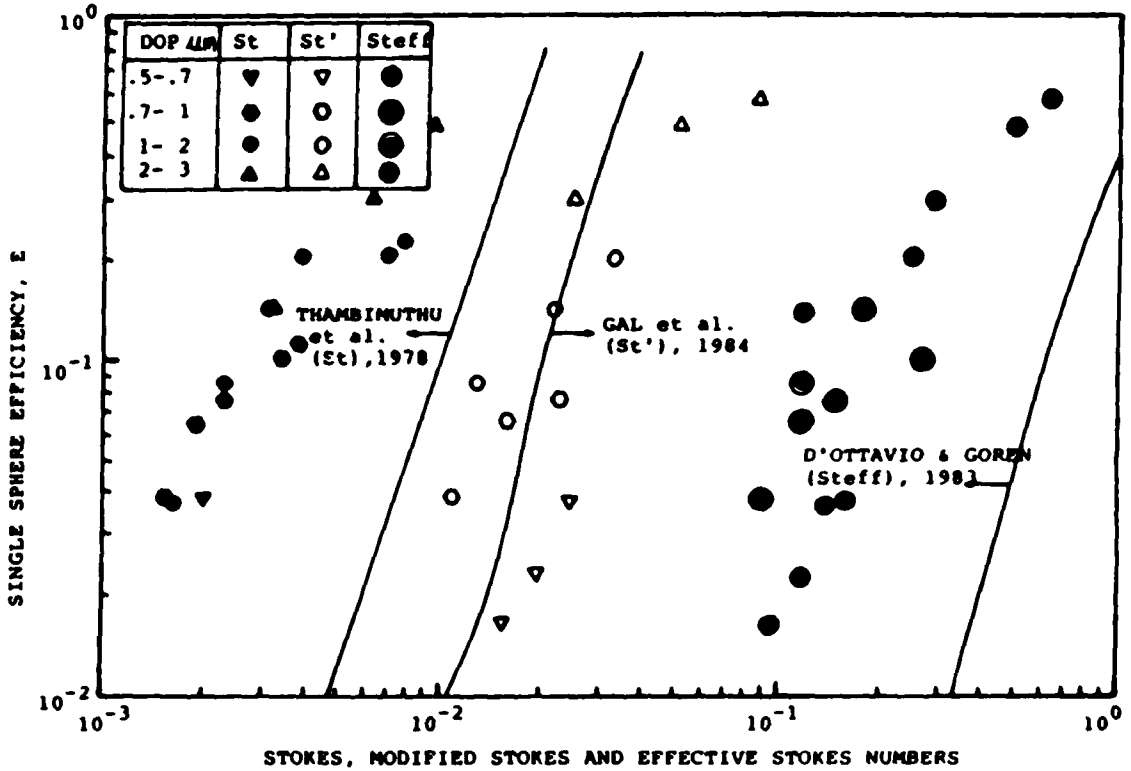

Figure A19. Single sphere efficiency for DOP aerosol as a function of Stokes, modified Stokes and effective Stokes numbers using 0.3 cm diameter polyethylene granules. Bed thickness, L = 3 cm; Bed porosity, ϵ = 0.4, Rotating speed, W = 345 RPM; Relative humidity, RHu = 45-47 %.

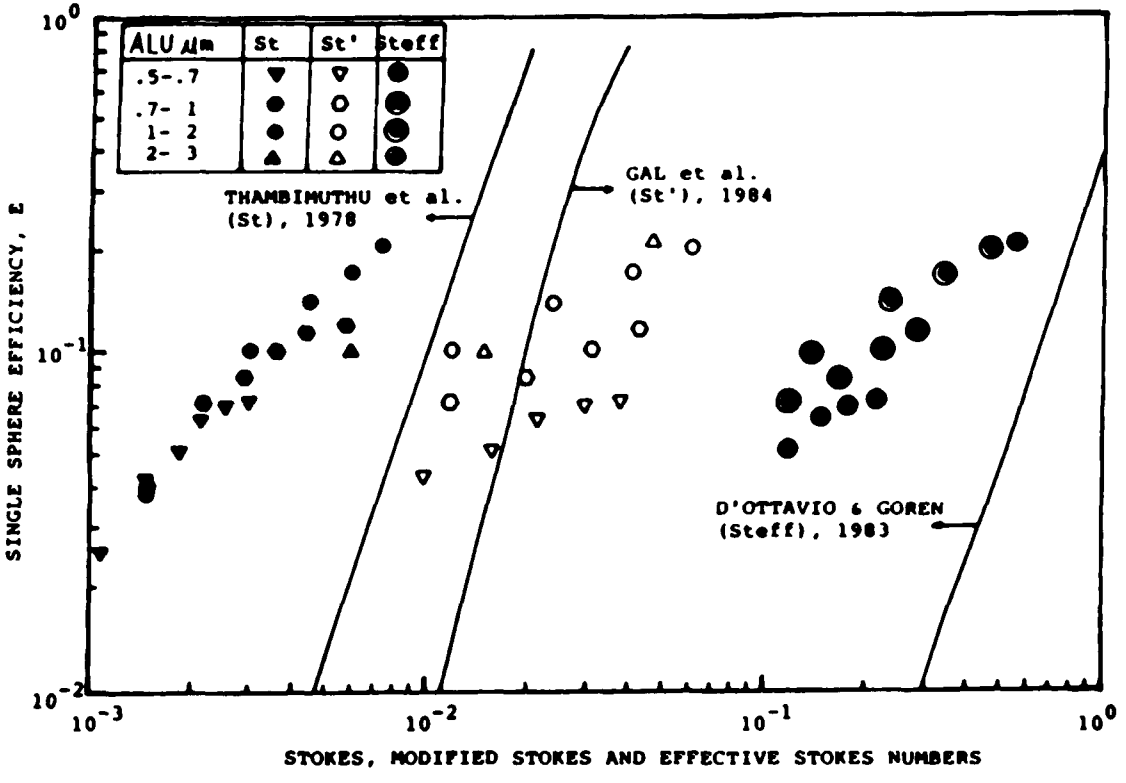

Figure A20 *Single sphere efficiency for alumina dust as a function of Stokes, modified* Stokes and effective Stokes numbers using 0.3 cm diameter polyethylene granules. Bed thickness, L = 3 cm; Bed porosity, ϵ = 0.4; Rotating speed, W = 345 RPM; Relative humidity, RHu = 45-47 %.

(D'Ottavio and Goren, 1983). Thus at higher values of the modified Stokes number, St', where the kinetic energy of the alumina dust is high (the mass of alumina dust is almost twice that of DOP), the deviation of the experimental results from the model is more significant as shown in Figure A20; c) the entrainment of aerosol particles already captured on the granules by the high velocity air and possibly by bubble formation in the RFBF when the air velocity exceeds the critical minimum fluidization may also contribute to the lower efficiency observed.

D'Ottavio and Goren calculate the trajectories of aerosol particles as they flow past an isolated sphere using a sphere-in-cell model. These authors are successful in predicting the general trend of the filtration efficiency as a function of the Stokes number but underestimate the filtration efficiency and the effect of the Reynolds number. The correction factor to the Stokes number in this calculation depends on $Re^{0.5}$ (see Table A1) so that the experimentally calculated effective Stokes numbers, $St_{eff.}$ are smaller than the correlation predicts and most experimental points fall to the left of the correlation curve. The correlation by Thambimuthu et al. (1978) also underestimate the filtration efficiency for the experimental data presented here.

A.2. THE INFLUENCE OF ELECTROSTATIC CHARGES

In addition to diffusion, gravitation and inertial effects which all are purely mechanical filtration mechanisms, there exists another class of capture process which results from the attraction or repulsion between electrostatic charges or image of charges on the bed granules and the aerosol particles.

Many experimental and theoretical studies (Kirsh, 1972; Nielsen and Hill, 1976; Dietz, 1981) have shown that electrical forces can significantly enhance the collection efficiency of fine particles in granular beds and fibrous filters. The electrical forces become considerably important in the range of low Stokes numbers (low air velocity and/or small aerosol particles) where inertial effects are negligible and the filtration efficiency is low. A fluidized bed may be electrically charged by an external electric field or by triboelectrification. Triboelectrification, or electrostatic charging of the fluidized granules and of the container, is a common phenomenon in an operating fluidized bed arising from collision between granules and between granules and the wall of the container during fluidization. The effect is more pronounced when the fluidized granules and the fluidization vessel is not grounded (Tardos and Pfeffer, 1980). The electrostatic charge on the granules depends on the granular material and the air humidity which determines the rate of charge relaxation. Increasing humidity increases conductivity (Zahedi and Melcher, 1976) and thus reduces the charge relaxation time. All electrostatic charges generated during our experiments are due to triboelectrification and no external electric field is applied.

The effect of humidity

Figure A21 shows the single sphere efficiency of DOP aerosol and alumina dust as a function of Stokes numbers for a 3 cm thick bed containing 0.3 cm diameter polyethylene granules, where the semi-empirical expression for the single sphere efficiency, E is given as:

$$E = -\frac{4a}{3L(1-\epsilon)} \ln (1-\eta) \qquad (A8)$$

where a is the radius of the granule, L is the bed thickness, ϵ is the bed porosity and η is the total filtration efficiency. Figure A21 clearly shows that mechanisms other than diffusion, gravitation and inertia are involved in enhancing the filtration efficiency especially that of small particles (less than 1 μm) at low Stokes numbers. For instance, at a relative humidity of 5-10% and Stokes number of 0.003, the single sphere efficiency for the 0.5-0.7 μm (empty inverted triangle) and 0.7-1 μm (empty hexagon) diameter DOP aerosols is very low - 6.5 and 5.2% respectively, as compared to 13 and 12% , respectively for the 0.5-0.7 μm (solid inverted triangle) and 0.7-1 μm (solid hexagon) diameter alumina dust. However, as the relative humidity increases the filtration efficiency of alumina dust decreases and at relative humidity of about 45-50% the filtration efficiency of the two types of aerosols - DOP and alumina dust, is about the same for an equal Stokes numbers. The single sphere filtration efficiency for the 0.5-0.7 μm (half-solid inverted triangle) and 0.7-1 μm (half-solid hexagon) diameter alumina dust, at Stokes number of about 0.003 and relative humidity of 45-50% is 6.3 and 7% respectively. On the other hand, the filtration efficiency of DOP aerosols does not vary

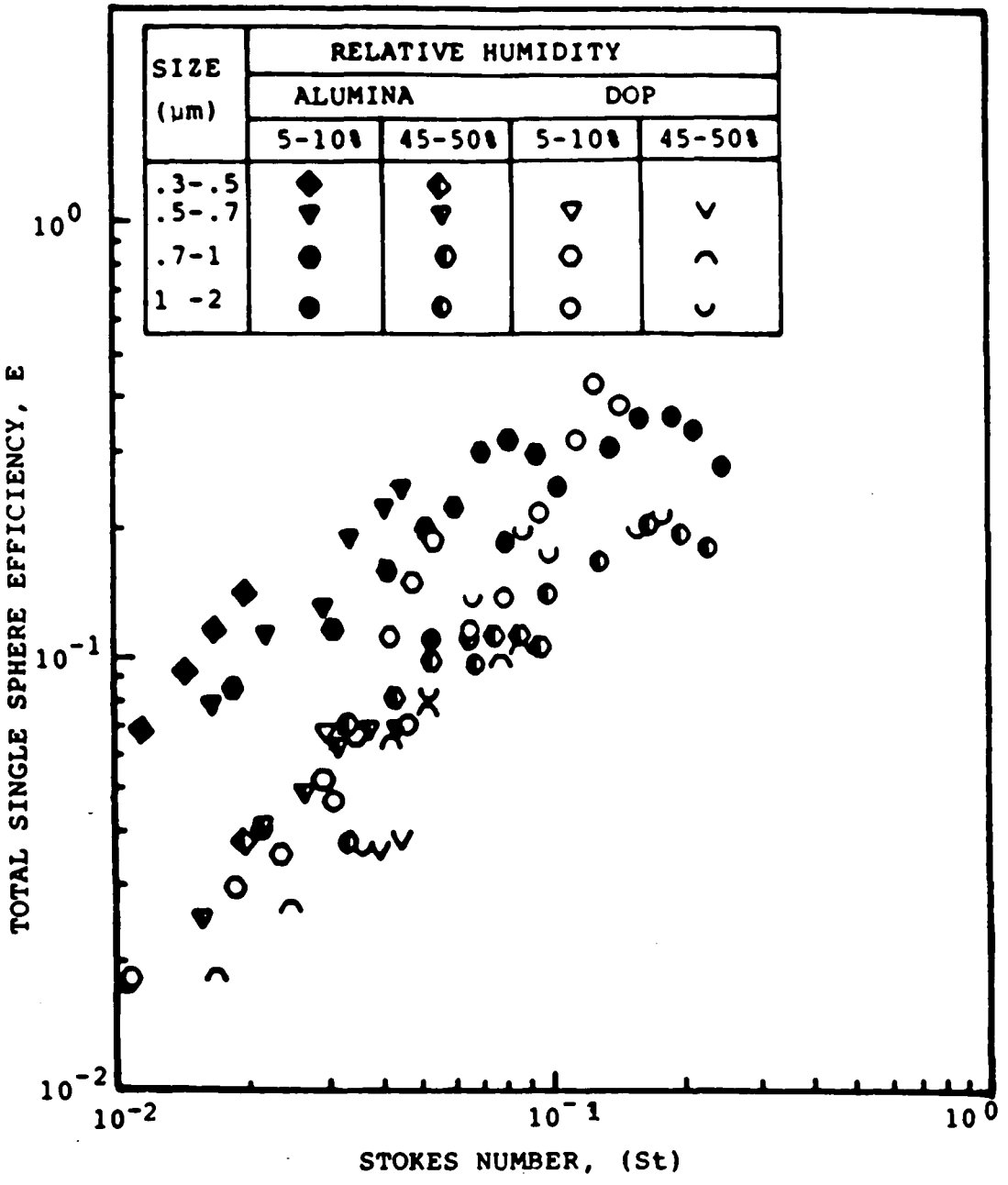

Figure A21. Single sphere efficiency as a function of the Stokes number for DOP aerosol and alumina dust in the RFBF containing 0.3 cm diameter polyethylene granules. Bed thickness, L = 3 cm; Bed porosity, ϵ = 0.4.

significantly as the relative humidity changes as shown in Figure A21. The fact that relative humidity and the type of aerosols affect the filtration efficiency is due mainly to electrostatic effects which occur primarily due to triboelectrification. This phenomenon, which by nature produces both negative and positive charges, in combination with the magnitude of the electric field in the voidage of the bed affects the filtration efficiency, thus renders the quantitative evaluation of electrostatic effects rather difficult.

Aerosol charge measurement

The average electrostatic charge on the aerosol particles is measured simultaneously with the filtration efficiency using a side stream of dusty air just before it enters the bed as shown in Figure 5. The flow rate of the side stream is kept equal to the sample flow rate of air to the particle analyzer, using a vacuum pump and a rotameter. The side stream of dusty gas flows through an absolute filter which is situated in a second Faraday cage as shown Figure A22. All airborne aerosol particles are assumed to be captured in the absolute filter and the cage is connected to the electrometer where the current is measured. The cage is double-shielded to diminish any outside electrical noise since the current level generated in the cage is of the order of 10^{-14} to 10^{-13} Ampere. From the measurement of the current produced which is the net flow of all charges on the dust particles flowing per unit time, the number of aerosol particles of each size range, j flowing through the Faraday cage per unit time, N_j, the average charge per unit area, $\bar{Q}_p$ is:

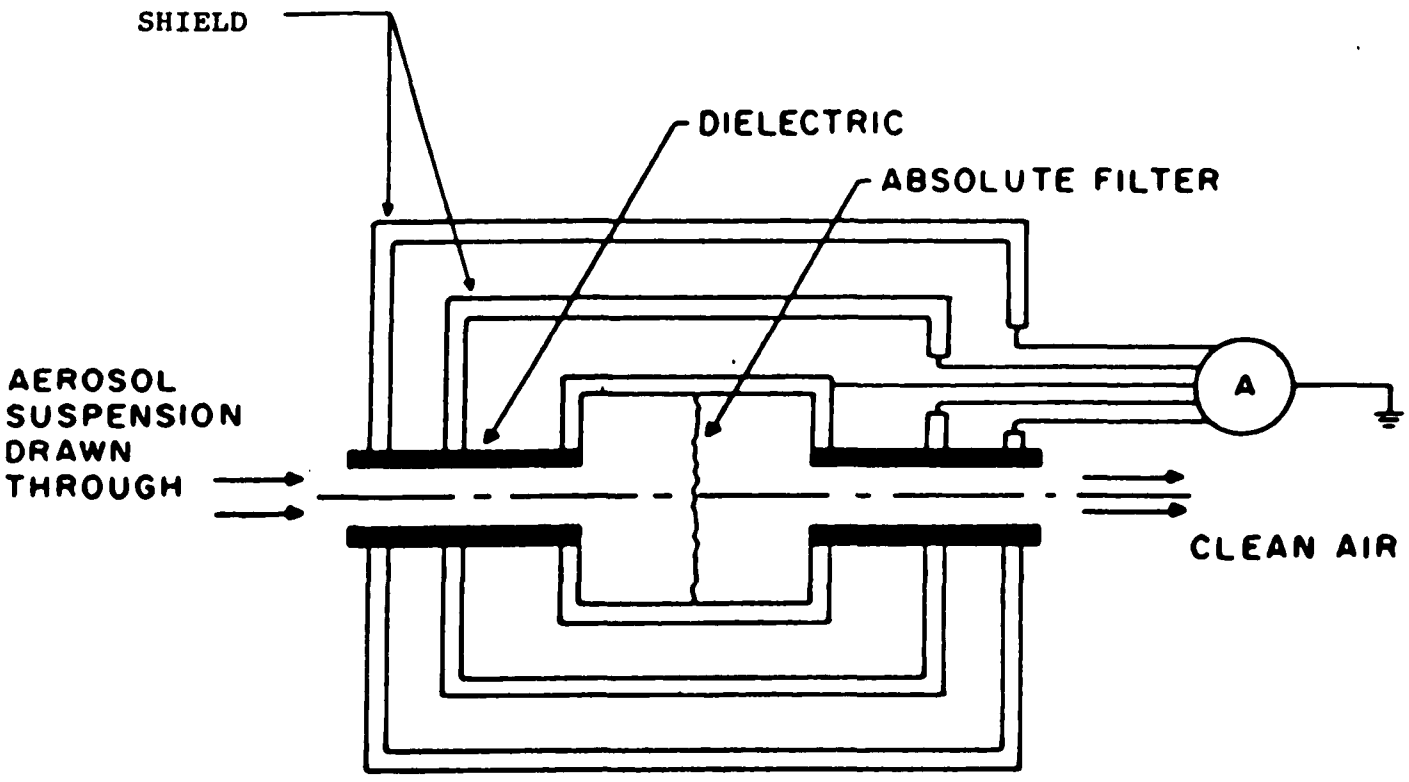

Figure A22. Faraday Cage for the measurement of electrostatic charge on dust particles.

$$\bar{Q}_p = \frac{I}{\sum_{j=1}^{m} N_j A_j} \qquad (A9)$$

where A_j is the average surface area of aerosol particles in the size range j. Figure A23 shows the charge variation for the DOP aerosol and alumina dust due to changes in the relative humidity. Since the relative humidity is not controlled during the experiments, the results are given over the range of humidities rather than at a fixed value. The electrostatic charge on the alumina dust particles is of the order of 10^{-10} Coulomb/cm^2 while the charge on the DOP aerosol is of the order of -0.1×10^{-10} Coulomb/cm^2.

The results in Figure A23 clearly explain the much higher filtration efficiency of alumina dust as compared to DOP at low relative humidities (see Figure A21). The difference in filtration efficiency between alumina dust and DOP aerosol for the same Stokes number is the result of stronger electrostatic forces on the alumina dust. The magnitude of the charge on the naturally charged alumina dust is about ten times as high as that of the naturally charged DOP at high relative humidities and about 3 times as high at low relative humidities. The electrostatic charge on the DOP aerosol is small and is not affected by humidity and consequently the filtration efficiency of the DOP aerosols is independent of the relative humidity as shown in Figure A21.

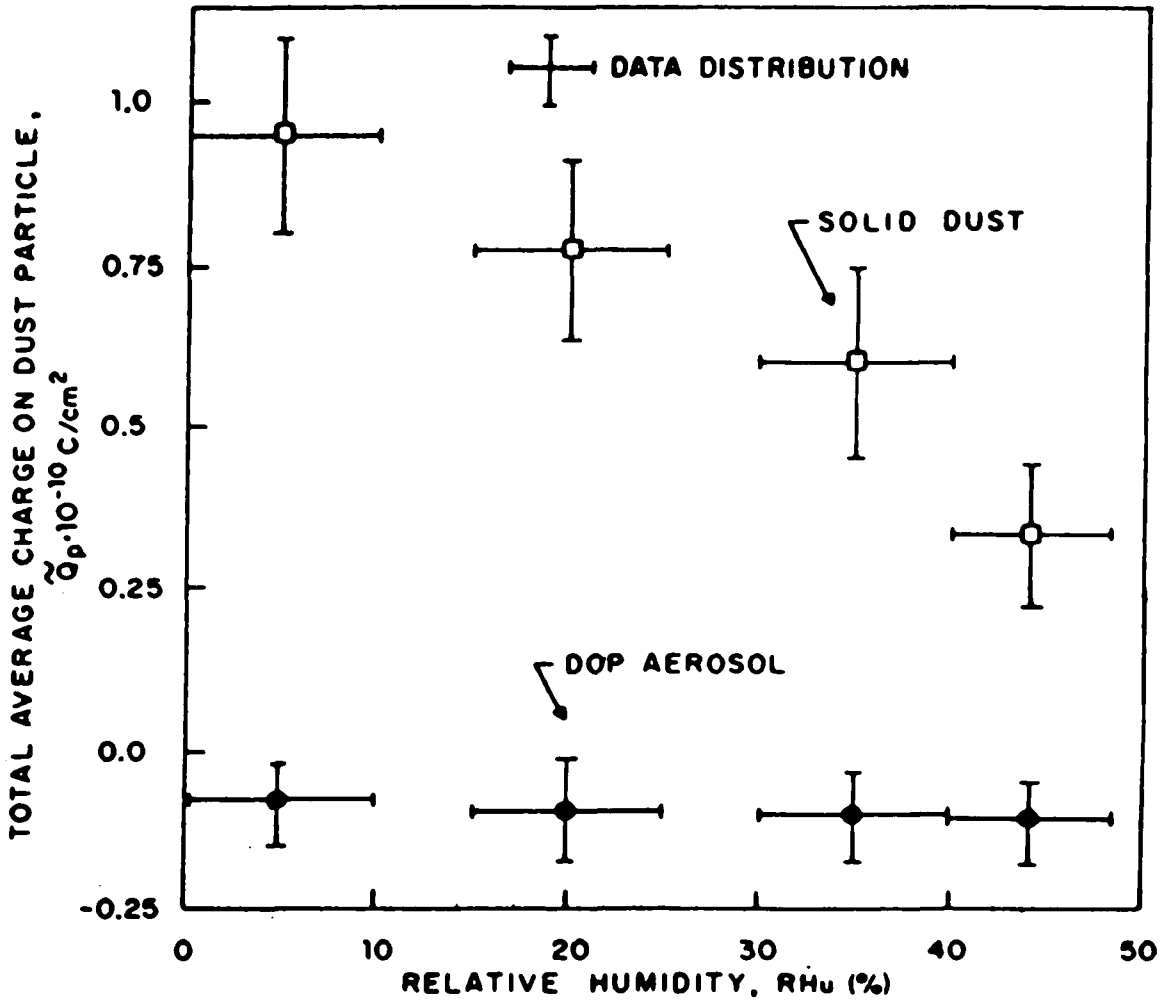

Figure A23. Total average charge on aerosol particles as a function of humidity.

Granule charge distribution

Electrostatic charge on bed granules is measured during the present work using a modified procedure suggested earlier by Tardos and Pfeffer (1980). It consists of taking a side stream of out-going granules into a Teflon vessel located inside a Faraday cage as shown in Figure 5. If a granule entering the cage has electric charge, it produces an electric field inside the cage which induces an equal charge on the copper vessel which forms the cage. This charge is measured by the Keithly 610C electrometer and by the HP 3438A voltmeter. The data collected is simultaneously stored in the microcomputer for analysis.

The electric potential reading is recorded continuously and each time a charged particle enters the cage there is a step change in the reading. The step change may be positive or negative according to the charge on the incoming granule. The number of step changes in the electric potential reading is compared to the actual number of particles collected in the Teflon vessel and was found to be within 85-100% in all experiments. The fact that the number of granules collected is often larger than the number of step changes indicates the presence of electrically neutral granules. The electrostatic charge distribution on the 0.3 cm diameter polyethylene granules in a 3 cm thick bed, as shown in Figure A24, is obtained by controlling the flow of granules to be low enough so that granules only enter the Teflon vessel one at a time. As shown, the distribution curve is the average from measurements on 300 to 500 granules performed over several runs. The results clearly show that both positive and negative charges exist in the bed. The charge is evenly distributed between negative and

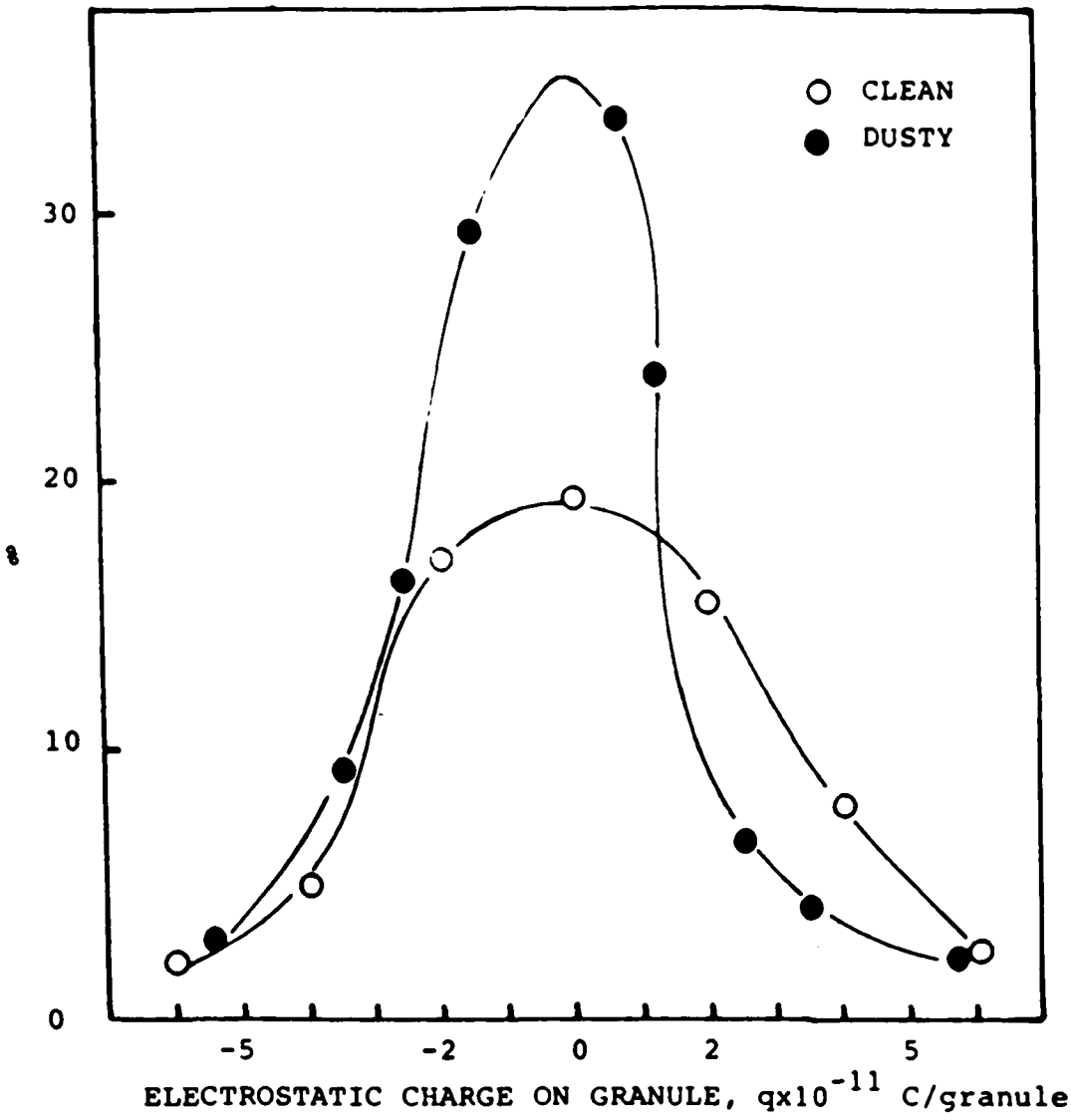

Figure A24. Electrostatic charge distribution on 0.3 cm (.12 in) diameter polyethylene granules in the RFBF.
Bed thickness, L = 3 cm; Bed porosity, ε = 0.4;
Relative humidity, RHu = 45-50%.
Clean gas: $\tilde{q}_c = 1.73 \times 10^{-12}$ C/granule
$\hat{q}_c = 2.95 \times 10^{-11}$ C/granule
Dirty gas: $\tilde{q}_c = -1.96 \times 10^{-12}$ C/granule
$\hat{q}_c = 1.65 \times 10^{-11}$ C/granule.

positive both in magnitude as well as in the number of charged granules. The net average charge per granule, $\tilde{q}_c$, is defined as:

$$\tilde{q}_c = \sum_{i=n}^{n} q_i / n \qquad (A10)$$

where q_i is the individual charge on each granule and n is the number of granules counted. From Figure A24, the net average charge per granule, $\tilde{q}_c$ is the value obtained by a line that divides the area under the distribution curve into two equal parts. As seen, the value of $\tilde{q}_c$ is extremely small and fluctuates around zero depending upon the distribution curve. One can also define the absolute average charge per granule as:

$$\hat{q}_c = \sum_{i=1}^{n} |q_i| / n \qquad (A11)$$

where $|q_i|$ is the absolute value of the charge on individual granule. The values found for $\tilde{q}_c$ are smaller by about an order of magnitude as compared to the absolute average charge, $\hat{q}_c$. Since the electrostatic effects are more pronounced at low relative humidity (Tardos and Pfeffer, 1980) which leads to a wider charge distribution curve, it is believed that the absolute average charge, $\hat{q}_c$ will increase at a relative humidity lower than the one presented in Figure A24 (there, the range of relative humidity is 45-50 %).

When a charged aerosol particle is captured by a granule with opposite charge, there is a reduction in the net charge of the granule. As charged aerosols flow through the rotating fluidized bed, the electrostatic charge on the granules becomes smaller as shown by the narrower charge distribution curve in Figure A24 resulting in the drop of absolute average charge of about 44%. In addition, there are other parameters that affect the charge distribution in Figure A24 including the magnitude and sign of charge on the aerosol particles, aerosol concentration, air flow rate, collection efficiency, granule material and the effect of aerosols coating the granules and changing their conductivity.

The drop in the average absolute charge on the granules when dusty air is flowing through the bed (Figure A24) indicates that the charged dust particles are captured on the granules with opposite charge hence reducing the total charge of the bed.

V.2. APPENDIX B: DUST DEPOSITION IN ELECTROSTATICALLY ENHANCED FIBROUS FILTERS

CONTENTS

B.1. INTRODUCTION

The removal of small charged dust particles from a gas stream using an external electric field is common in many industrial applications such as electrostatic precipitators, impactors, granular and fibrous filters, etc. In the majority of these applications, the purpose is to separate the hazardous and/or toxic particles from the gas stream by applying strong electric fields across the filter. Recently, numerous authors have studied the filtration phenomenon of charged particles in electrostatic fibrous filters (EFF) because of its practical importance (Bergman et al., 1978; Nielsen, 1978; Kallio et al., 1979; Frederick, 1980; Harriot and Saville, 1980; Ho and Wang, 1981; Henry and Ariman, 1981,1983; Kallio and Dietz, 1981; Henry et al., 1982; Tardos and Snaddon, 1984). This type of filter has been proven to be very effective in the removal of small particles in the size range between 0.1 to 2 microns. The physical phenomena in an electrostatic fibrous filter are similar to those in electrostatic precipitators. The advantage of the electrostatic fibrous filter over the electrostatic precipitator is the significant increase in collection surface per unit volume or the reduction in size of the device required for a given gas throughput.

In 1969, Hochrainer and Hidy demonstrated the influence of the electrical forces on the slow motion of small charged particles around a circular cylinder. Using Oseen flow to describe the gas flow and linear superposition of the aerodynamic flow field and the electrical field, these authors took into account the dipole induced by polarization of the cylinder due to charged particles approaching it. The experimental results showed reasonable agreement. These authors however only considered one cylinder in an infinite fluid i.e. they

neglected the influence of neighboring fibers. Emi et al. (1973, 1977) considered the influence of neighboring fibers and the effect of Reynolds number. However, the authors used a cell model which does not take into account the fibers' orientations and the electrostatic effects were not included.

Nielsen (1978) computed the collection of fine, inertialess, charged particles on a single circular cylindrical collector situated in a gas stream under the influence of electrical forces and gravitation. This study included potential flow, Oseen flow, stationary-vortex flows, and Kuwabara cellular flow and considered the effect of the coulombic force and a uniform external electric field. Ho and Wang (1981) took into account the effects of particle inertia, direct interception, charges on airborne particles, and the polarization of the particles. In neither paper (Nielsen, 1978 and Ho and Wang, 1981), however, was the effect of neighboring fibers on the electrical forces taken into consideration.

Henry and Ariman (1981,1983) introduced the effect of neighboring fibers on the electric field using a staggered array as a model of a fibrous filter with electrical enhancement. In these studies, the particle inertia effect was not taken into account and the finite difference method used to solve the flow field in the fibrous array was too cumbersome to describe the particle's trajectories. Furthermore, the results were not compared to experimental data.

In the present study, the effects of neighboring fibers on the flow field as well as on the electrical field are being considered. The model takes into account inertia, interception, and electrostatic forces on the dust particles in the filter. Moreover, the theoretical results are verified by careful experiments.

One has to note here the essential difference between the electrostatic fabric filter studied during this work and the electrostatically enhanced (stimulated) filter under development at among other places at the Textile Research Institute in Princeton, NJ. The filter considered during this work is a "deep bed" type separator in which dust is collected on each and every one of the fibers while the electric field is applied parallel to the flow by two mesh electrodes situated on both sides of the filter. By contrast the electrically stimulated filter (Morris et al., 1986; VanOsdell et al., 1986; Hovis et al., 1986; Lamb and Jones, 1986; Banks and Griffin, 1986; VanOsdell et al., 1986) is a "cake" type filter where the filtration of dust takes place in superimposed dust layers and the fabric only serves as a support. The electric field in this case is applied parallel to the cake i.e. perpendicular to the gas flow by metalic wires woven into the fabric. The theoretical model developed during the present work does not apply in its present form to this type of cake filtration.

B.2. THE MATHEMATICAL MODEL AND METHOD

Consider the flow of fine, charged, airborne particles through a fibrous bed of regularly arranged uniform dielectric fibers with an external electric field applied parallel to the gas flow. Figures B1 and B2 show the geometry of the system: the gas flows in the plane of the figures and perpendicular to the fibers with a superficial velocity U_o. Each fiber is considered to be surrounded by a square unit cell of size, ℓ as shown in Figure B2. The difference between the two chosen

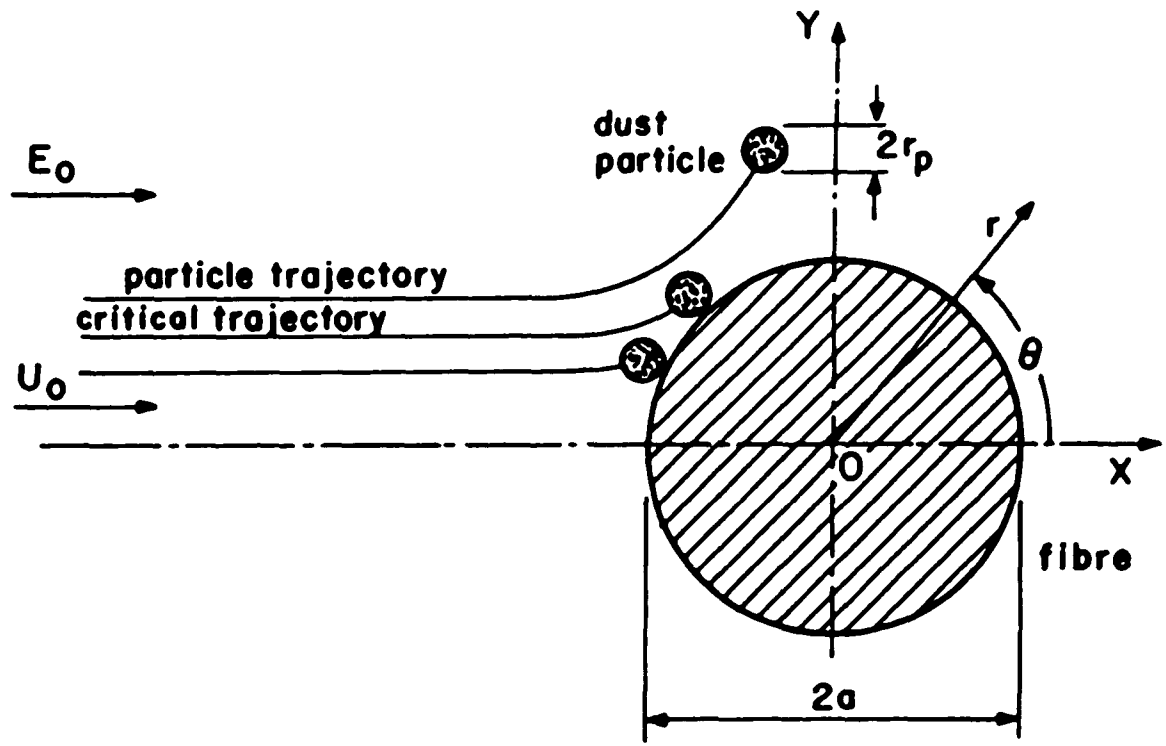

Figure B1. Deposition of particles on a fiber.

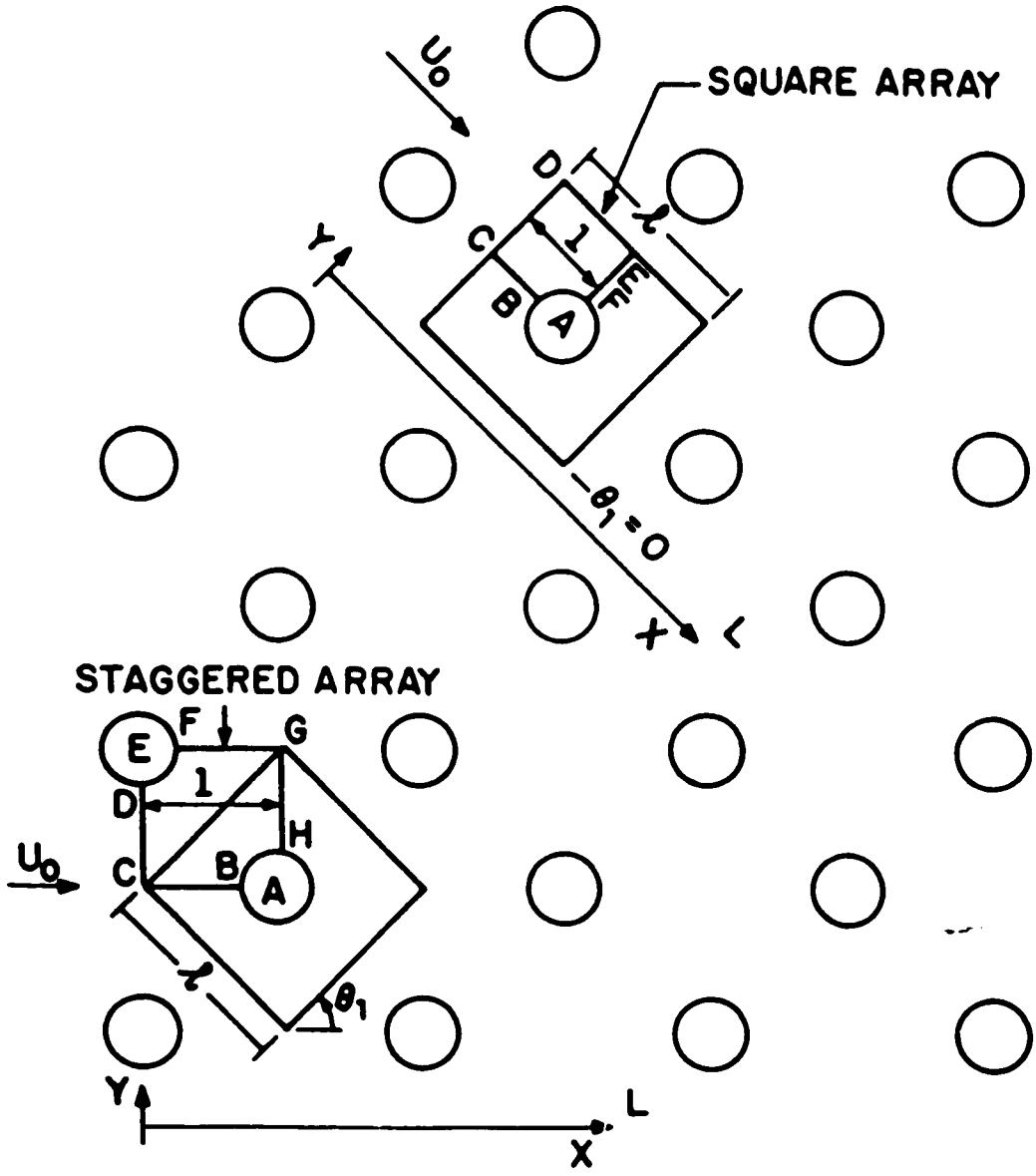

Figure B2. The configuration of the fibrous bed.

geometries, which we call the square and the staggered array, is only in the orientation of the gas flow.

The flow field

The steady motion of an incompressible viscous fluid (creeping flow), through the geometry depicted in Figure B2 was studied by Sangani and Acrivos (1982). These authors calculated the stream function, ψ, for these two cases and gave the solution in the form of an infinite series as:

$$\psi = a_1[r^3 - \frac{4a^2 r\ln r}{2\ln a+1} + \frac{a^4(2\ln a-1)}{2\ln a+1}(\frac{1}{r})]\sin\theta + b_1[a^2 r - \frac{2a^2 r\ln r}{2\ln a+1} - \frac{a^4}{2\ln a+1}(\frac{1}{r})]\sin\theta + \sum_{n=2}^{N}\{a_n[r^{2n+1} - 2na^{4n-2}r^{3-2n} + (2n-1)a^{4n}r^{1-2n}] + b_n[a^2r^{2n-1} - (2n-1)a^{4n-2}r^{3-2n} + 2(n-1)a^{4n}r^{1-2n}]\}\sin(2n-1)\theta \qquad (B1)$$

where a is the radius of the fiber, a_1, b_1 ..... a_n, b_n are the coefficients determined from the configuration of the fibrous array and the boundary conditions on the unit cell and r and θ are cylindrical coordinates. Values for all coefficients a_1, b_1 ..... a_n, b_n are given in Table B1. Equation (B1) can be applied only for cases when the characteristic Reynolds number is very small (Re < 0.1).

The velocity of the flow in Cartesian coordinates is then given by

$$U_x^f = \frac{1}{r}\frac{\partial\psi}{\partial\theta}\cos\theta + \frac{\partial\psi}{\partial r}\sin\theta$$

$$U_y^f = \frac{1}{r}\frac{\partial\psi}{\partial\theta}\sin\theta - \frac{\partial\psi}{\partial r}\cos\theta \qquad (B2)$$

TABLE A1. The coefficients of the flow model in the square and staggered arrays at 0.87 porosity

	Square array		Staggered array	
n	a_n	b_n	a_n	b_n
1	-0.500	7.02	-0.972	24.16
2	6.14×10^{-2}	-1.35	-0.256	5.52
3	-2.00×10^{-3}	-3.42×10^{-2}	2.26×10^{-2}	0.196
4	2.59×10^{-3}	-5.65×10^{-2}	3.68×10^{-2}	-0.850
5	-1.82×10^{-4}	1.60×10^{-3}	-2.17×10^{-3}	6.83×10^{-3}
6	9.93×10^{-5}	-1.47×10^{-3}	-9.46×10^{-3}	0.132
7	-1.59×10^{-5}	2.39×10^{-4}	4.73×10^{-3}	-6.48×10^{-2}
8	4.69×10^{-6}	-5.08×10^{-5}	-1.15×10^{-3}	1.70×10^{-2}
9	-1.25×10^{-6}	1.95×10^{-5}	1.43×10^{-3}	-1.65×10^{-2}
10	2.28×10^{-7}	-1.44×10^{-6}	-2.10×10^{-3}	2.56×10^{-2}
11	-9.58×10^{-8}	1.45×10^{-6}	1.90×10^{-3}	-2.52×10^{-2}
12	1.14×10^{-8}	-1.83×10^{-8}	-1.51×10^{-3}	2.04×10^{-2}
13	-7.10×10^{-9}	1.02×10^{-7}	1.35×10^{-3}	-1.79×10^{-2}
14	5.58×10^{-10}	2.35×10^{-9}	-1.28×10^{-3}	1.70×10^{-2}
15	-5.11×10^{-10}	6.86×10^{-9}	1.13×10^{-3}	-1.53×10^{-2}
16	2.25×10^{-11}	3.58×10^{-10}	-9.27×10^{-4}	1.26×10^{-2}
17	-3.31×10^{-11}	4.21×10^{-10}	7.11×10^{-4}	-9.74×10^{-3}
18	-1.09×10^{-13}	3.91×10^{-11}	-5.06×10^{-4}	6.88×10^{-3}
19	-1.40×10^{-12}	1.74×10^{-11}	3.16×10^{-4}	-4.33×10^{-3}
20	-9.35×10^{-14}	2.57×10^{-12}	-1.72×10^{-4}	2.30×10^{-3}
21			7.84×10^{-5}	-1.05×10^{-3}
22			-3.08×10^{-5}	3.87×10^{-4}
23			8.60×10^{-6}	-1.08×10^{-4}
24			-2.10×10^{-6}	2.30×10^{-4}

The electric field

For an uniform electric field, E_o, applied across the fibrous array, the total electric potential function can be derived by superimposing the potential functions for each cylinder and fitting the boundary conditions on every cylinder's surface. Applying this method initially suggested by Jackson (1975) and Lamb (1932) for two cylinders, for the case of a regular array as shown in Figure B2, one obtains:

$$\phi_o^e = -E_o x + \epsilon E_o a^2 \sum_{i=1}^{n} \frac{(x-x_i)}{(x-x_i)^2+(y-y_i)^2} \left[1 - \sum_{j=1}^{m} \epsilon \frac{a^2}{d_{ij}^2}\right] \qquad (B3a)$$

where (x_i, y_i) are the locations of the fibers, d_{ij} is the distance between fibers i and j and x and y are Cartesian coordinates. The polarization coefficient is given by $\epsilon = \frac{\epsilon_f/\epsilon_o - 1}{\epsilon_f/\epsilon_o + 1}$ where ϵ_f is the dielectric constant of the fiber and ϵ_o is the dielectric constant of air.

Henry and Ariman (1981, 1983) obtained a similar expression for the potential function using the method of images in complex coordinates, which reads:

$$W(Z) = \phi_o^e + i\psi_o^e \approx -E_o Z + \epsilon E_o a^2 \sum_{i=1}^{n} \left[\frac{1}{Z-Z_i} - \sum_{j=1}^{n} \left(\frac{a^2}{|Z_j|^2}\right) \frac{1}{Z-Z_{ij}}\right] \qquad (B3b)$$

where Z_i is the position of the ith cylinder and Z_{ij} is the position of the first-order image of cylinder j in cylinder i.

Comparing the resulting functions from equations (B3a) and (B3b), it can be seen that a polarization coefficient, ϵ, is missing in the last term of equation (B3b) but otherwise the equations are identical.

Due to the electric potential ϕ_o^e, the electric velocity is given by:

$$\vec{u}^e = -\omega_p \nabla \phi_o^e \qquad (B4)$$

where ω_p is the electric mobility of the particle. For small particles where Stokes law is applicable, particle mobility is related to the electrical charges on the particles by

$$\omega_p = CQ_p/3\pi\mu D_p \qquad (B5)$$

where C is the Cunningham correction factor, μ is the gas viscosity and D_p is the diameter of the particle.

The dimensionless electric velocity is defined as:

$$\vec{U}^e = \vec{u}^e/U_o \qquad (B6)$$

so that it's x and y components can be written as:

$$U_x^e = Kex - \epsilon Kex \sum_{i=1}^{n} \frac{(Y-Y_i)^2 - (X-X_i)^2}{[(X-X_i)^2 + (Y-Y_i)^2]^2} \left(1 - \sum_{j=1}^{m} \frac{\epsilon}{D_{ij}^2}\right)$$

$$U_y^e = \epsilon Kex \sum_{i=1}^{n} \frac{2(X-X_i)(Y-Y_i)}{[(X-X_i)^2 + (Y-Y_i)^2]^2} \left(1 - \sum_{j=1}^{m} \frac{\epsilon}{D_{ij}^2}\right) \qquad (B7)$$

where the dimensionless electric number, Kex, is defined as

$$Kex = \omega_p E_o/U_o = CQ_p E_o/3\pi\mu D_p U_o \qquad (B8)$$

The trajectory equation

The flow and electric field models described above can be used in the trajectory equation to predict filtration efficiencies in a fibrous filter. The aerosol particle in the flow is considered to be a point mass, which does not affect the flow or the electric fields when moving in the proximity of a fiber. Its critical trajectory, i.e. the one for which the particle just misses the fiber, has to be computed (see Figure B1). The general equations of motion of a small particle in the filter bed taking into account the gas flow and the electric field can be written in the form (Tardos and Snaddon, 1984):

$$\frac{d^2\vec{X}}{dT^2} = \frac{1}{St}(\vec{U}^f + \vec{U}^e - \frac{d\vec{X}}{dT}) \qquad (B9)$$

where $\vec{X}$ is the dimensionless position vector, T is the dimensionless time given by, $T=tU_o/a$, and St is the Stokes number, $St=2C\rho_p U_o r_p^2/9\mu a$. The initial conditions for the trajectory equation are:

$$\vec{X}(T=0) = \vec{X}_o \qquad (B10a)$$

$$\frac{d\vec{X}(T=0)}{dT} = \vec{U}^f + \vec{U}^e \qquad (B10b)$$

where it is assumed that the velocity of the particle is identical to the superposition of the flow and the electric velocity at time, T=0. The actual initial velocity of the dust particle is exactly equal to the superposed velocities for zero Stokes number, St, but is lower for larger Stokes numbers. Thus, using the initial conditions as shown above introduces a small error in the trajectory calculation for small Stokes numbers which increases however with increasing Stokes numbers.

The trajectory equation may be solved numerically. Each particle is assumed to be travelling in the X direction with the main stream

velocity, until it reaches the cell boundary which is taken as the starting point of each trajectory (see Figure B1). Each successive position of the particle in the stream around the fiber is calculated by the superposition of the field velocities, the particle inertia as measured by the Stokes number, and the position of the particle a small time interval earlier. The computer is programmed to calculate the points step by step, using a fourth order Runge-Kutta method until the complete trajectories are developed. The coordinate of the trajectory starting point is successively increased until the particle misses the fiber. The critical trajectory is then calculated by interpolation, using the bisection method, between the last two trajectories. The finite particle size, the interception effect, is allowed for by increasing the effective capture size of the fiber by an amount equal to the radius of the particle.

Unit cell efficiency and total bed efficiency

As a first step, the unit cell collection efficiency was computed using the trajectory equation. The flow in the cell is taken to be in the positive X direction and the dust concentration is assumed to be very small and uniform. All dust particles whose trajectories are below the critical trajectory are assumed to be captured (see Figure B1). The unit cell collection efficiency, E, is defined as the ratio of the flux of dust particles through the area from which they are captured to the total flux of particles flowing through the unit cell.

$$E = \frac{\text{Flux captured by the fiber}}{\text{Total flux inside the unit cell}}$$

The total bed collection efficiency, η, can be computed directly from the unit cell collection efficiency. If the bed is assumed to be a series of collection units of length, ℓ, (see Figure B2) then the total bed efficiency is (Payatakes et al., 1982):

$$\eta = 1 - (1-E)^{m_b} \qquad (B11)$$

where m_b is the number of unit cell layers in the bed and is given by

$$m_b = L/\ell\cos\theta_1 \qquad (B12)$$

where L is the filter thickness and θ_1 is the angle between L and ℓ (see Figure B2).

B.3. FILTER EFFICIENCY AND PARTICLE CHARGE MEASUREMENTS

The experimental set-up for efficiency measurements

Filtration efficiencies in a fibrous filter bed can be obtained experimentally by passing a dusty gas stream through the filter and measuring the inlet and outlet particle concentrations, n_{in} and n_{out}. The total bed collection efficiency is then given by:

$$\eta = 1 - \frac{n_{out}}{n_{in}} \qquad (B13)$$

A schematic drawing of the apparatus used in these experiments is shown in Figure B3. Dry clean compressed air is pumped through the system at flow rates up to 400 ft^3/hr. The humidity of the air in the system is controlled by a humidifier and can be adjusted to anywhere between 0 to 95%. Monodispersed latex particles of known size are generated from a solution of methanol. Liquid aerosols of

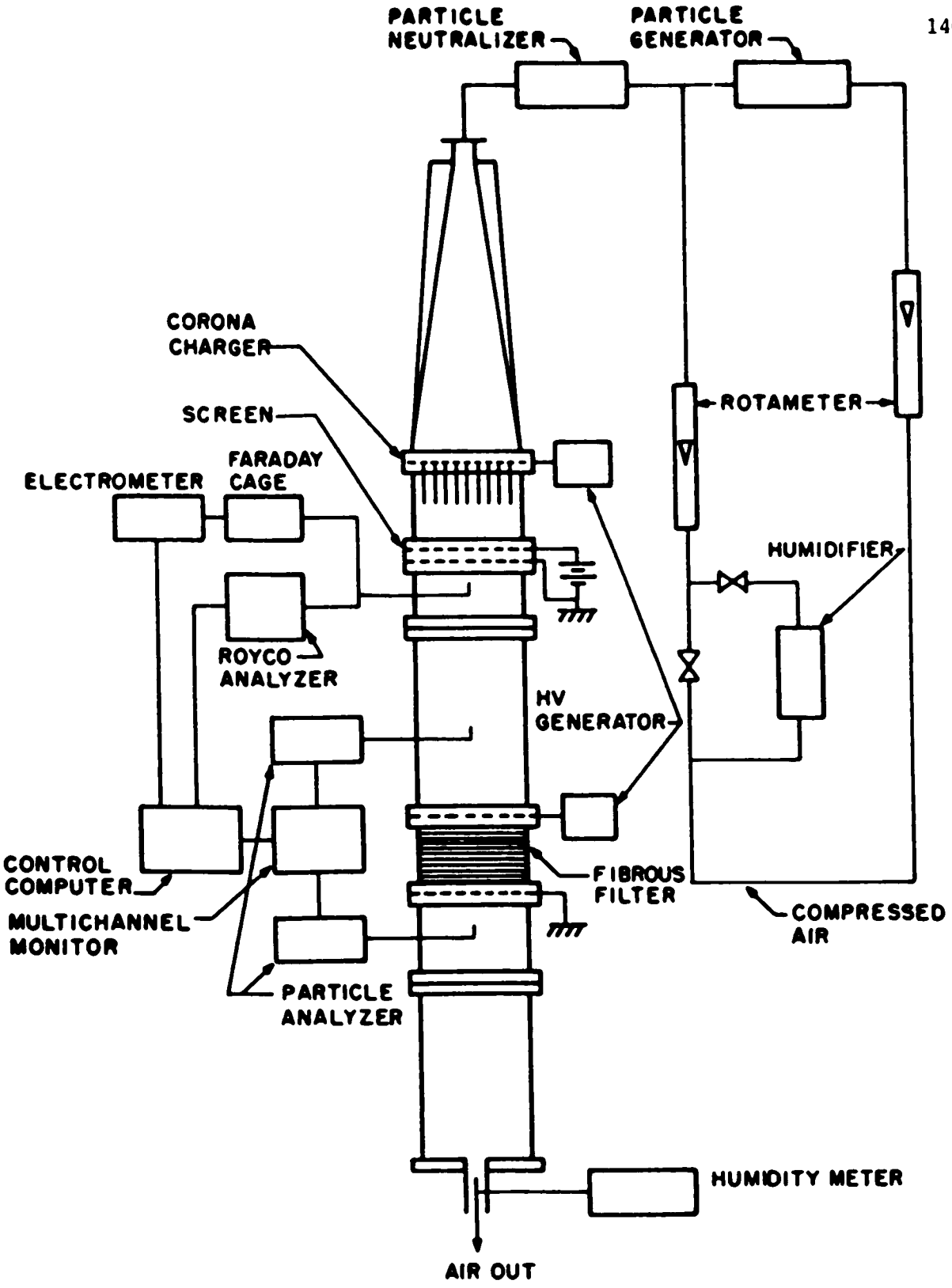

Figure B3. Schematic representation of the experimental set-up.

dioctylphtalate (DOP) were generated by an atomizer and alumina particles were generated by a powder disperser. The particle concentration was kept at about 60,000 particles/ft^3 for latex particles and about 600,000 particles/ft^3 for DOP and alumina particles. The concentration was measured simultaneously at the inlet and outlet of the fibrous bed using Climet CI-225 and CI-208S sensors and a Climet CI-210 multichannel monitor. The particles were charged by a corona charger prior to entering the filter bed and the particle charges were measured both by a Faraday cage with an electrometer (using a ROYCO 4100 particle counter for concentration measurements) and by a mobility analyzer. All data were collected and analyzed by a DEC microcomputer.

The fibrous bed was placed in a long square duct to allow for fully developed flow to form and a good mixing of the aerosols in the gas to occur. The filter beds were constructed out of textile fibers with a diameter of 0.4 mm and were placed in the rectangular duct. The fibers were arranged exactly as described in the theoretical model used (see Figure B2). Two beds, one using a staggered array arrangement with ten layers and the other with a square array arrangement with seven layers (see Figure B2) were constructed. Both had the same porosity, α=0.87, and fiber radius, a = 0.2 mm and, therefore, were operating under the same superficial velocity and the same Stokes numbers.

Particle charge measurements

The filtration efficiency of fibrous filters can be significantly increased by charging the aerosol particles and applying an electric field across the fibrous filter. In the experiments, the aerosol particles were charged using a (point) needle-and-flat plate corona charger. The charge on the particles is dependent on the current in the corona charger and the relative humidity of the inlet stream. In order to measure particle charge, a radial-flow parallel-plate mobility analyzer as well as a Faraday cage were used. The procedure and method used to perform these measurements are described in detail by Tardos et al (1984).

Practical corona charger devices tend to produce a distribution of charges even on monodisperse particles. A wide distribution of particle charges was obtained with monodispersed particles and a corona charger by Tardos (1982) and Tardos et al (1984). It was also shown during this work that the particle mobility distribution produced on the particles can be expressed by the semi-empirical equation:

$$N(\omega_p) = \left(\frac{Qd}{AV_s}\right)^2 \omega_p^{-3} e^{-(Qd/AV_s)\omega_p^{-1}} = \frac{\bar{\omega}_p^2}{\omega_p^3} e^{-[\bar{\omega}_p/\omega_p]} \qquad (B14)$$

where Q, d, A and V_s are the flow rate through the mobility analyzer, the separation distance between the plates, the area of the collecting surface of the analyzer and the saturation voltage, where an efficiency of 63% is achieved, respectively. The number averaged mean particle mobility is defined by

$$\bar{\omega}_p = \int_0^\infty \omega_p N(\omega_p) d\omega_p \; / \; \int_0^\infty N(\omega_p) d\omega_p = Qd/AV_s \qquad (B15)$$

and, as seen, can be computed from a few measured quantities in the mobility analyzer.

The average particle charge can also be measured by using the Faraday cage, an electrometer, and a particle analyzer to measure concentrations (Tardos et al. 1984). The charged aerosol particles pass through the cage and are separated from the gas stream by an insulated absolute filter. The average particle charge is given by

$$Q_a = \frac{I}{n_{in} v_F} \qquad (B16)$$

where I is the current from the cage to ground measured by the electrometer; n_{in} is the particle concentration at the inlet stream measured by the particle analyzer and v_F is the gas flow rate through the Faraday cage. Particle mobilities can be computed from the knowledge of the particle charge using equation (B5).

Figure B4 shows a comparison between results of particle charge measurements from both the mobility analyzer and the Faraday cage as a function of gas humidity. A reasonably good agreement between results obtained from the analyzer and the Faraday cage can be seen. The particle charge is increasing with relative humidity especially in the high humidity region above 80%. The somewhat higher values obtained from the Faraday cage experiment in the high humidity region are probably due to the formation of charged water mist which cannot be detected by the ROYCO particle counter but still carry some electric charge.

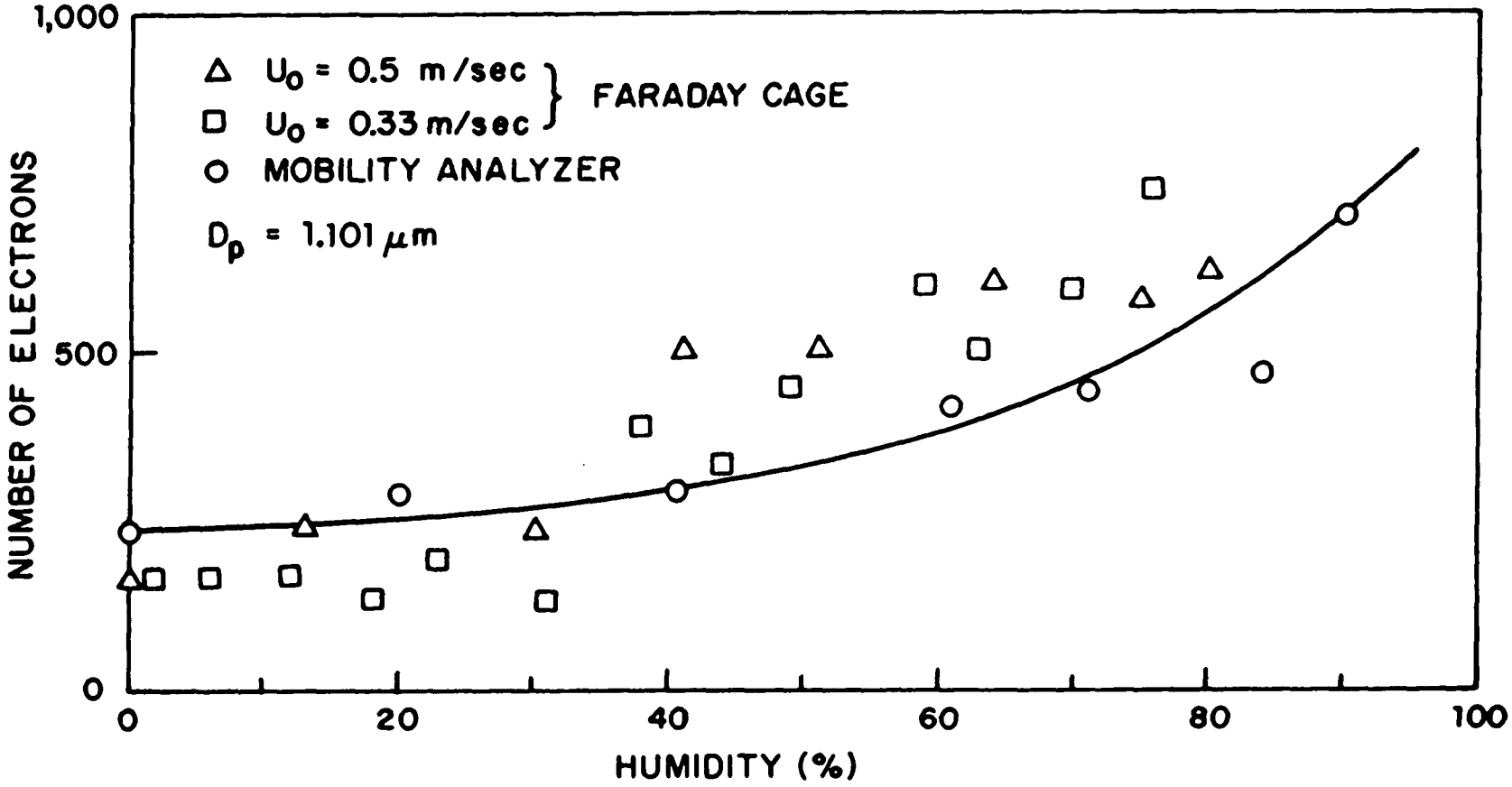

Figure B4. The influence of humidity on acguired particle charge.

B.4. THEORETICAL AND EXPERIMENTAL RESULTS AND DISCUSSION

Absence of electrostatic effects

When the dimensionless electric number, Kex, is equal to zero (see equation (B8)), at a zero value of the applied electric field, the collection mechanisms include only inertia and interception effects. In this case, the characteristics of the flow field can be checked by measuring the unit cell collection efficiency.

In Figure B5, theoretical results for the single cell collection efficiency are presented for zero applied electric fields as a function of the Stokes number with the bed porosity, α, as a parameter. As seen in Figure B5, the collection efficiency decreases with increasing porosity of the filter as expected; a staggered array of fibers is used in this case. At Stokes numbers larger than 0.5, the very high efficiencies are due to the inertia effect; at Stokes number smaller than 0.1, only the interception effect is important.

In order to verify the theoretical computations for both arrays experiments were performed as described in the previous section but with no applied electric fields. The theoretical and experimental results (for a porosity of α=0.87) are shown in Figure B6, as total bed efficiencies as a function of Stokes number. The solid lines represent calculated values, the empty symbols represent experiments with the staggered array while the full symbols, experiments with the square array. Experiments were performed for both arrays with air and helium. Helium was used because it has similar viscosity as air but a much lower density and therefore experiments can be performed with similar Stokes numbers while the corresponding Reynolds numbers are much lower (Gal et al, 1985).

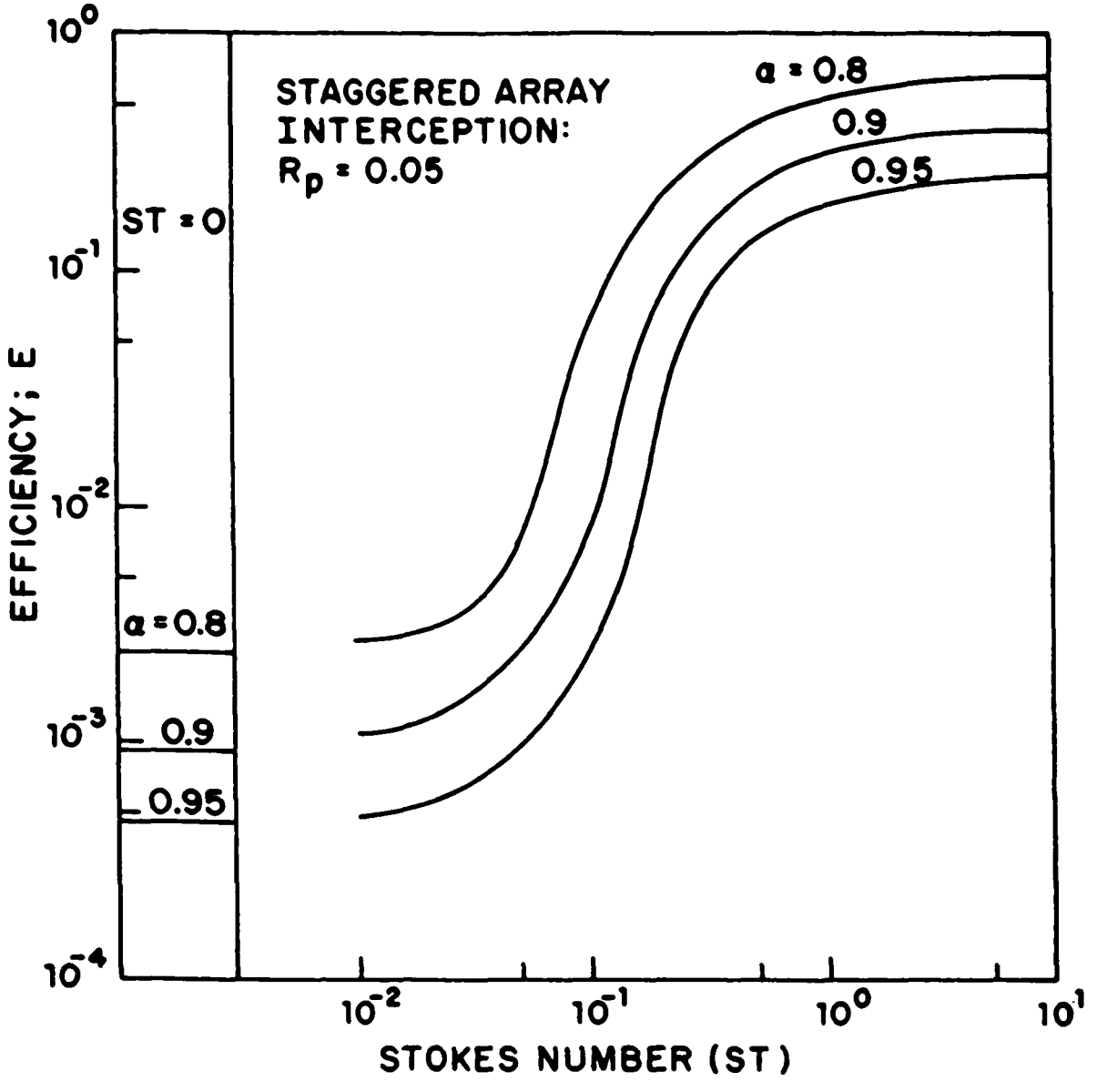

Figure B5. Unit cell collection efficiencies for different porosities in a staggered array. No electrical effects.

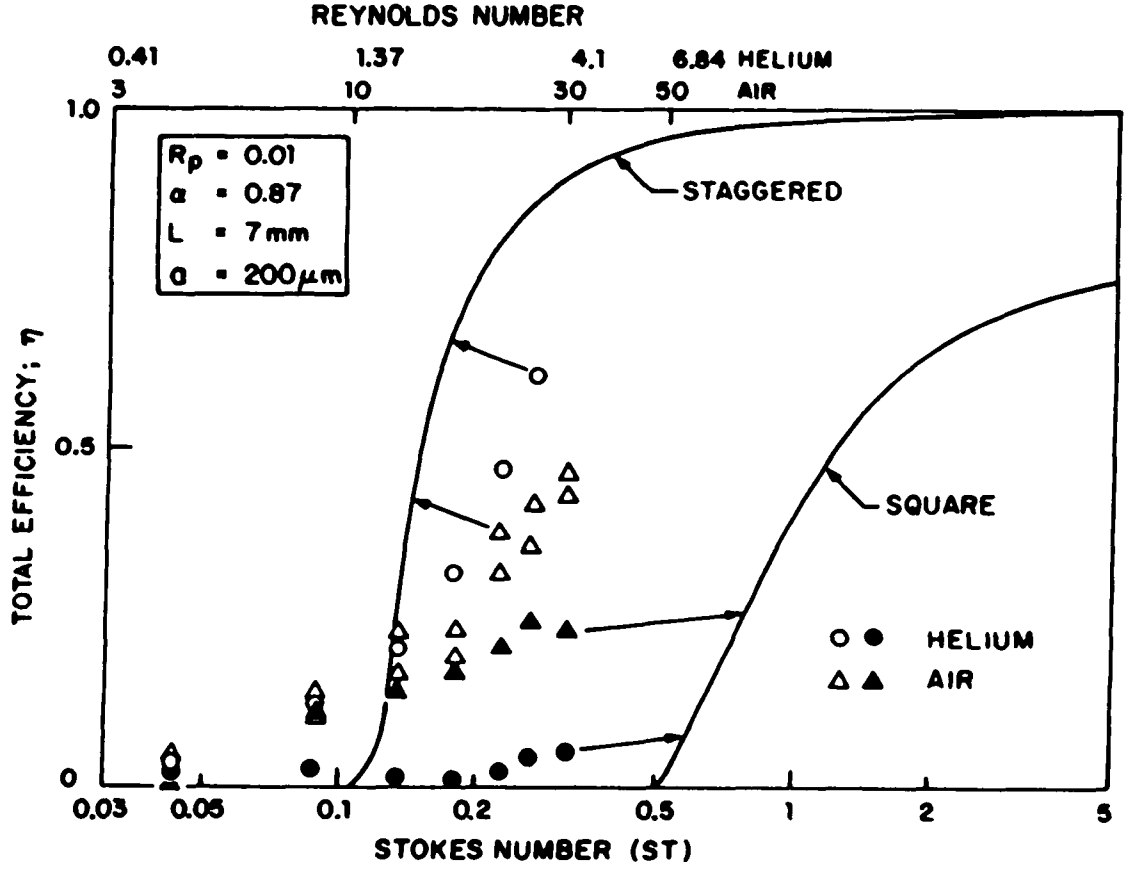

Figure B6. Comparison of experimental data for total bed collection efficiencies with the theoretical model. No electrical effects.

The circles in Figure B6 represent experimental results with helium while the triangles represent results obtained with air. As seen, the experiments with helium follow the calculated values quite closely while those with air do not. One has to note here that the calculated values (solid lines in the figure) were obtained for a zero Reynolds number (creeping flow). This explains why the experimental efficiency values obtained with helium (low Reynolds numbers) are closer to the theoretical values than those obtained with air (higher Reynolds numbers) [see values for the effective Reynolds numbers for the two gases at given Stokes numbers at the top of the Figure]. These results demonstrate both the correctness of the theoretical calculations and the very different nature of the flow in the two fiber arrays.

Presence of electrostatic effects

The collection efficiency increases significantly as the electric field is applied to the filter as seen in Figures B7 and B8 which give calculated values. The electrostatic forces are clearly dominant in Figure B7 with the efficiencies rising from zero at no applied field to 40% and above at moderate applied field strengthes for the unit cell for both the square and the staggered arrays. Also shown is the effect of the dielectric constant of the fibers. Higher dielectric constants result in better collection. As seen, there is no significant difference between efficiencies of the two arrays when electric forces become dominant. The following results in this chapter are therefore all given for the square array only.

Figure B8 shows the influence of the Stokes number and the electric number, Kex, on the total bed filtration efficiencies of the

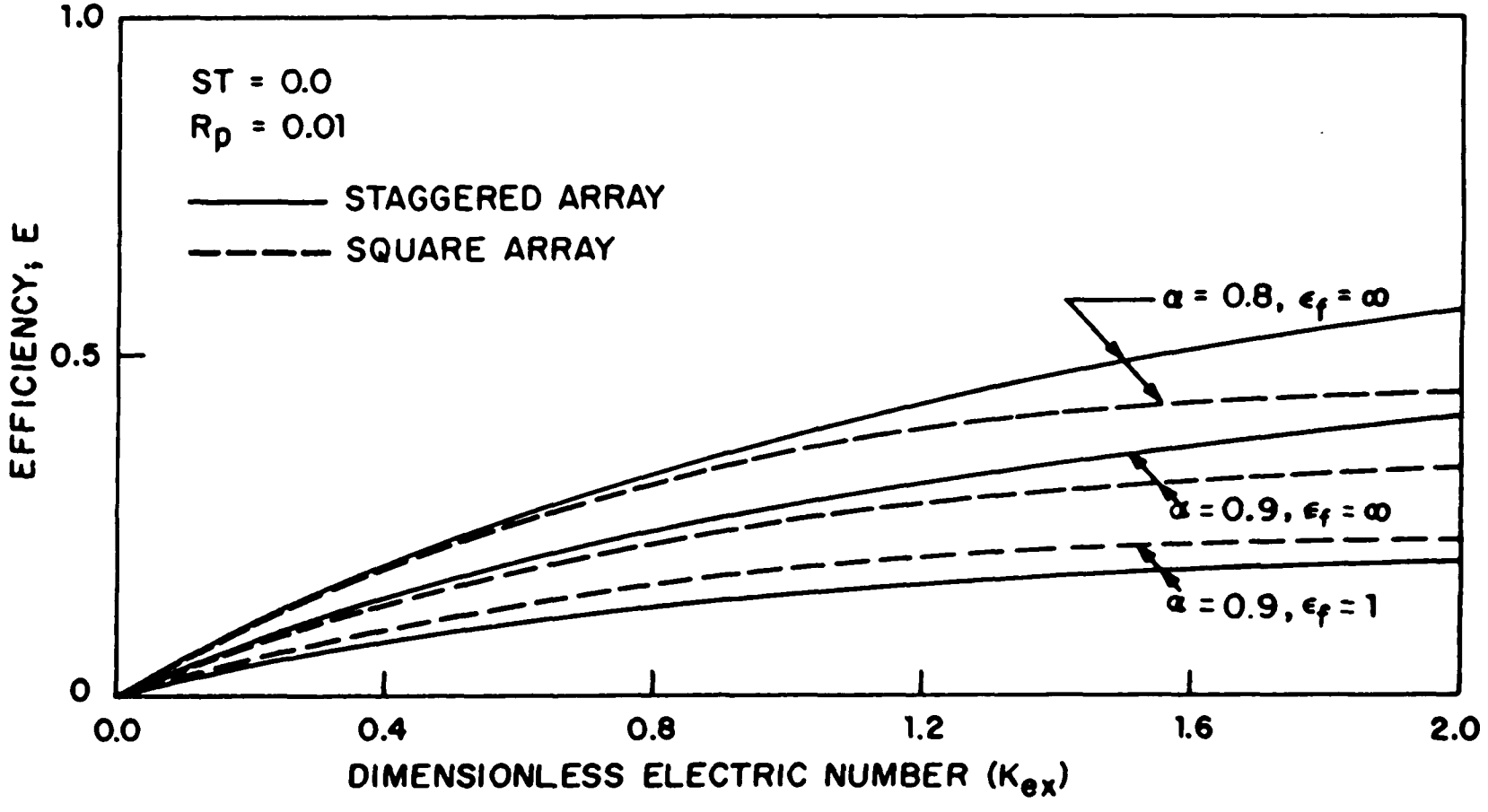

Figure B7. The influence of the dielectric constant of the fiber and of the porosity on filtration efficiency.

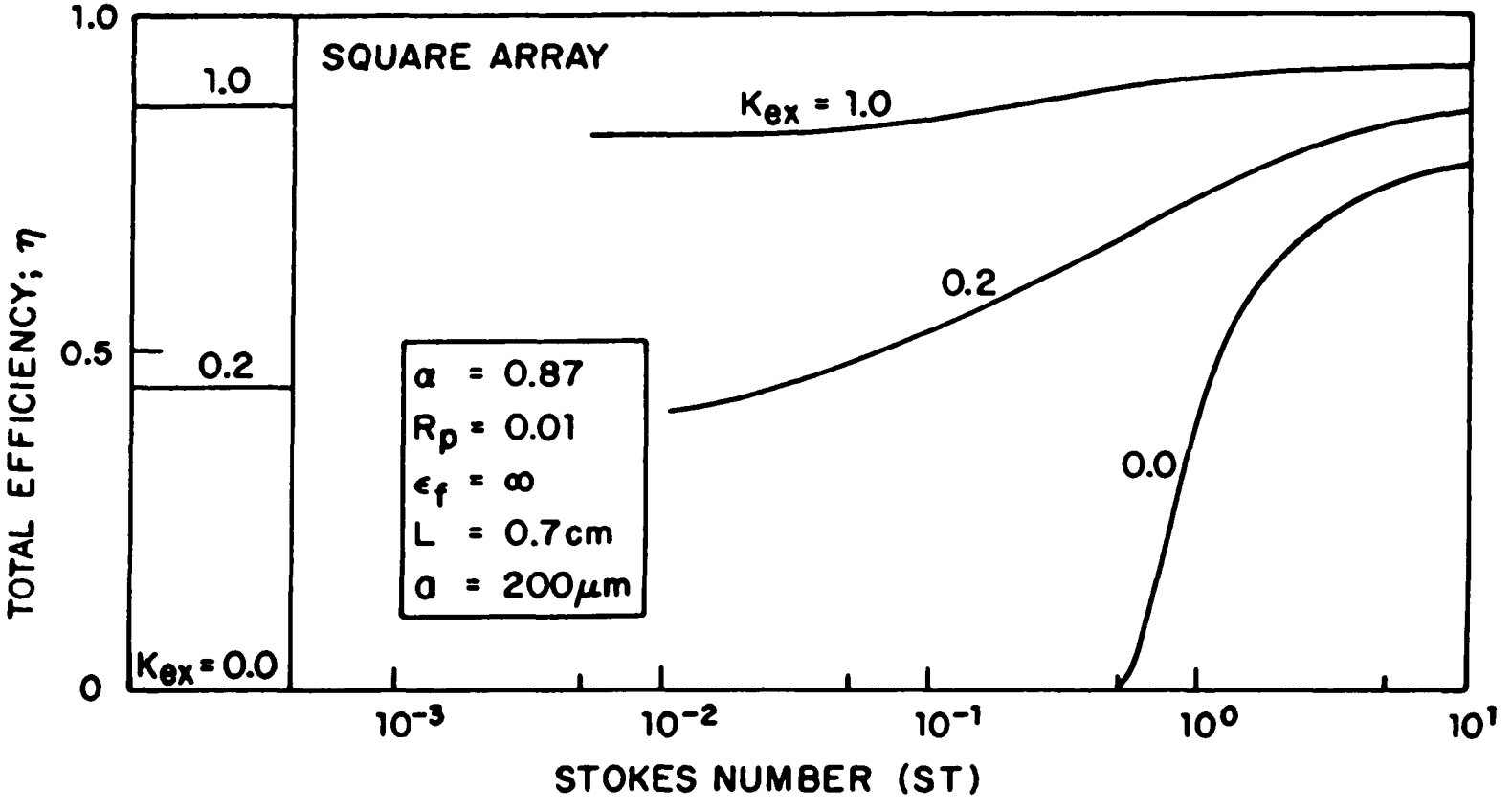

Figure B8. Total bed filtration efficiency of the square array as a function of Stokes number.

square array. The influence of electrostatic forces is more significant at low Stokes numbers: the total bed collection efficiency can be increased by increasing the electric number so that the efficiencies rise from 0 to 80% for Kex=1.0. The electric number is increased by increasing the electric field strength, raising the amount of electric charge on the particles or lowering the superficial gas velocity in the bed.

In Figure B9, experimental results using 1 μm in diameter latex particles for the square array containing textile fibers under the influence of electric forces are shown for two different average particle mobilities, $\bar{\omega}_p$ (or charge, see Eq. B5). As shown before, the particles charged by a corona charger have a wide mobility distribution and the filter efficiency is a function of particle mobility. Therefore, the distribution of particle mobility must be taken into account in the theoretical computation. There are three methods by which this can be done as shown in Figure B9. First, by assuming that all particles have the same mobility equal to two thirds of the measured average particle mobility:

$$\omega_p = \frac{2}{3}\bar{\omega}_p \qquad (B17)$$

as was demonstrated earlier by Tardos (1982). Second, by integrating the filter efficiency over the whole range of particle mobility distribution. The total efficiency is given in this case by

$$\eta = \int_0^\infty \eta(\omega_p) N(\omega_p) d\omega_p \qquad (B18)$$

where $\eta(\omega_p)$ is the filter efficiency which is obtained from trajectory calculations with the particle mobility, ω_p as a parameter. Third, by fitting the values of the filter efficiency as a function of mobility

with an exponential curve and substituting into equation (B18). The exponential curve was assumed to be of the form

$$\eta(\omega_p) = 1 - \exp(-2Kex) \qquad (B19)$$

The results depicted in Figure B9 show no significant difference for the three methods used and the agreement is very good indeed. In the following computations, therefore, the first method is preferred because of its simplicity.

The charge on the aerosol is influenced by the humidity of the gas stream as shown in Figure B4 and, therefore, the total bed efficiency changes as the humidity changes. The influence of humidity on the total bed efficiency for the square array of fibers is shown in Figure B10. The relative humidity was varied from 0 to above 90%. The three solid lines in the figure were computed for three values of the dielectric constant ϵ_f= 1, 2 and ∞, respectively. As seen, all data show very good agreement with the theoretical computations even thought particle charging increases with increasing humidity because the dimensionless electric number ,Kex, includes the influence of particle mobility (or of particle charge).

Experiments with DOP and alumina particles

In industry, filters have to handle large amounts and wide size ranges of dust particles and still maintain high filtration efficiencies with low pressure drops through the filters. From the theoretical computations and from experiments with monodisperse latex particles (D_p= 1.1 μm) and shallow fibrous beds (L = 0.7 cm) of high porosity (α = 0.87), it was demonstrated above that these goals can be

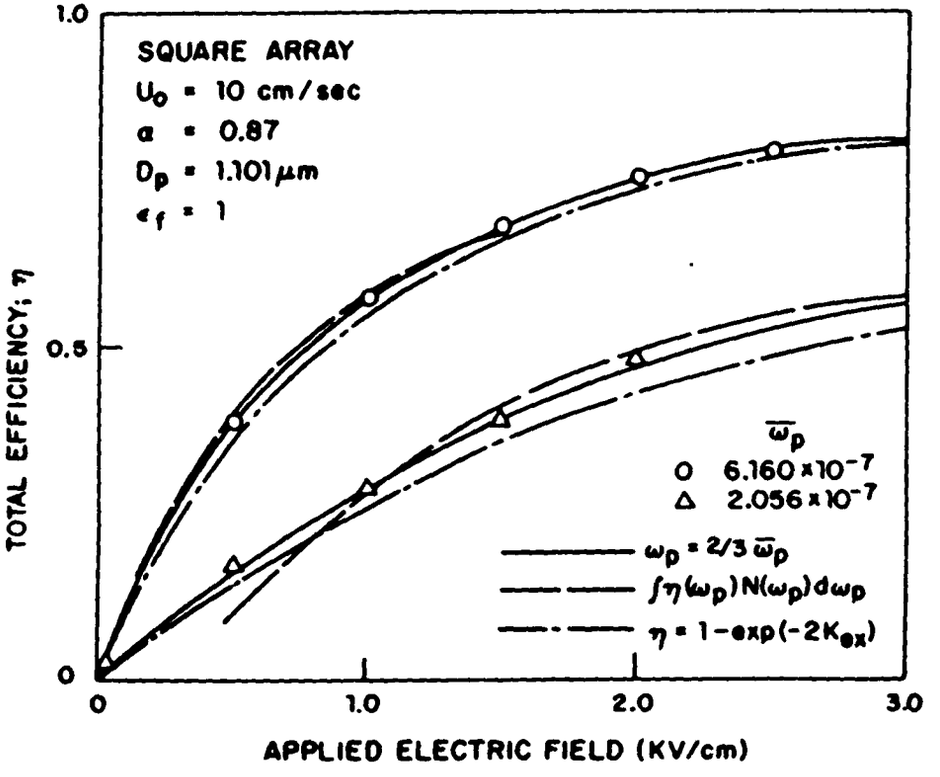

Figure B9. Filtration efficiency for the square array as a function of applied electric field.

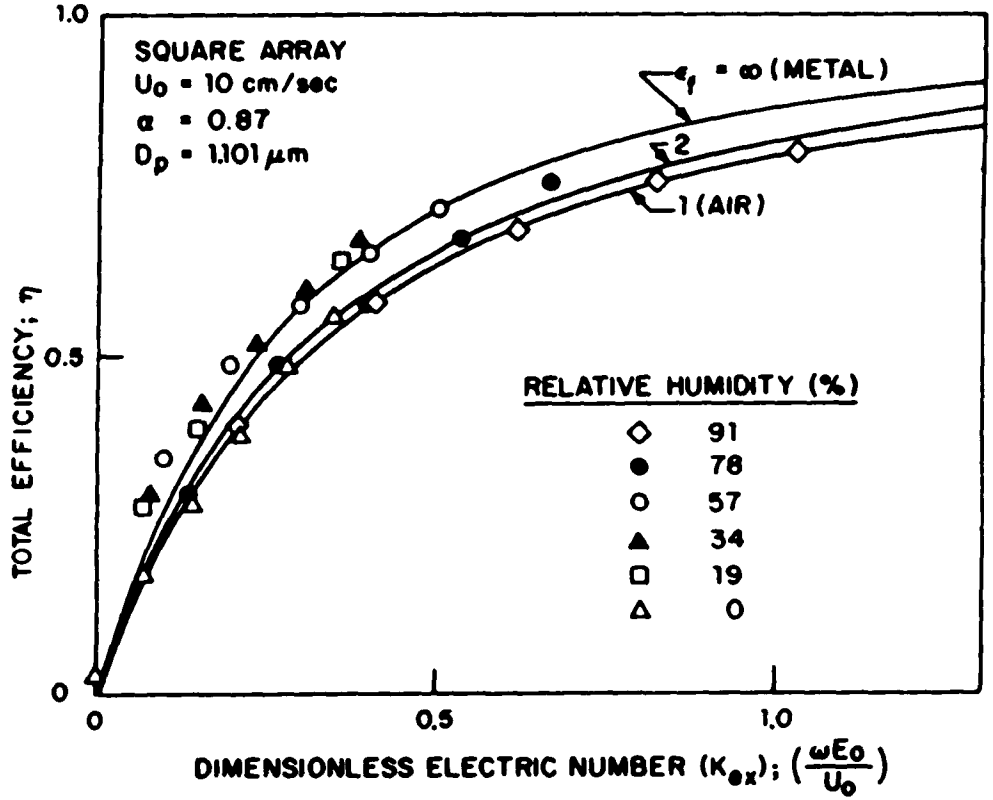

Figure B10. Filtration efficiency of the square array as a function of the dimensionless electric number for different humidities. Charges on the aerosol particles taken from Figure B4.

easily achieved. In order to demonstrate the possibility of industrial applications of the electrostatic fibrous filter, DOP and alumina dust particles were used to test the model staggered and square fibrous filters with a wide size range of dust particles at the filter inlet. Figure B11 shows an example of the filtration efficiency of DOP and alumina particles as a function of the applied electric field across the filter using a square array. At low electric fields (2.0 KV/cm), the filtration efficiency of DOP increases from zero to more than 50% for all particles. Alumina dust particles show an even higher efficiency than DOP particles because they carry some rezidual charges which are often generated in the powder disperser. Alumina particles therefore show efficiencies of about 10 to 20% even at zero external electric fields. It is believed that 99% efficiency can be easily obtained by increasing the electric field across the filter to higher levels (8-9 KV/cm) and using a thicker fibrous bed.

In order to compare the direct measurements to theoretical calculations the electric charge on DOP particles was also measured in the mobility analyzer for different particle sizes. The number of electric charges was found to be proportional to the surface area of the DOP particles: the larger the particles the higher the acquired charges. Also, as found before, the amount of charges on the particles increased with increasing gas relative humidity.

Figure B12 shows the efficiency of the square array as a function of the dimensionless electric number, Kex, for different humidities and different gas velocities. Comparison with theoretical calculations is difficult in this case because particle sizes counted into a certain channel of the Climet counter are between two limits for example between 1 and 2 microns. The particle charge might be therefore four

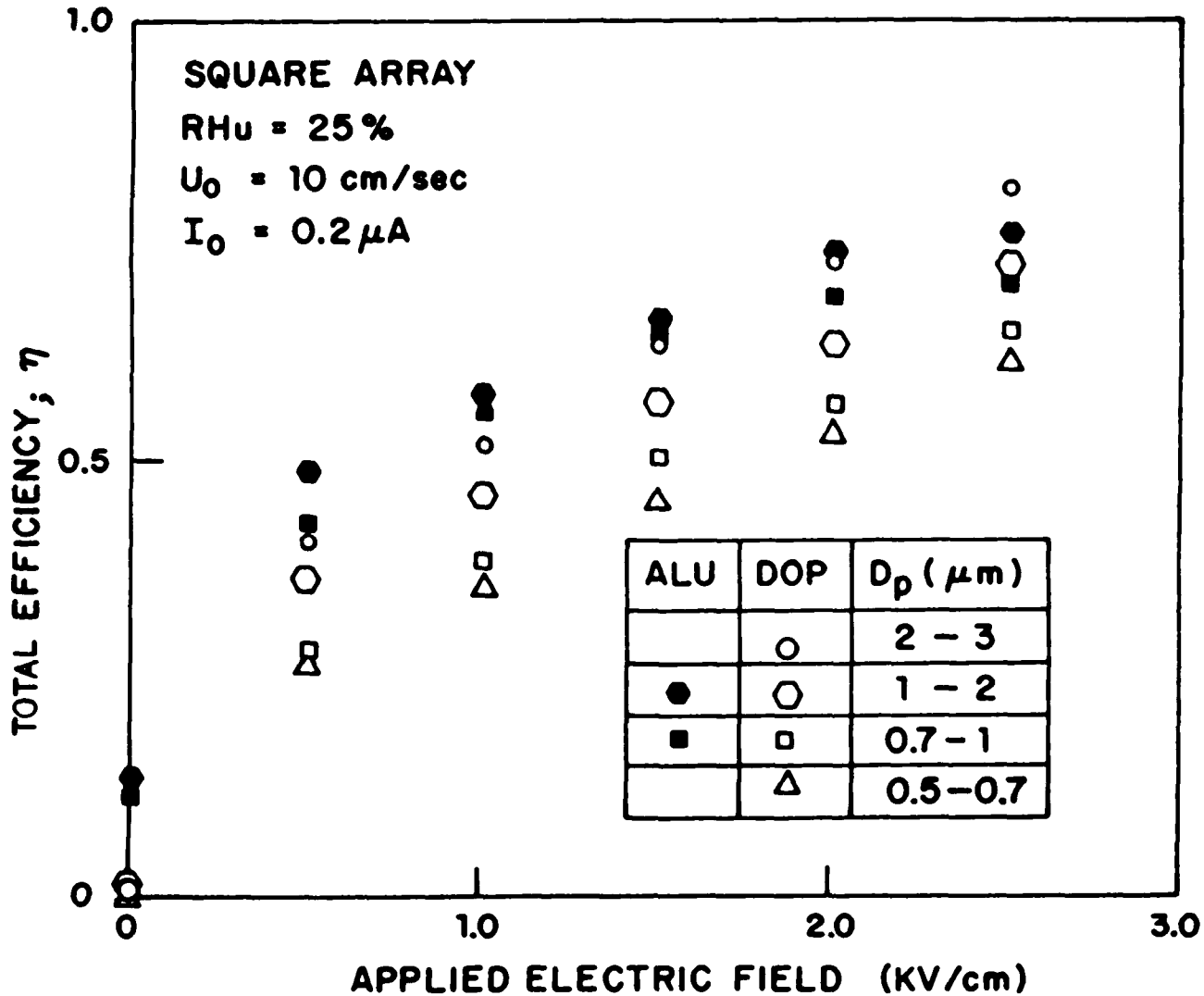

Figure B11. Filtration efficiency of the square array for DOP and alumina dust particles (ALU).

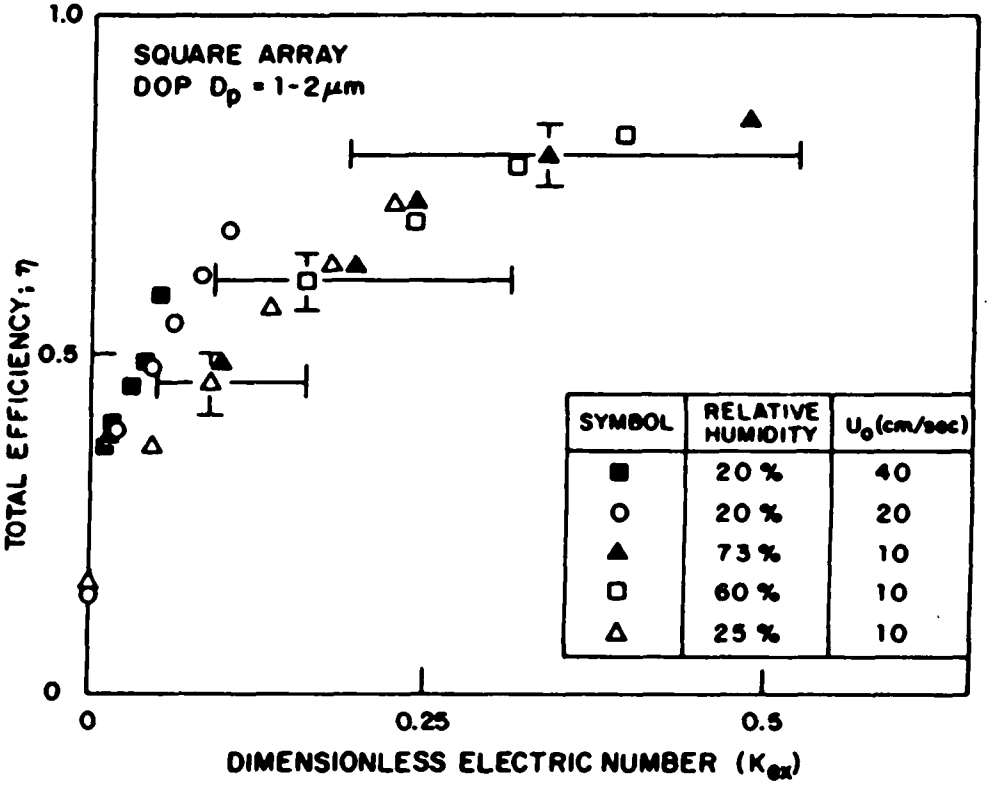

Figure B12. Filtration efficiency of the square array as a function of the dimensionless electric number for DOP particles.

times higher on a 2 micron particle as compared to a one micron particle. If maximum and minimum values of particle charges are taken for the two micron and one micron particles for example, the values of the dimensionless electric number will cover a wide range as shown in the figures and the calculated efficiencies will also vary, as shown. Furthermore, there are other very small sized particles which cannot be measured by the Climet counter. Those particles might carry some charge and influence the aerosol filtration efficiency of the fibrous bed. The most important point is that the filters can be operated under high velocities and still maintain high efficiencies (during the present experiments, the velocities were increased four times). This observation is very important in scale-up and industrial applications for handling large amounts of gas.

B.5. CONCLUSIONS

A filtration model predicting both the unit cell and the total bed collection efficiencies for regular arrays of fibrous filter with electrostatic fields was developed. The model, using the flow field developed by Sangani and Acrivos (1982) and an electric potential field considering the effect of neighboring fibers, is based on trajectory calculation. The collection mechanisms taken into account are inertia, interception, and electrostatic effects. Furthermore, the influence of the humidity of the gas stream was also studied.

In the present work both flow and electrostatic fields using actual configurations of fibrous filters were considered together with the influences of the inertia, interception, and the electrostatic effects. The model predictions showed very good agreement with experimental data. The results show that inertia effects are strong

for Stokes number larger than unity. For small Stokes numbers, the filtration efficiencies can be significantly increased by using a corona charger to charge the dust particles and applying an external electric field across the fibrous bed. The particle charges and the electric fields are also influenced by the humidity of the gas stream in that the particle charges increase with increasing humidity.

V.3. APPENDIX C: COMPUTER PROGRAMS

Program 1: Program to collect data from the Climet system using an IBM PC

```
10   CLS
20   INPUT "NUMBER OF RUNS                          ";N
30   INPUT "AIR FLOW RATE, cu ft/min                ";Q
40   INPUT "ROTATING SPEED, RPM                     ";W
50   INPUT "BED THICKNESS, cm                       ";L
60   INPUT "PRESSURE DROP, in Water                 ";P
70   INPUT "RELATIVE HUMIDITY, RHu                  ";R
80   INPUT "FILE NAME FOR DATA                      ";F$
90   OPEN F$ FOR OUTPUT AS #2
100  OPEN "COM1:300,E,7,1,CS,DS,ASC" FOR INPUT AS #1
110  PRINT#2,N,Q,W,L,P,R
120  FOR I=1 TO N
130  PRINT:PRINT TAB(0);"RUN";I
140  FOR J=1 TO 5
150  LINE INPUT#1,A$
160  IF J=1 GOTO 200
170  B$=RIGHT$(A$,68)
180  PRINT B$
190  PRINT#2,B$
200  NEXT J
210  NEXT I
220  CLOSE 1
230  CLOSE 2
240  PRINT
250  INPUT "CONTINUE COLLECTING DATA Y/N";V$
```

```
260 PRINT
270 IF V$="Y" OR V$="y" GOTO 20
280 RUN "A:CLIMIT.BAS
290 END
```

PROGRAM 2: Program to compute the total bed filtration efficiency using an IBM PC and sample data calculation

```
10   DIM A(16),T(16),E(8)
20   CLS
30   INPUT "NAME OF DATA FILE ";F$
40   OPEN F$ FOR INPUT AS #2
50   INPUT#2,N,Q,W,L,P,R
60   PRINT "NUMBER OF RUNS              ";N
70   PRINT "AIR FLOW RATE, cu ft/min    ";Q
80   PRINT "ROTATING SPEED, RPM         ";W
90   PRINT "BED THICKNESS, cm           ";L
100  PRINT "PRESSURE DROP, in Water     ";P
110  PRINT "RELATIVE HUMIDITY, RHu      ";R
120  PRINT
130  FOR K=1 TO 16
140  T(K)=0
150  NEXT K
160  FOR I=1 TO N
170  PRINT "RUN:";I
180  M=0
190  FOR J=1 TO 4
200  LINE INPUT#2,A$
210  FOR K=1 TO 4
220  M=M+1
230  K1=12+(K-1)*17
240  B$=LEFT$(A$,K1)
250  AT=VAL(RIGHT$(B$,6))
260  A(M)=CINT(AT)*10^(CINT((AT-CINT(AT))*10))
```

```
270  T(M)=T(M)+A(M)
280  NEXT K
290  PRINT A$
300  NEXT J
310  PRINT
320  NEXT I
330  CLOSE 2
340  PRINT "THE AVERAGE FILTRATION EFFICIENCY OF THE RFBF:"
350  PRINT
360  PRINT TAB(1);"CHANNEL";TAB(12);"EFFICIENCY";TAB(30);
     "IN CONC. (#/LITER)";TAB(55);"OUT CONC. (#/LITER)"
370  TI=0
380  TO=0
390  TE=0
400  FOR J=1 TO 8
410  E(J)=0
420  IF T(J) >= T(J+8) GOTO 440
430  E(J)=(1-T(J)/T(J+8))*100
440  T(J)=T(J)/N/2.8317
450  T(J+8)=T(J+8)/N/2.8317
460  TI=TI+T(J+8)
470  TO=TO+T(J)
480  PRINT TAB(4);J;
490  PRINT TAB(14) USING "###.##";E(J);
500  PRINT TAB(32) USING "########";T(J+8);
510  PRINT TAB(58) USING "########";T(J)
520  NEXT J
530  IF TO >= TI GOTO 550
```

```
540  TE=(1-TO/TI)*100
550  PRINT
560  PRINT "TOTAL CONCENTRATION";TAB(32) USING "########";TI;
570  PRINT TAB(58) USING "########";TO
580  PRINT "TOTAL EFFICIENCY OF RFBF %: "USING "###.##";TE
590  PRINT
600  INPUT "CONTINUE ANOTHER DATA FILE Y/N";V$
610  IF V$="Y" OR V$="y" GOTO 30
620  RUN "A:CLIMET.BAS
630  END
```

Sample data calculation

```
NUMBER OF RUNS              5
AIR FLOW RATE, cu ft/min    250
ROTATING SPEED, RPM         465
BED THICKNESS, cm           1
PRESSURE DROP, in Water     14.6
RELATIVE HUMIDITY, RHu      43

RUN: 1
C01   1188.2PC   C02   7528.1PC   C03   4958.1PC   C04   3202.1PC
C05   2192.0PC   C06   0806.0PC   C07   0363.0PC   C08   0000.0PC
C09   1513.2PC   C10   8396.1PC   C11   8498.1PC   C12   1041.2PC
C13   1268.1PC   C14   1391.0PC   C15   0000.0PC   C16   0000.0PC

RUN: 2
C01   1176.2PC   C02   7428.1PC   C03   4774.1PC   C04   2850.1PC
C05   0579.0PC   C06   0122.0PC   C07   0070.0PC   C08   0000.0PC
C09   1504.2PC   C10   8311.1PC   C11   8368.1PC   C12   1019.2PC
C13   1218.1PC   C14   1275.0PC   C15   0001.0PC   C16   0000.0PC

RUN: 3
C01   1167.2PC   C02   7317.1PC   C03   4731.1PC   C04   2856.1PC
C05   0509.0PC   C06   0117.0PC   C07   0061.0PC   C08   0000.0PC
C09   1486.2PC   C10   8167.1PC   C11   8330.1PC   C12   1011.2PC
C13   1208.1PC   C14   1354.0PC   C15   0001.0PC   C16   0000.0PC

RUN: 4
C01   1184.2PC   C02   7536.1PC   C03   4833.1PC   C04   2928.1PC
C05   0486.0PC   C06   0085.0PC   C07   0060.0PC   C08   0000.0PC
C09   1511.2PC   C10   8313.1PC   C11   8521.1PC   C12   1030.2PC
C13   1229.1PC   C14   1341.0PC   C15   0001.0PC   C16   0000.0PC

RUN: 5
C01   1159.2PC   C02   7309.1PC   C03   4702.1PC   C04   2839.1PC
C05   0550.0PC   C06   0131.0PC   C07   0058.0PC   C08   0000.0PC
C09   1477.2PC   C10   8165.1PC   C11   8274.1PC   C12   1007.2PC
C13   1231.1PC   C14   1338.0PC   C15   0000.0PC   C16   0000.0PC

THE AVERAGE FILTRATION EFFICIENCY OF THE RFBF

CHANNEL   EFFICIENCY   IN CON. (#/LITER)   OUT CONC. (#/LITER)
   1         21.59          52908               41487
   2         10.24          29206               26216
   3         42.85          29658               16950
   4         71.27          36077               10365
   5         92.99           4347                 305
   6         81.18            473                  89
   7          0.00              0                  43
   8          0.00              0                   0

TOTAL CONCENTRATION        152670               95455
TOTAL EFFICIENCY OF RFBF %:        37.48

CONTINUE ANOTHER DATA FILE Y/N?
```

PROGRAM 3: Program to collect data for electrostatic charge measurements on granules in the RFBF

```
10   DEF SEG = $HC000
20   A%=0:FLG%=0:BRD%=0
30   CMA$ = "SYSCON MAD=3,CIC=1,NOB=1,BAO=&H300"
40   BT=0
50   IE488=0
60   INPUT "FILE NAME FOR CHARGE ";F$
70   INPUT "NUMBER OF DATA RUNS  ";N
80   OPEN F$ FOR OUTPUT AS #1
90   PRINT#1, N
100  FOR J=1 TO N
110  REM COLLECTING DATA USING ACQU IEE488 BOARD
120  CALL IE488 (CMA$,A%,FLG%,BRD%)
130  CMD$ = "OUTPUT 9[$]"
140  BRD%=0
150  A$="DCV3"+CHR$(13)
160  CALL IE488 (CMD$,A$,FLG%,BRD%)
170  B$=SPACE$(20)
180  CMDD$ = "ENTER 9[$,0,18]"
190  CALL IE488 (CMD$,B$,FLG%,BRD%)
200  REM FINISHED OF IEE488
210  PRINT J,B$
220  BV=VAL(B$)
230  PRINT#1,BV
240  NEXT J
250  CLOSE 1
260  END
```

PROGRAM 4: Program to analyze charge distribution on granules in the RFBF

```
10   DIM CHARGE(1000),CH(1000)
20   INPUT "FILE NAME                    ";F$
30   INPUT "ORDER OF COULOMBUS READING   ";O$
40   INPUT "TYPE OF AEROSOL              ";A$
50   OPEN F$ FOR INPUT AS #1
60   INPUT #1,N
70   FOR I=1 TO N
80   INPUT #1,BV
90   CH(I)=BV
100  NEXT I
110  CLOSE 1
120  INPUT "LOWER LIMIT OF THE DIFFERENCE BETWEEN TWO DATA":LOWER
130  INPUT "UPPER LIMIT OF THE DIFFERENCE BETWEEND TWO DATA":UPPER
140  L=0
150  MIN=0
160  MAX=0
170  NC=0
180  PC=0
190  SNC=0
200  SPC=0
210  REF=CH(1)
220  FOR I=2 TO N
230  C=CH(I)-REF
240  IF ABS(C) < LOWER GOTO 360
250  IF ABS(C) > UPPER GOTO 360
260  L=L+1
```

```
270  IF MAX<C THEN MAX=C
280  IF MIN>C THEN MIN=C
290  CHARGE(L)=C
300  IF C >= 0 GOTO 340
310  NC=NC+1
320  SNC=SNC+C
330  GOTO 360
340  PC=PC+1
350  SPC=SPC+C
360  REF=CH(I)
370  NEXT I
380  IF NC=0 GOTO 400
390  AVNEG=SNC/NC
400  IF PC=0 GOTO 420
410  AVPOS=SPC/PC
420  SUM=NC+PC
430  PRINT TAB(16);"TOTAL # OF CHARGED GRANULES:";SUM
440  PRINT:INPUT "WANT A SUMMARY, Y/N  ";Y$
450  IF Y$ <> "y" AND Y$ <> "Y" THEN GOSUB 800
460  NETAV=(SNC+SPC)/SUM
470  ABSAV=(ABS(SNC)+SPC)/SUM
480  PRINT "FILE NAME:";F$;TAB(24);"AEROSOL :";A$
490  PRINT:PRINT TAB(2);"# OF NEGATIVE CHARGED GRANULES:";NC
500  PRINT TAB(2);"# OF POSITIVE CHARGED GRANULES:";PC
510  PRINT:PRINT "TOTAL  # OF CHARGED GRANULES  :";SUM
520  PRINT "NET AVERAGE CHARGE       :";NETAV
530  PRINT "ABSOLUTE AVERAGE CHARGE  :";ABSAV
540  IF MIN<0 THEN MIN=INT(MIN) ELSE MIN=1+INT(MIN)
```

```
550  IF MAX>0 THEN MAX=1+INT(MAX) ELSE MAX=INT(MAX)
560  PRINT:INPUT "INCREMENT FROM MINIMUM TO MAXIMUM";INCR
570  PRINT TAB(3)"FROM";TAB(19);"TO";TAB(33);"# GRANULES";TAB(54);"%"
580  FOR I=MIN TO MAX STEP INCR
590  IF ABS(I-MAX)<=.0001 GOTO 700
600  COUNT=0
610  FOR K=1 TO L
620  IF ABS(I)<=.0001 GOTO 650
630  IF CHARGE(K)>I AND CHARGE(K)<I+INCR THEN COUNT=COUNT+1
640  GOTO 660
650  IF CHARGE(K)>I AND CHARGE(K)<=I+INCR THEN COUNT=COUNT+1
660  NEXT K
670  PRINT TAB(3);I;TAB(17);I+INCR;TAB(35);COUNT;
680  PRINT TAB(51) USING "###.##";100*COUNT/SUM
690  NEXT I
700  PRINT "LOWER LIMIT:";LOWER
710  PRINT "UPPER LIMIT:";UPPER
720  PRINT TAB(19);"*-*-*-*-*-*-*-*-*-*-*-*-*-*"
730  INPUT "CHANGE THE INCREMENT, Y/N";Y$
740  IF Y$ <> "y" AND Y$ <> "Y" THEN 750 ELSE 560
750  INPUT "CHANGE THE LIMIT, Y/N";Y$
760  IF Y$ <> "y" AND Y$ <> "Y" THEN 770 ELSE 120
770  PRINT:INPUT "ANOTHER FILE, Y/N";Y$
780  IF Y$ <> "y" AND Y$ <> "Y" THEN END ELSE 20
790  END
800  INPUT "CHANGE THE LIMIT, Y/N";Y$
810  IF Y$ <> "y" AND Y$ <> "Y" THEN 770 ELSE 120
820  END
```

V.4. APPENDIX D: RODOS 12 SR PARTICLE GENERATOR

The Rodos-type dust particle feeder is capable of generating an aerosol concentration of up to about 1 g/m^3. This high aerosol concentration is necessary to test the RFBF at conditions similar to those present in an industrial environment. The feeding and dispersion in the Rodos system is accomplished by means of a well defined subdivision of operations into consecutive functional stages. This has a wide range of applications whenever the feeding of dispersed solids in the form of an aerosol jet at constant flow rate is required. The system is shown in Figure D1 and its schematic diagram, in Figure D2.

The feeding process starts from the feed hopper (1) with the use of a vibrating chute feeder (2) which pours powder into the annular groove of a rotary table (3) whose rotational speed can be regulated (12). The cone of particulate material which remains in the groove of the rotary table turning under the vibrating chute is subsequently levelled to a preselected hight by an adjustable plough scraper (4). It is then compacted by a stationary roller (5) mounted above the groove in such a manner that the groove cross-section is completely and uniformly filled, even in the case of bulk materials with inferior flow properties. Any solid material adhering to the outer edge of the rotary blade is then removed by the rubber cleaning brush (17).

The dispersion of solid materials into individual particles begins with the entry of material into the ejector (6) and (7). The secondary flow in the central suction tube of the injector (8) is induced by a primary propellant jet in accordance with the aspirator principle. The propellant jet is generated at a present pressure by means of a compressed air system (14). The vacuum necessary for the suction is

thus generated. If necessary, the cascade impactor (9) serves as a supplementary dispersion in the case of difficult solids.

In the present experiments using an existing somewhat oversized feeder, it was possible to generate about 50 mg of fly ash per meter cube of air flowing through the RFBF which is about 50 to 100 times higher than the concentration used previously by the in house generator. However, the concentration of fly ash generated is still below the accepted industrial standard. It was also found that fly ash generated by the Rodos is at relatively low pressure. Operation with high air velocities creates a back pressure from the RFBF system and sometimes obstructs the fly ash pass of the Rodos feeder. This may be corrected by introducing a Venturi tube in the system or by sucking air from the outlet of the RFBF to create a low pressure for the Rodos' injecting system to avoid the blocking of the fly ash stream.

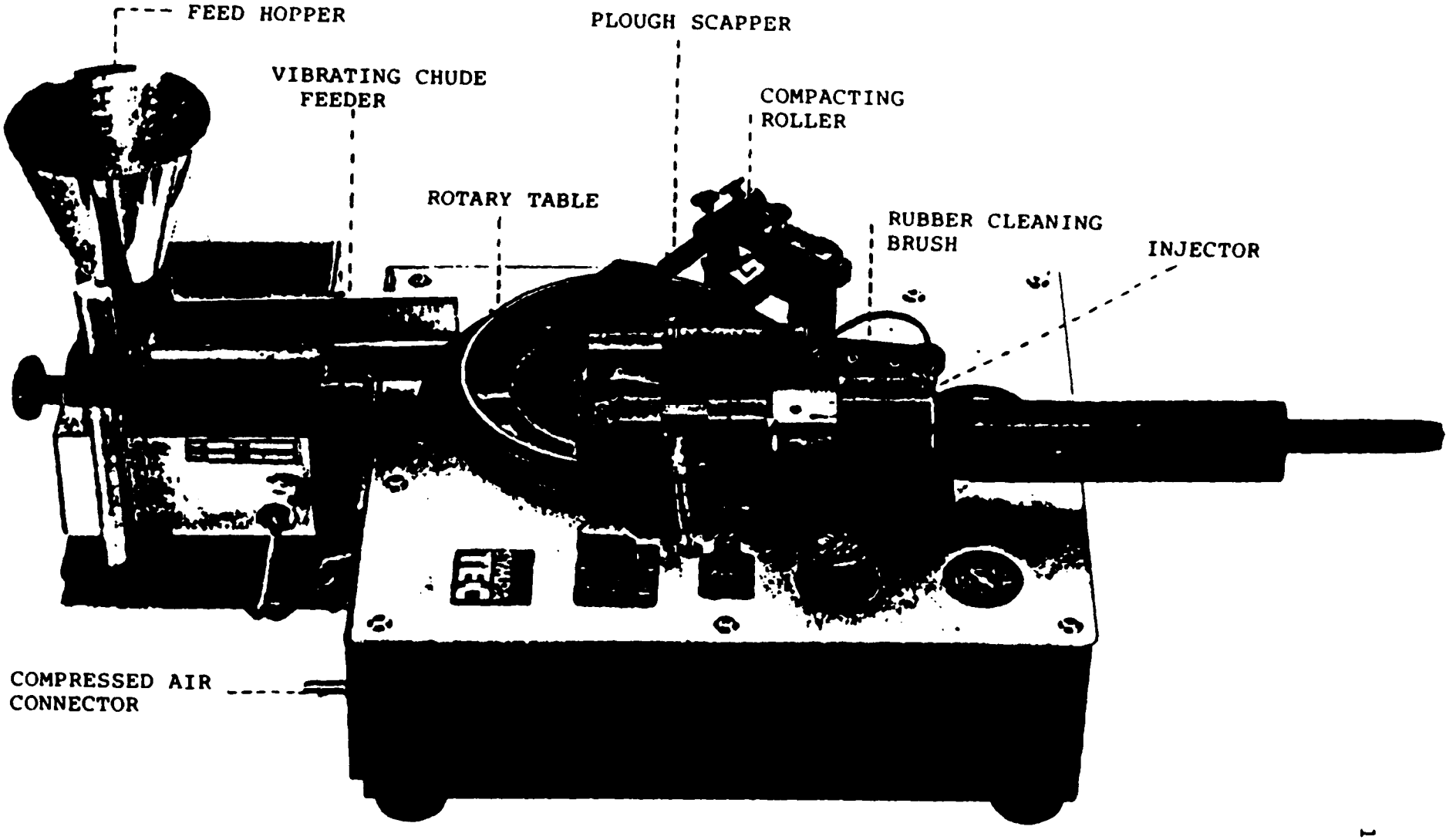

Figure D1. RODOS 12 SR particle generator.

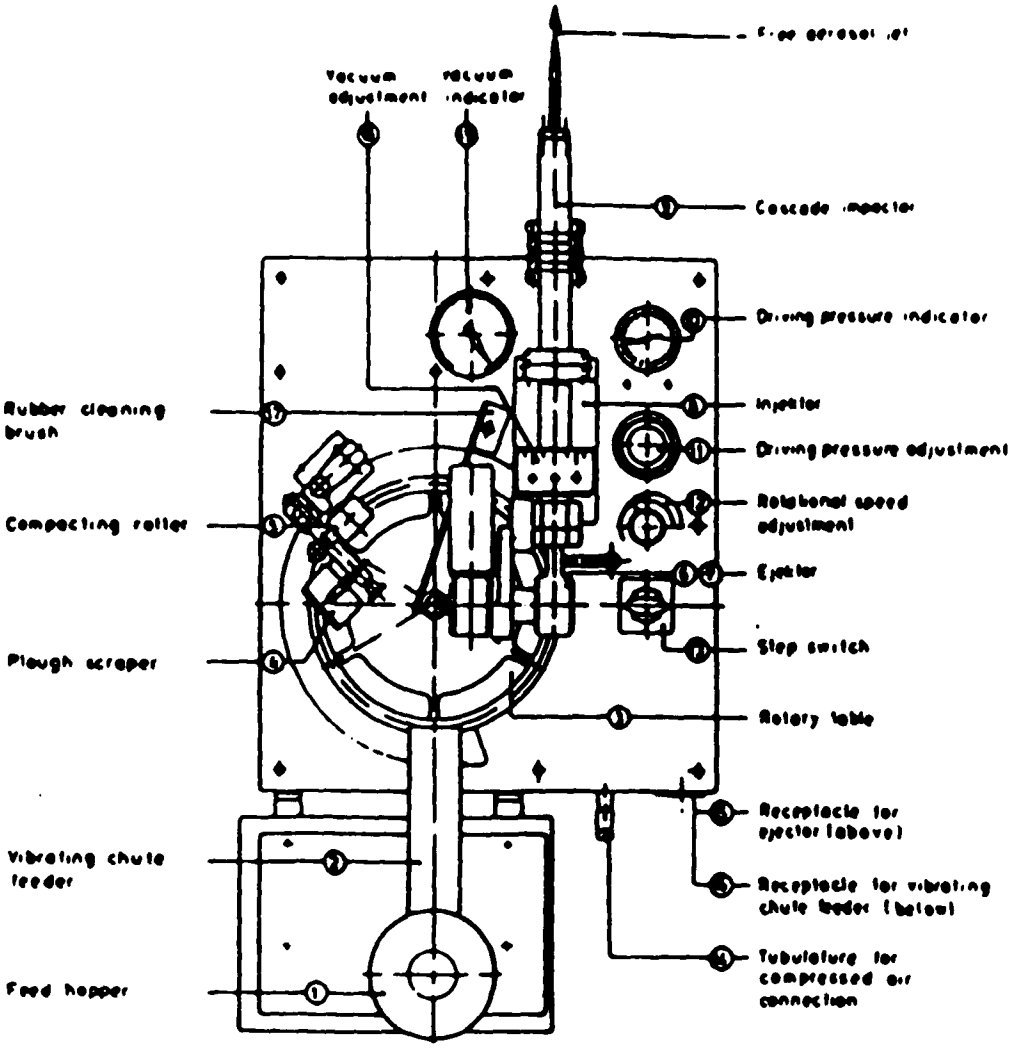

Figure D2. Construction of RODOS model 12 SR.

VI. NOTATION

a radius of granule

a_r radial acceleration

A_j average surface area of aerosol particles in the size range j

C Cunningham correction factor

C_o concentration of granules in the feed

C_t concentration of granules in the effluent at time t

d_g granule diameter

d_p dust particle size, diameter

E single sphere efficiency

F_{dust} amount of dust in the gas stream

$\vec{F}_{ext}$ external forces

g gravitational acceleration

h height of the cylinder bed

I current in Faraday cage

I_c current in corona charger

L thickness of RFBF

L_{load} dust particle loading on the granules

M particle size distribution in the boiler outlet

m_p mass of the aerosol particle

n number of granules counted

n_{in} number concentration of dust particles in the inlet stream

n_{out} number concentration of dust particles in the outlet stream

N_j number of aerosol particles of size range j

P pressure

ΔP_f pressure drop across the fluidized bed

ΔP_p pressure drop across the packed bed

$\tilde{q}_c$ average charge per granule

$\hat{q}_c$ absolute average charge per granule

q_i individual granule charge

Q total air flow rate

Q_{gas} volumetric flow rate of the gas

$\tilde{Q}_p$ average particle charge

r radius (coordinate)

r_i radius of the inner surface of the granule bed

r_o radius of the RFBF

r_p radius of the aerosol particle

Re_g granule's Reynolds number, $d_g \rho_f U_o / \mu$

RHu relative humidity

RPM round per minute

St Stokes number

t time

t_{sat} saturation time of granules

T dimensionless time

$\vec{u}$ air velocity

$\vec{U}$ dimensionless air velocity

U_{mf} average minimum fluidization velocity

U_{mf_c} critical minimum fluidization velocity

U_{mf_s} surface minimum fluidization velocity

U_o superficial air velocity based on the outside radius, r_o

U_r superficial air velocity as a function of radius, r

U_t local tangential velocity

V_g volume of granules in the RFBF

W rotating speed

W_g weight of the granules

W_p weight of the dust particles

$\vec{x}$ position vector

x, y coordinates

$\vec{X}$ dimensionless position vector

X, Y dimensionless coordinates

Greek letters

α volume fraction of the dust particles in the granule's surface layer

ϵ void fraction

η total bed filtration efficiency

$\eta_{overall}$ overall filtration efficiency of the RFBF

ν feed rate of granules

μ gas viscosity

ρ_f air density

ρ_g granule density

ρ_p aerosol particle density

ϕ_s sphericity of granule

θ angular coordinate

τ residence time

Notations for electrostatic fibrous filters

a fibrous (cylindrical) radius

a_n, b_n, c_n, d_n coefficients of stream function

A area of the collecting surface of the analyzer

C Cunningham correction factor

d separation between the plates in mobility analyzer

d_{ij} distance between fibers i and j

D_{ij} dimensionless distance between fibers i and j

D_p dust particle diameter

E unit cell efficiency

E_o applied electric field strength

I current in Faraday cage

Kex dimensionless electric number

ℓ unit cell length

L fibrous bed length

m number of cylinders around the center cylinder

m_b number of the unit cell layer in the bed

n number of cylinders taken into account in electric field

N number of points in the unit cell boundary to compute coefficients of stream function

n_{in}, n_{out} number concentrations of dust particles in the inlet stream and the outlet stream

Q the flow through the mobility analyzer

Q_a average particle charge

Q_p particle charge

r radius (coordinate)

r_p particle radius

R_p interception parameter

St Stokes number

t time

T dimensionless time

U_o superficial velocity

$\vec{u}^e$ velocity of electric field

$\vec{U}^e$ dimensionless velocity of electric field

U_i^f dimensionless flow velocity in the i direction

U_i^e dimensionless electric field velocity in the i direction

V applied voltage across the mobility analyzer

v_F gas flow rate through the Faraday cage

V_s voltage at which a removal efficiency of 63 percent

W complex potential function

x, y coordinates

X, Y dimensionless coordinates

$\vec{X}$ position vector

(X_i, Y_i) position of fiber i

Z position in complex coordinates

Z_i position of cylinder i

Z_{ij} position of first-order image of cylinder j in cylinder i

Greek letters

α fibrous bed porosity

μ gas viscosity

ψ stream function

ψ_o^e electric stream function

θ coordinate

$\epsilon = \frac{\epsilon_f/\epsilon_o - 1}{\epsilon_f/\epsilon_o + 1}$ polarization coefficient

ϵ_o dielectric constant of air

ϵ_f dielectric constant of fiber

ω vorticity

ω_p particle electric mobility

$\bar{\omega}_p$ average particle electric mobility

ρ_p particle density

ϕ_o^e electric potential function outside the fibers

ϕ_i^e electric potential function inside the fibers

η total filter efficiency

VII. REFERENCES

Banks, R. B. and J. W. Griffin, "Development of Electrostatic Enhancement for Commercial Fabric Filters," The Sixth Symposium on the Transfer and Utilization of Particulate Control Technology, New Orlean, Louisiana, February 25-28, 1986.

Bergman, W., R.D. Taylor, H. H. Miller, A. H. Biermann, H. D. Hebard, R. A. daRosa, and B. Y. Lum, "Enhanced Filtration Program ar LLL - A Progress Report," DOE Contract W-F405-EMG-48, 1978.

Black, G. H. and R. W. Boubel, "Effectiveness of a Fluidized Bed in Removing Submicron Particulate From an Air Stream", I&EC Process Design Develop., Vol. 8, 573, 1979.

Carr, R. C. and W. B. Smith, "Fabric Filter Technology for Utility Coal-Fired Power Plants - Part II: Application of Baghouse Technology in the Electric Utility Industry", J. of the Air Pollution Control Association, Vol. 31, No. 2, 178, 1984a.

Carr, R. C. and W. B. Smith, "Fabric Filter Technology for Utility Coal-Fired Power Plants - Part III: Performance of Full-Scale Utility Baghouse", J. of the Air Pollution Control Association, Vol. 31, No. 3, 281, 1984b.

Carr, R. C. and W. B. Smith, "Fabric Filter Technology for Utility Coal-Fired Power Plants", J. of the Air Pollution Control Association, Vol. 34, No. 1, 79, 1984c.

Chen, Y. M., "Fundamentals of a Centrifugal Fluidized Bed", AIChE Journal, in press, 1986.

Dietz, P. W. "Electrostatic Filtration of Inertialess Particles by Granular Beds", J. Aerosol Sci., Vol. 12, 27, 1981.

Dorman, R. G., 'Dust Control and Air Cleaning", Pergamon Press, Oxford 1974.

D'Ottavio, T. and S. L. Goren, "Aerosol Capture in Granular Beds in the Impaction Dominated Regime", Aerosol Sci. and Technol., Vol. 2, 91, 1983.

Emi, H., K. Okuyama and M. Adachi, "The Effect of Neighbouring Fibers on the Single Fiber Inertia-Interception Efficiency of Aerosols," J. Chemical Engineering of Japan, Vol. 10, No. 2, pp. 148-153, 1977.

Emi, H., K. Okuyama and N. Yoshioka, "Prediction of Collection Efficiency of Aerosols by High-Porosity Fibrous Filter," J. Chemical Engineering of Japan, Vol. 6, No. 4, pp. 349-354, 1973.

Ergun, S., "Fluid Flow Through Packed Column", Chem. Eng. Progr., Vol. 48, 89, 1952.

Fan, K. C., and J. W. Gentry, "Effect of Packing Density on Collection Efficiencies of Charged Fibers," Ind. Eng. Chem. Fundom., Vol. 18, No. 4, pp. 306-311, 1979.

Fan, L. T., C. C. Chang, Y. S. Yu, T. Takahashi and Z. Tanaka, "Incipient Fluidization Condition for a Centrifugal Fluidized Bed", AIChE Journal, Vol 31, No. 6, 999, 1985.

Frederick, E. R., JAPCA, Vol. 30, No. 4, pp. 426-431, 1980.

Gal, E., "Dust Filtration in Granular Beds", Ph.D. Dissertation, The City University of New York, 1984.

Gal, E., G. I. Tardos and R. Pfeffer, "An Experimental Evaluation of the Rotating Fluidized Bed Filter", World Filtration Congress III, 1982.

Gal, E., G. I. Tardos and R. Pfeffer, "A Study of Inertial Effects in Granular Bed Filtration", AIChE Journal, Vol. 31, No. 7, 1093, 1985.

Happel, J., "Viscous Flow Relative to Arrays of Cylinders," Am. Inst. Chem. Eng. J., Vol. 5, pp. 174-177, 1959.

Harriot, G. M., and D. A. Saville, "Electrically Stimulated Aerosol Filtration in Packed Beds," AIChE Journal, Vol. 26, No. 3, pp. 398-402, 1980.

Harrop, J. A., and J. I. T. Stenhouse, "The Theoretical Predication of Inertial Impaction Efficiencies in Fibrous Filters," Chem. Eng. Sci., Vol. 24, pp. 1475-1481, 1969.

Henry, F., and T. Ariman, "The Effect of Neighboring Fibers on the Electric Field in a Fibrous Filter," J. Aerosol Sci., Vol. 12, pp. 137-149, 1981.

Henry, F. S., and T. Ariman, "An Evaluation of the Kuwabara Model," Particulate Science & Tech., Vol. 1, pp. 1-20, 1983.

Henry, F., and T. Ariman, "A Staggered Array Model of a Fibrous Filter with Electrical Enhancement," Particulate Sci. & Tech., Vol. 11, No. 2, pp. 139-154, 1983.

Henry, F., W. F. Podolski, and S. C. Saxena, "Electrostatically Augmented Gas Cleanup Devices for Particulate Removal," presented at the annual meeting of the Industrial Applications Society of the IEEE, San Francisco, California, 1982.

Ho, C. P., and C. S. Wang, "Collection of Solid Particles on Single Cylinders by Particle Inertia and Electrical Forces," Recent Develop. in Gas/Particle Separation, NSFA, No. INT 78-21376, 109, 1981.

Hochrainer, d., and G. M. Hidy, "Creeping Motion of Charged Particles around a Cylinder in an Electrical Field," J. of Colloid and Interface Sci., Vol. 30, No. 4, pp. 553-567, 1969.

Hovis, L. S., Y. J. Chen and R. P. Donovan, "Laboratory Studies of electrically enhanced fabric filtration," Proceedings: Fifth Symposium on the Transfer and Utilization of Particulate Control Technology, held in Kansas City, Missouri, 1984, Vol. 3, CS-4404-Research Project 1835-6, February 1986.

Jackson, J. D., Classical Electrodynamics, Second Ed., New York: John Wiley & Sons Inc., 1975, ch. 4, pp. 147-152.

Kallio, G. A., and P. W. Dietz, "Image Charge Collection of Fine Particles in Granular Beds," presented at the 7th TDFM Conference on Gas Borne Particles, Oxford, England, 1981.

Kallio, G. A., D. W. Dietz, and C. Gutfinger, "Theoretical and Experimental Filtration Efficiencies in Electrostatically Augmented Granular Beds," Proc. of the Symp. on the Transfer and Utilization of Particulate Control Technology, Denver, 1979.

Kao, J., R. Pfeffer and G. I. Tardos, "On Partial Fluidization in Rotating Fluidized Beds," AIChE Journal, Vol. 33, No. 5, pp. 858-861, 1987.

Kao, J., G. I. Tardos and R. Pfeffer, "Dust Deposition in Electrostatically Enhanced Fibrous Filters," IEEE Transactions on Industry Applications, Vol. IA-23, No. 3, pp. 464-473, 1987.

Kao, J., P. Vinh, G. I. Tardos and R. Pfeffer, "Development of a Rotating Fluidized Bed Dust Filter," Interim Annual Report to NYERDA, 819-ERER-BEA-86, 1987.

Kirsh, A. A., J. Aerosol Sci., Vol. 3, 25, 1972.

Krupp-Koppers, British Patent No. 1921684, 1974.

Kuwabara, S., "The forces Experienced by Randomly Distributed Parallel Circular Cylinders or Spheres in a Viscous Flow at Small Reynolds Numbers," J. of the Physical society of Japan, Vol. 14, No. 4, pp. 527-532, 1959.

Lamb, G. E. R. and R. I. Jones, "Pressure Drop for a Filter Bag Operating with a Lightning - Rod Precharger," Proceedings: Fifth Symposium on the Transfer and Utilization of Particulate Control Technology, held in Kansas City, Missouri, 1984, Vol. 3, CS-4404-Research Project 1835-6, February 1986.

Lamb, S. H., Hydrodynamics, Sixth Ed., London: Cambridge University Press, 1932, pp. 133-135.

Levy, E. K. and J. C. Chen, "Centrifugal Fluidization: A Review", Int. Power and Bulk Solids Handling and Processing Conf., Rosemont, IL, 1977.

Levy, E. K., N. Martin and J. Chen, "Minimum Fluidization and Start-Up of a Centrifugal Fluidized Bed", in Fluidization, J. F. Davidson and D. L. Keairns, Editors, Cambridge University Press, Cambridge, 1978.

McElroy, M. W., R. C. Carr, D. S. Ensor and G. R. Markowski, "Size Distribution of Fine Particles from Coal Combustion," Science, Vol. 215, No. 4528, pp. 13-19, 1982.

Morris, B. A., G. E. R. Lamb and D. A. Saville, "Modeling Studies of Pressure Drop Reduction in Electrically Simulated Fabric Filtration," Proceedings: Fifth Symposium on the Transfer and Utilization of Particulate Control Technology, held in Kansas City, Missouri, 1984, Vol. 3, CS-4404-Research Project 1835-6, February 1986.

Nielsen, K. A., "Collection of Inertialess Particles on Circular Cylinders with Electrical Forces and Gravitation," J. of Colloid and Interface Sci., Vol. 64, No. 1, pp. 131-142, 1978.

Nielson, K. A. and J. C. Hill, "Collection of Inertialess Particles on Spheres with Electrical Forces", I&EC Fundamental, Vol. 15, 149, 1976.

Oglesby, S. Jr. and G. B. Nichols, "Electrostatic Precipitation", Marcel Dekker, Inc., New York, 1978.

Paretsky, L. C., L. Theodore, R. Pfeffer and A. M. Squires, J. Air Pollution Control Assoc., Vol. 21, 204, 1971.

Paytakes, A. C., C. Tien, and R. M. Turian, "A New Model for Granular Porous Media: Part I - Model formulation," AIChE J., Vol. 28, pp. 677-686, 1973.

Pfeffer, R. and F. B. Hill, "a Feasibility Study on the Use of a Rotating Fluidized Bed as a Dust Filter", BNL 50990, 1978.

Pfeffer, R., G. I. Tardos and E. Gal, "The Use of a Rotating Fluidized Bed as a High Efficiency Dust Filter", Eng. Found. Conf., Fluidization V, Denmark, 1986.

Pontius, D. H., P. V. Bush and L. E. Sparks, "Performance of Large-Diameter Wires as Discharge Electrodes in Electrostatic Precipitators", J. of Air Pollution Control Association, Vol. 34, No. 12, 1203, 1984.

Reynolds, J., S. Kreidenweis and L. Theodore, "Results of a Baghouse Operation and Maintenance Survey on Industry and Utility Coal-Fired Boilers", J. of the Air Pollution Control Association, Vol. 33, No. 4, 352, 1983.

Sangani, A. S., and A. Acrivos, "Slow Flow Past Periodic Array of Cylinders with Application to Heat Transfer," Int. J. Multiphase Flow, Vol. 8, No. 3, pp. 193-206, 1982.

Snaddon, R. W. L. and P. W. Dietz, "Interstitial Flow Intensification within Packed Granular Bed Filters: Experiments and Theory", General Electric Internal Report No. 00CRD290, 1980.

Squires, A. M., "Preliminary Economic Evaluation of the RFBF," Report to NYERDA, 819-ERER-BEA-86, 1987.

Stairmand, G. J., "Removal of Grit Dust and Fume from Exhaust Gases from Chemical Engineering Processes", The Chemical Engineer, December 1965.

Takahashi, T., Z. Tanaka, A. Itoshima and L. T. Fan, "Performance of a Rotating Fluidized Bed", J. of Chemical Engineering of Japan, Vol. 17, No. 3, 333, 1984.

Tardos, G. I., "The Granular Bed Filter - Theory and Experiments", Ph. D. Dissertation, Technion-Israel Institute of Technology (1977)

Tardos, G., "Studies in Electrohydrodynamics of Small Charged Particles," GE/CRD Report, 1982.

Tardos, G. I., C. Gutfinger and N. Abuaf, Isr. J. Technol., Vol. 12, 184, 1974.

Tardos, G. I. and R. Pfeffer, "A Method to Measure Electrostatic Charge on a Granule in a Fluidized Bed", Chem. Eng. Comm., Vol. 4, 665, 1980.

Tardos, G., R. W. L. Snaddon, and P. W. Dietz, "Electrical Charge Measurements on Fine airborne Particles," IEEE Transactions on Industry Applications, Vol. IA-20, No. 6, pp. 1978-1982, Nov. 1984.

Tardos, G., and R. W. L. Snaddon, "Separation of Charged Aerosols in Granular Beds with Imposed Electric Fields," AIChE Symposium Series, Vol. 80, pp. 60-69, 1984.

Thambimuthu, K. V., Y. Doganoglu, T. Farrokhalae and R. Clift, Symposium of Deposition and Filtration of Particles from Gases and Liquids, Society of Chemical Industry, London, 107, 1978.

VanOsdell, D. W., R. P. Donovan and L. S. Hovis, "Flow Resistance Reduction Mechanisms for Electrostatically Augmented Filtration," Proceedings: Fifth Symposium on the Transfer and Utilization of Particulate Control Technology, held in Kansas City, Missouri, 1984, Vol. 3, CS-4404-Research Project 1835-6, February 1986.

VanOsdell, D. W., A. S. Viner and K. D. Carter, "Fundamental Study of Electrically Stimulated Fabric Filtration," The Sixth Symposium on the Transfer and Utilization of Particulate Control Technology, New Orlean, Louisiana, February 25-28, 1986.

Wen, C. Y. and Y. H. Yu, "A Generalized Method for Predicting the Minimum Fluidization Velocity", Chem. Eng. Symp. Ser., Vol. 67, 100, 1966.

Whitby, K. T., "Calculation of the Clean Fractional Efficiency of Low Media Density Filters," Am. Soc. Heating, Refrig. air Cond. Engrs. J., p. 56, September 1965.

White, H. J., "Industrial Electrostatic Precipitation", Addison-Wesley Publishing Company, Inc., London, 1963.

Zahedi, K. and J. R. Melcher, "Electrofluidized Beds in the Filtration of a Submicron Aerosol", AIChE Journal, Vol. 26, 345, 1976.